Space-Time Processing: An Experimental Test Platform and Algorithms

A thesis submitted in fulfilment

of the requirements for the Degree of

Doctor of Philosophy

in Electrical and Computer Engineering

from the University of Canterbury

Christchurch, New Zealand

Peter John Green

B.Sc.,M.E.

May 2002

In loving memory of my mother

Abstract

This Thesis describes the concept, architecture, development and demonstration of a Smart Antenna Software Radio Test System (SASRATS). SASRATS was designed and developed as a functional and flexible system to facilitate the field testing of space-time processing architectures and algorithms. It is designed to facilitate the correlation of theoretical, simulated and measured performance. The SASRATS architecture has the capability of batch, pseudo-real and real time implementation of signal processing algorithms. It is used here to verify the work done by the author and others in the field of signal enumeration and blind beamforming.

The Thesis develops a robust method to enumerate the incident signals impinging on a uniform but variable size linear array independant of the extent of their correlation in a Rayleigh flat fading channel environment. The method self-optimizes the array size by minimizing the number of antennas with respect to the number of signals and adapts continously to maintain optimum performance in a mobile environment where users (signals) come and go. An algorithm is formulated with simulation and field results presented.

A robust channel order estimation algorithm using multiple antennas is also presented. We show that the approach has better performance than the conventional information theoretic based channel order estimation algorithms. It operates over a wide range of signal-to-noise ratios and is tolerant to correlation between channels. Algorithm performance is evaluated via computer simulation.

Acknowledgments

A million thanks to my wife, Anne for her love, patience, encouragement and total support of my work at Canterbury University. Thank you for being there for me and the kids.

I wish to also thank everybody who has helped me in my work. Special thanks to my supervisor Professor Desmond P. Taylor for providing financial assistance, technical guidance, proof reading my papers and Thesis. I like to also thank him for funding my trips to Globecom'98, Sydney, Australia and ICASSP 2001, Salt Lake City, USA. Thanks also to Professor Peter Gough for supporting the hardware development of the smart antenna system used in this Thesis.

My thanks also to Dr. Casey Miller who has helped me with the software development of the hardware system and his friendship, energy and enthusiasm on our numerous field trips.

Special thanks go all the technicians in the department for their help and assistance during the development of the smart antenna system. The smart antenna system would not have materialized without their help.

I wish to acknowledge and thank Telecom New Zealand for the Telecom Fellowship in Telecommunication Enginnering from 1998 to 2000. I am also grateful to the Public Good Science Fund for financial support through the years.

Last but not least, I wish to thank all my post-graduate friends and staff of the University of Canterbury whom I have been associated with for their friendship, support and guidance.

PETER JOHN GREEN

The University of Canterbury

May 2002

Contents

List of Figures

List of Tables

Chapter 1

Introduction

1.1 General Introduction

Wireless communications has become an essential part of our lives today. The millions of subcribers to wireless mobile cellular communication services is proof enough. It is anticipated that the growth of wireless systems will continue well into the future despite the current global recession and stagnant growth of the telecommunication and networking industries. This anticipated increase in the number of subscribers and the expectation of new services and systems with exciting multi-media features will pose technological challenges that must be met [1]. These systems must make full use of the limited and expensive frequency spectrum resource by increasing the spectrum efficiency of future wireless networks. The second generation wireless communication systems focussed on the development of modulation, coding, framing and protocols [2]. Antenna-related technologies were considered secondary functions and have received significantly less attention up to now. Current systems utilize antennas with limited directivity [3, 4]. This results in an expenditure of extra energy that is wasted and serves no useful purpose in maintaining a reliable communication link. This energy can also create interference to parallel links [5] and thus reduce the capacity of the system.

The demand for capacity, coverage, quality and a high level of services together with the reality of limited spectrum and the hostility of the wireless environment will require development of all aspects of radio technology for the third generation systems and beyond [2]. One key technology facilitator is the use of

adaptive or smart antennas. Smart antenna techniques use multiple antenna elements combined with signal processing to improve performance [6]. 'Intelligent' or 'self-configured' systems will be another key facilitator that is needed to achieve the ambitious requirements of future wireless systems [7]. These self-configuring systems will eliminate the current practise of "custom" tuning of antennas. These future systems must provide flexibility and programmability well beyond the conventional systems of today. It will be able to adapt to changing requirements of the customer, environment or operating standards with relatively ease. Such a system must therefore be software based. The ultimate software radio systems would allow full flexibility in frequency band, radio frequency channel bandwidth, air interface, and network protocols, with enough processing power to deal with future features and air interface standards [2, 8].

1.2 System Goals

The goal of this Thesis is to investigate smart antenna system architectures and to propose a smart antenna architecture that is simple yet flexible and employs software radio programming features that can be use for the evaluation of smart antenna architectures and algorithms. Another goal is to develop robust and adaptive algorithms to deal with the problems faced in real smart antenna systems. Many smart antenna algorithms developed in research labs around the world assume apriori knowledge of critical parameters that in practice are unknown and must be determined from the received signals corrupted by the hostile environment to work properly [9, 10]. Most are simulated and never field tested. Some will fail in the field when the mathematical models fail to match the real physical world [11]. Thus robustness and adaptability of algorithms that can reliably determine these critical parameters operating under real environmental conditions is another key goal of this Thesis.

1.3 Thesis Contents

Chapter 2 provides background information on the use of smart or intelligent antennas in wireless communication systems. This Chapter covers the use of intelligent antenna techniques such as beamforming and diversity to overcome wireless system impairments. It also introduces to the reader, the concepts of space and/or time processing. The concept of software radios in the design and development of a smart antenna test system platform is also covered. The main research topics on signal enumeration and channel order estimation are introduced in this Chapter.

Chapter 3 covers the concept, architecture, development and demonstration of a Smart Antenna Software Radio Test System platform dubbed SASRATS which is used to verify the algorithms developed in the later chapters. A robust blind beamforming algorithm using cyclostationarity properties of the received signal is simulated, verified and demonstrated using the platform.

Chapter 4 describes a robust algorithm developed to enumerate the number of signals arriving on an antenna array as many high resolution parameter estimation algorithms used in modern array processing rely on this knowledge to function correctly. The theory, simulation and field results of this algorithm using SASRATS are covered in this Chapter.

Chapter 5 decribes a robust algorithm for blind channel order estimation. The algorithm will correctly estimate the channel order over a wide range of signal to noise ratios using multiple antennas. It will also work correctly even when the channels picked up from the various antennas are highly correlated. Channel order estimation is critical to many channel estimation and equalization algorithms.

The final Chapter concludes the achievements and contributions of this Thesis. It also includes suggestions for future work.

1.4 Thesis Contributions

The original contribution of this Thesis consists of three components. The first is the architecture of the SASRATS platform, the second is the signal enumeration algorithm and the third contribution is the channel order estimation algorithm. The publications from this research and submissions are also cited.

1.4.1 Contributions to Smart Antenna Technologies

In this area, the original contribution is the development of a system architecture which facilitates the testing of a wide variety of smart antenna algorithms. A test platform was designed and developed based on the architecture. The platform has enabled the author to develop and verify smart antenna algorithms under real signal conditions. This approach ensures that the algorithms developed are robust enough to work in real conditions unlike those which are simulated but never field tested and usually fail under real signal conditions. Chapter 3 covers the research in detail and the result is summarised in the paper below

- P.J. GREEN AND D.P. TAYLOR, "Smart Antenna Software Radio Test System", *Proceedings of the First IEEE International Workshop on Electronic Design, Test, and Applications (DELTA 2002)*, pp. 68-72, Jan. 2002.

1.4.2 Contribution to Signal Enumeration

The original contribution in the area of signal enumeration is a robust method to enumerate the incident signals impinging on a uniform but *variable* size linear array independant of the extent of their correlation in a Rayleigh flat fading channel environment. The method also self-optimizes by minimizing the number of antennas to the number of signals and adapts continously to maintain optimum performance in a mobile environment where users (signals) come and go. The technique is a modification of the matrix decomposition method of Cozzens and Sousa [12]. The algorithm has a new set of stability, stopping and adaptive control criteria. A conference paper summarizes the research which includes the verification of the algorithm in the field using SASRATS. A journal paper covers the theory and algorithm is detail.

- P.J. GREEN AND D.P. TAYLOR, "Dynamic Enumeration Algorithm using Array Antenna", *Proceedings of IEEE International Conference on Acoustics, Speech and Signal Processing*, vol. 5, pp. 2861-2864, May 2001

- P.J. GREEN AND D.P. TAYLOR, "Dynamic Signal Enumeration Algorithm for Smart Antennas", *IEEE Transactions on Signal Processing*, vol. 50, pp. 1307-1314, June 2002

1.4.3 Contribution to Channel Order Estimation

The original contribution in channel order estimation is a robust algorithm which uses a linear prediction error filter approach to estimate the channel order using multiple antennas. Previous approaches operate only over a limited range of signal to noise ratios and are sensitive to channel correlation. A paper describing this research will be submitted in the near future.

Chapter 2

Background Information

2.1 Introduction

The major digital wireless cellular systems deployed today include code-division multiple access (CDMA) with IS-95, and time-division multiple access (TDMA) with IS-136 and the Global System for Mobile Communications (GSM)[13]. These second generation (2G) digital systems offer significant performance and capacity improvements over 1st-generation mobile systems, which are analog. Just as 2G systems have been deployed, work is well underway to develop third generation (3G) wireless networks [1]. The 2G systems are limited to data rates of approximately 9.6 Kbits per second (Kbps) and are too slow for broadband applications.

Third generation mobile systems also known as the International Mobile Telecommunications 2000 (IMT-2000) [3] by the International Telecommunication Union (ITU), will add broadband data transfers up to 2 Mbps to support video, Internet access, and other wireless high speed data services [14]. The ITU has outlined a family of standards to migrate the existing 2G networks to 3G in a common frequency band throughout the world [1]. The primary objectives are to provide high quality service for multimedia applications with a high degree of commonality of design worldwide, compatibility of services with IMT-2000 and with fixed networks and worldwide roaming capability. Key IMT-2000 technology facilitators [2] at the radio level are envisioned to be; battery technologies, digital signaling processor (DSP)/intergrated circuit (IC) technologies, antenna technologies and software radios.

Extensive research and development is being carried out worldwide to meet these objectives. The next section will cover in detail the problems associated the with wireless communication channel that must be solved to meet 3G objectives.

2.2 Wireless System Impairments

Wireless cellular communication systems are limited in performance and capacity by three major impairments; multipath fading, delay spread and co-channel interference. The combination of these effects makes the design of high-capacity systems a complex task.

Multipath fading occurs due to a signal from a transmitter taking many paths to a receiver due to signal scattering. The signal components that arrive at the receiver interfere with each other as the phases of the signals arriving at the receiver do not match and cause the received signal to fade. It is made worse by the fact that movement of the transmitter and/or receiver adds time-varying effects. This leads to the notion of slow and fast fading (time-selectivite fading). Time-selective fading [15] is characterised by the *coherence time*, T_c of the channel which measures the period of time over which the fading process is correlated. In other words, it is the period of time after which the correlation function of two samples of the channel response taken at the same frequency but different time instants drops below a certain predetermined threshold. The coherence time is inversely proportional to the *Doppler spread*. That is [3],

$$T_C \approx \frac{1}{f_m} \tag{2.1}$$

where f_m is the maximum Doppler shift given by $f_m = \frac{v}{\lambda}$ where v is the mobile velocity and λ is the wavelength of the received signal. The fading is said to be slow if the symbol time duration T_s is smaller than the channel's *coherence time* T_C; otherwise, it is considered to be fast. In slow fading, a particular fade level will affect many successive symbols, which leads to burst errors, whereas in fast fading the fading decorrelates from symbol to symbol. Multipath fading is relatively fast and is therefore responsible for short-term signal variation. If the multipath fading envelope varies in time according to the Rayleigh distribution then the fading channel

is characterised as a Rayleigh fading channel. In this Thesis, only signals from fixed terminals are considered and the effects of Doppler shift will not be observed.

Another form of multipath interference is delay spread. The main concern here is that multiple paths of the same signal arrive at different times and cause the phenomenon called intersymbol interference (ISI). The data symbols of one or many paths are relatively delayed in time such that the received symbols overlap one another. Delay spread [15] causes frequency-selective fading which implies that fading now depends on frequency.

Frequency selectivity is thus an important characteristic of fading channels. If all the spectral components of the transmitted signal are affected in a similar manner, the fading is said to be *frequency nonselective* or, equivalently, *frequency flat.* This is the case for *narrowband* systems in which the transmitted signal bandwidth is much smaller than the channel's *coherence bandwith* B_C. This bandwidth measures the frequency range over which the fading process is correlated and is defined as the frequency bandwidth over which the correlation function of two samples of the channel response taken at the same time but at different frequencies falls below a suitable value. In addition, the coherence bandwidth is related to the *maximum delay spread* τ_{max} by

$$B_C \approx \frac{1}{\tau_{max}} \tag{2.2}$$

On the other hand, if the spectral components of the transmitted signal are affected by different amplitude gains and phase shifts, the fading is said to be *frequency selective.* This applies to *wideband* systems in which the transmitted bandwidth is bigger than the channels's coherence bandwidth.

Co-channel interference (CCI) arises from users in other cells or systems using the same frequency. In time division multiple access (TDMA) systems, the co-channel interference is predominantly from one or two users, while in code division multiple access (CDMA) systems there are typically many strong interferers both within the cell and from adjacent cells [13]. Co-channel interference from multiple users sharing the same frequency within the same cell is called multi-user interference (MUI).

Interference from signals adjacent in frequency to the desired signal is called adjacent channel interference (ACI) [16]. ACI is caused by imperfect filtering at

the receiver which allows energy from transmitters operating close to the receiver frequency to leak into the passband. ACI however, can be minimized through careful filtering and channel assignments.

The specification of 3G wireless systems place heavy demands on the system capacity [3, 14]. As the available spectrum is limited and expensive, the need for additional capacity must also go hand in hand with techniques that improve spectral efficiency. To achieve the ambitious requirements of 3G wireless systems, new 'intelligent' or 'self-configured' systems will be needed [17].

Current 2G modems use temporal signal processing via equalizers that use a weighted sum of signal samples to mitigate interference. Temporal signal processing however, cannot effectively address the problem of CCI that arises from frequency re-use. It is shown in [5] that joint ISI and CCI cancellation is impossible with time-only processing when the received signal is sampled at the symbol rate. One way to mitigate CCI is to exploit the spatial dimension by using more than one antenna [5, 18]. Attention has recently turned to spatial filtering methods using advanced antenna techniques called smart, intelligent or adaptive antennas. The next section describes the use of intelligent antennas and space-time processing to mitigate interference.

There are numerous single-channel (one antenna) interference rejection techniques used for non spread-spectrum and spread-spectrum schemes [19]. Spread spectrum techniques employ a transmission bandwidth that is several orders of magnitude *greater* than the minimum required signal bandwidth compared to non spread-spectrum techniques. These interference rejection techniques will be mentioned but not discussed in detail as they are beyond the scope of this thesis. Interference rejection techniques for *non* spread-spectrum schemes include adaptive equalization and maximum likelihood sequence estimation (MLSE) [15], with the former employing adaptive approaches including the constant modulus algorithm [20, 21], neural networks [22], exploitation of spectral correlation [23], non-linear techniques [24] and higher order statistics [25].

Interference in spread spectrum systems can be classified as narrowband and wideband [19]. Spread spectrum tends to have a wide and flat spectrum. Narrowband interference is characterized by spikes in the spectrum. Narrowband interfer-

ence rejection techniques for direct sequence spread spectrum include adaptive notch filling [19], decision feedback [26], adaptive analogue to digital conversion [27] and non-linear techniques [28].

Wideband interference on the other hand is found in CDMA systems, where all users (each with his own spread spectrum signal) share the same band and interfere with each other. Wideband interference rejection is important to facilitate increased capacity in the licensed bands that deploy CDMA. Wideband interference rejection techniques for direct sequence spread spectrum include single-user and multi-user detection (MUD) [29, 19, 30]. Single-user detection means that only one user's spreading code and delay are known at the receiver and the interference from other users is treated as additive noise. The concept of multi-user detection regards all signals, both desired and undesired, as known at the receiver. Information regarding other users' signals enables the receiver to cancel or remove the effect of these signals, thereby lowering the limiting "noise floor" and increasing the overall capacity [29, 6].

Frequency hopping is another interference rejection method used in spread spectrum. Frequency hopping involves a periodic change of transmission frequency [3]. A frequency hopping signal may be regarded as a sequence of modulated data bursts with time-varying, pseudorandom carrier frequencies. At the receiver, the transmitted signal is first *dehopped* and then demodulated by a conventional receiver.

2.3 Intelligent Antennas

Intelligent antenna techniques use multiple antenna elements combined with signal processing to improve performance. The signals received by multiple antenna elements are weighted and combined to generate an output signal that can combat multipath fading of the desired signal and suppress interfering signals, thereby permitting greater coverage and capacity of a wireless system [13]. The current need for increased capacity and interference protection in wireless multi-user systems is at present treated through, among other techniques, limited microdiversity at the cell sites, sectorization and switched multibeam schemes [4].

Current systems employ 120^o sectorization. This means that a traditional

cellular base station with an omnidirectional antenna response is subdivided into 3 equal sectors using directional antennas looking out from the same base station location. Sectored antennas increase the possible reuse of a frequency channel by reducing potential interference across the original cell. However, sectorization efficiency decreases [4] as the number of sectors increases due to the effects of the overlapping beams.

When a mobile moves into a different cell while a conversation is in progress, a sophisticated switching technique called a *handoff* enables a call to proceed essentially uninterrupted [3]. A handoff is called a *hard* handoff when the user is assigned a different radio channel. Hard handoff is used by channelised wireless systems such as TDMA. Soft handoff on the other hand is used in CDMA cellular systems where users share the same channel in every cell. With *soft* handoff, a different base station handles the radio communication task. The basestation that gives the best communication link is selected. With 120^o sectorization, there will be more handoffs as the number of sectors increases when a mobile moves through a single cell. A more sophisticated scheme will be needed to handle the increased number of handoffs [7].

The switched multibeam approach is also called *fixed* multibeam antennas [14]. It utilises multiple sets of antenna elements with each set dedicated to an individual sector. The elements in a single sector are phased together to form multiple narrows beams which are predefined and fixed. Together they cover the entire sector. The phasing is done in the analog domain at radio frequency (RF) using a Butler matrix. The base station monitors each beam and for a desired signal, selects the beam which gives the best signal-to-interference-plus-noise ratio (SINR).

While sectorization and switched multi-beams antennas can provide some of the benefits of intelligent antennas, we consider intelligent antennas in this thesis as *adaptive* antenna systems. Interference-rejection techniques often need to be adaptive because of the dynamic or changing nature of the interference and the channel [19]. Adaptive processing is rapidly achieving favour because it can simultaneously exploit all three of the potential gain mechanisms; aperture gain, diversity gain, and interference suppression to improve performance [6].

In addition to increased coverage and capacity, some additional benefits of intelligent antennas [7] are reduced base station transmit power, improved mobile

battery life, better signal quality at higher data rates and improved robustness to imperfect cell location. Operational benefits may also include the ability to support user location for emergency calls, location of fraud perpetrators, location-sensitive billing, on-demand location-specific services and vehicle and fleet management [7].

2.3.1 Approaches

All intelligent antenna techniques either explicitly or implicitly improve the signal-to-interference-plus-noise ratio (SINR) at the receiver output. They can be classified under the following categories:

- Beam-forming [14, 31]
- Adaptive optimal combining [4, 10]

Beam-forming

Beamforming approaches for the mobile wireless communications environment were adapted from phase array antenna technology originally developed for radar applications [32, 31, 33]. The array is typically linear and composed of identical elements and assumes that the incoming signals are plane waves. The methods typically use $\lambda/2$ antenna element spacing, combine the signals to enhance desired signal reception and attempt to place nulls in the direction of interferers. The elements are typically combined at baseband in the digital domain using complex weights. The weights can be predetermined to form fixed beams or they can be adaptive. Historically, adaptive techniques were first developed by Howells [34], for application in a sidelobe canceler for adaptive nulling, and later Applebaum [35] developed a feedback control algorithm for maximizing the signal-to-interference-and-noise ratio (SINR). Simultaneously, Widrow [36, 32] developed the least-mean-square (LMS) algorithm for adaptively canceling interferers in the presence of the signals of interest. Yet another important milestone was the work of Capon, who proposed an adaptive antenna system [37] using a look-direction constraint that resulted in the minimum variance distortionless beam former. Further advances were made by Frost [38] and Griffiths and Jim [39] among several others. These techniques were

applied to analog signals for continuous operation and iteratively cancelled interferers in the presence of signals of interest. With the advent of digital technology, these techniques were re-employed, this time dealing with digitally sampled data and processing at baseband in the digital domain.

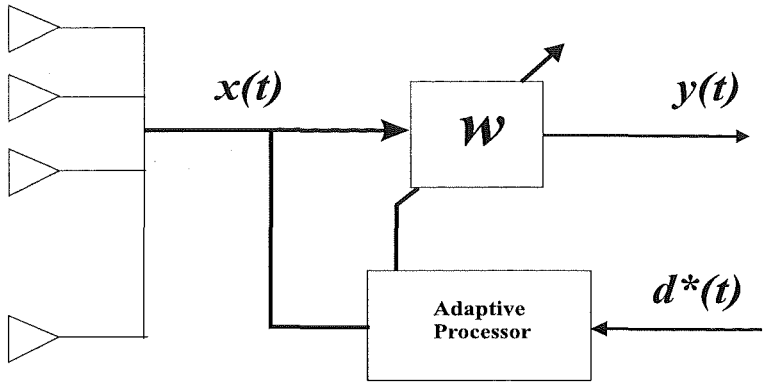

Figure 2.1: A generic adaptive beamforming system

A generic adaptive beam-forming system is shown in Figure 2.1. The choice of the weight vector $\boldsymbol{w}$ is based on the statistics of the the signal vector $\boldsymbol{x}(t)$ received at the array. Using a prescribed criterion of optimality, the objective is to optimize the beam former response so that the output $\boldsymbol{y}(t)$ contains minimal noise and interference. $\boldsymbol{d}^*$ is called the reference signal which closely represents or is at least highly correlated with the desired signal. Historically, the problem of finding the optimum weight vector was solved by Kolmogorov [40], in the analysis of stationary time series, and, simultaneously, by Wiener, in the control of antiaircraft guns [41]. Their methodology chose weights that minimize the mean-square error (MSE) between the beam former output and the reference signal, where the MSE is given by

$$\epsilon^2(t) = [d^*(t) - \boldsymbol{w}^H \boldsymbol{x}(t)]^2 \tag{2.3}$$

where H indicates the Hermitian transpose. Taking the expected values of both sides, we have [31]

$$E\{\epsilon^2(t)\} = E\{d^2(t)\} - 2\boldsymbol{w}^H \boldsymbol{r} + \boldsymbol{w}^H \boldsymbol{R}\boldsymbol{w} \tag{2.4}$$

where $\boldsymbol{r} = E\{d^*(t)\boldsymbol{x}(t)\}$ and $\boldsymbol{R} = E\{\boldsymbol{x}(t)\boldsymbol{x}^H(t)\}$. $\boldsymbol{R}$ is usually called the covariance matrix. To find the optimum weights, the expected value of the error needs to be

differentiated with respect to the weight vector $\boldsymbol{w}$, and the condition for minimum $\epsilon^2(t)$ leads to the orthogonality of the error with the input $\boldsymbol{x}(t)$. In other words, the optimum weight vector is the solution of

$$\nabla_w(E\{\epsilon^2(t)\}) = -2\boldsymbol{r} + 2\boldsymbol{R}\boldsymbol{w} = 0 \tag{2.5}$$

where ∇ is the complex gradient operator [42], and it follows that the solution is

$$\boldsymbol{w}_{opt} = \boldsymbol{R}^{-1}\boldsymbol{r} \tag{2.6}$$

which is commonly referred to as the Wiener-Hopf equation or the optimum Wiener solution.

Various criteria of optimality [4] such as maximum signal-to-noise ratio (SNR), minimum mean squared error (MMSE), maximum SINR, minimum variance distortionless response (MVDR) and maximum likelihood (ML) can be used. Highly important is the choice of adaptive algorithms [31] for deriving the adaptive criterion as it determines both the speed of convergence and complexity required to implement the algorithm. Some adaptive algorithms for continous adaptation are the least-mean squares (LMS) algorithm, direct sample covariance matrix inversion (SMI), recursive least squares (RLS) algorithm and the Hopfield neural network [31, 43].

The LMS algorithm is based on the steepest-descent method, a well known optimization method [43], that recursively computes and updates the weight vector. The primary virtue of the LMS algorithm is its simplicity, is numerically robust and its performance is acceptable in many applications. However, convergence can be slow if the eigenvalues of $\hat{\boldsymbol{R}}$ are widely spread. The SMI algorithm can be used to speed up the convergence rate by direct inversion of the covariance matrix $\boldsymbol{R}$ in (2.6). The SMI algorithm has two major problems: (1) increased computational complexity and (2) numerical stability resulting from the use of finite-precision arithmetic and the requirement of inverting a large matrix [31]. On the other hand, an important feature of the RLS algorithm is that the inversion of the covariance matrix is replaced at each step by a simple scalar division. The convergence rate of the RLS algorithm is typically an order of magnitude faster than that of the LMS algorithm, provided that the signal-to-noise ratio is high [31].

The various algorithms and criteria of optimality require a reference signal $\boldsymbol{d}^*$ in the adaptive optimization process. Explicit or implicit knowledge about the signals of interest must be known *a priori*. Spatial and temporal references are two categories of explicit reference.

The angle-of-arrival (AOA) of the desired signal is referred as an explicit spatial reference. If the AOA of the desired signal is known, the initial weights can be set to maximinize gain in the desired AOA and the received signal is used as the reference for later updating of the weights [44]. AOA information is usually obtained by applying a particular AOA estimation technique to the received array signal. A drawback with AOA-based approaches is the requirement of array calibration, in addition to the extra processing load required for estimating the AOA [31].

Examples of explicit temporal reference signals [31] include a special sequence in a data packet that is repeated at regular intervals by the desired signal (TDMA system) or a known pseudo-noise (PN) code in a CDMA system. In the IS-54 digital TDMA standard, there are three user slots in a time frame, each of which contains 324 bits, including a 28-bit synchronization sequence, 12-bit user identification sequence, and 260 data bits [45]. In [46], it is proposed that the known 28-bit synchronization sequence be used to generate the reference signal. In a GSM TDMA system, there is a training sequence in each data burst. This training sequence can be used to create a reference signal. Adaptive beamforming is highly suitable for a CDMA system, because the spreading codes can be used as references for beamforming.

An implicit reference on the other hand, is based on hidden or implicit structures of the wanted signal. It is primarily used in *blind* adaptive systems that do not require an explicit reference signal as each generates its own reference from knowledge of the implicit structures of the received signals. These hidden structures include spatial and temporal structures.

Spatial structure relates to the array manifold. The array manifold includes the effect of array geometry, element patterns, interelement coupling, scattering from support structures and nearby objects [5, 18]. The array manifold thus captures the spatial wavefront information. The array manifold is frequency dependent and needs to be calibrated at multiple points within the operating band.

The temporal structure relates to the properties of the desired signal and includes modulation format, pulse-shaping function, and symbol constellation. In many wireless applications, the transmitted waveform has a *constant* envelope. A typical example of a constant envelope waveform is the gaussian minimum shift keying (GMSK) modulation in the GSM system. The constant modulus algorithm (CMA) which exploits the constant modulus (CM) temporal structure, has been successfully applied to IS-54 TDMA signals [47], GSM signals [48] and 16-QAM signals [49].

The finite alphabet structure of digitally modulated signals is another important temporal structure in mobile communication signals. Such structure underlies all digitally modulated schemes. The modulated signal is a linear or nonlinear map of an underlying finite alphabet. For example, the IS-54 digital TDMA signal is a $\pi/4$ shifted differential quadrature phase shift keying (DQPSK) signal which has a set of finite phase shifts depending on the data. This finite set of phase shifts represents the finite alphabet structure.

Rather than make use of the constant modulus property or the finite alphabet structure of some communication signals, a number of algorithms make use of the cyclostationary properties of certain types of communication signals. The first algorithm that exploits the cyclostationary properties is called the spectral self-coherence restoral (SCORE) algorithm which was developed by Agree *et al.* [23].

Signals are said to exhibit cyclostationarity if their cyclic autocorrelation or cyclic conjugate correlation are nonzero either at some time delay τ or at some frequency shift α. The cyclic autocorrelation of a signal $s(n)$ is defined as

$$R_{ss}^{\alpha} = \langle s(n)s^*(n+\tau)e^{-j2\pi\alpha n}\rangle_{\infty} \triangleq \lim_{N\to\infty}\sum_{n=1}^{N} s(n)s^*(n+\tau)e^{-j2\pi\alpha n} \tag{2.7}$$

and the cyclic conjugate correlation is defined as

$$R_{ss^*}^{\alpha} = \langle s(n)s(n+\tau)e^{-j2\pi\alpha n}\rangle_{\infty} \tag{2.8}$$

When the signal $s(n)$ exhibits cyclostationarity at α_c (i.e., $R_{ss}^{\alpha_c} \neq 0$ or $R_{ss^*}^{\alpha_c} \neq 0$), α_c is referred to as the cycle frequency. The value of α_c for a particular signal is determined by the characteristics of that signal, such as the baud rate and the carrier frequency offset. Commonly used communication signals that possess cyclostationarity include [31]:

1. The double sideband amplitude modulation (DSB-AM) signals, which have a cycle frequency at $\alpha_c = 2\Delta f$, where Δf denotes the frequency offset from the carrier frequency;

2. The binary shift keying (BPSK) signals, which have cycle frequencies at $\{\alpha_c = 2\Delta f \pm kB_r$, for $k = 0, 1, \cdots\}$, where B_r represents the baud rate normalized with respect to the sampling frequency;

3. the GMSK signals, which have cycle frequencies at $\{\alpha_c = 2\Delta f \pm k\frac{B_r}{2}$, for $k = 0, 1, \cdots\}$

The SCORE algorithm for example, is based on the maximization of the cross-correlation coefficient between the outputs of the array and the reference signal that is constructed based on the cyclostationarity of the wanted signal. To generate the reference signal however, the *a priori* knowledge of both the delay and cycle frequency of the wanted signal, τ or α, respectively, is required.

An explicit reference signal is generally preferred as it is less complex, more accurate and leads to faster convergence of adaptive algorithms compared to an implicit reference signal [31]. In GSM, for example, about 17 percent of the bits in a data frame are dedicated to an explicit training/reference signal as the rapidly varying mobile channel requires frequent retraining [45]. However, if blind methods were to be used, the 17 percent could be used for data and thus improve the system capacity.

Beam-forming is a space-only processing technique as shown in Figure 2.2. It is shown in [5] that purely spatial combining can provide perfect cancellation of both ISI and CCI. However, this is not practical since real channels with rich multipath structure will require too many antenna elements. The solution is a combined space and time (ST) processing approach [50, 51, 52]. Such a ST structure is shown in Figure 2.3. Using the popular MMSE criteria of optimality, ST-MMSE has been shown to combine the strengths of time-only and space-only processing. CCI is primarily cancelled in the spatial dimension and ISI in the space or time dimension.

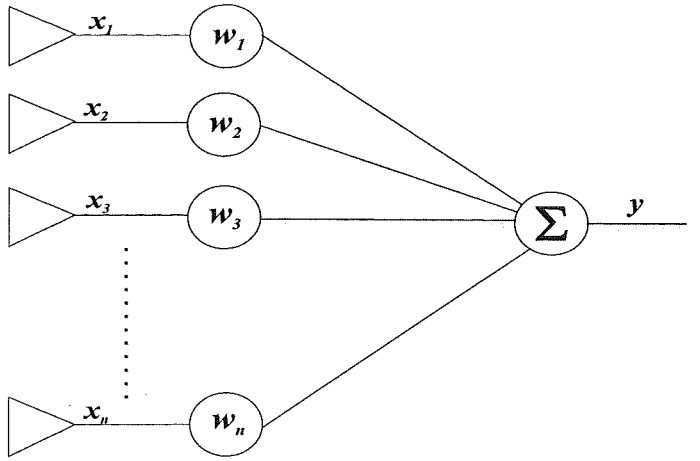

Figure 2.2: A generic space processing system

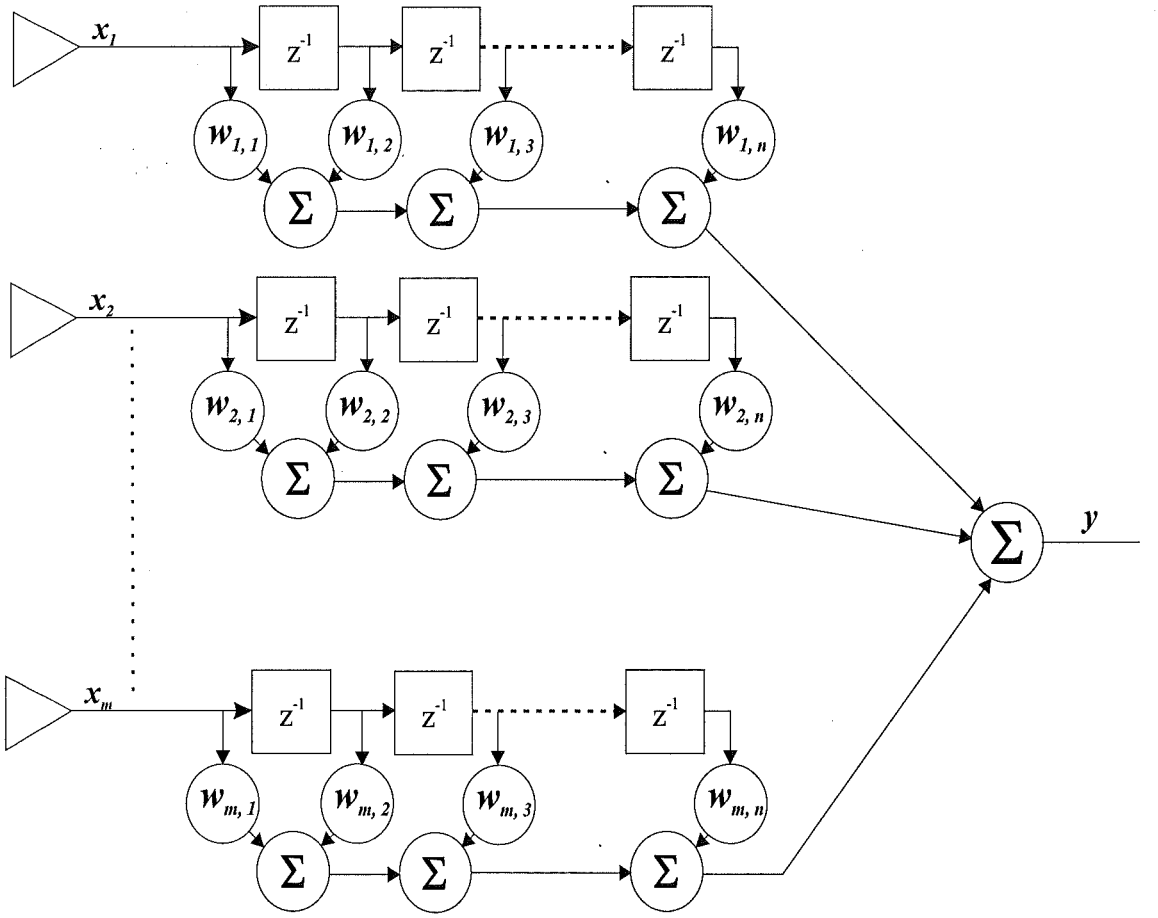

Figure 2.3: A generic space-time processing system

Adaptive optimal combining

In a typical wireless environment with multipath, the signals arrive from each user via multiple paths and angles of arrival. Angle spread at the receivers refers to

the spread of angles of arrival of the multipaths at the antenna array [5, 18, 53]. Angle spread causes space-selective fading, which means that the signal amplitude depends on the *location* of the antennas in space. Base stations are usually located at some considerable height above building rooftops and "see" a smaller angle spread compared to a radio handset operating close to ground level in a city environment. Signals from the base station arrive at the handset from almost all directions as they are bounced off numerous buildings and structures [4, 54]. Space-selective fading is characterized by coherence distance. Coherence distance [5, 53] represents the maximum separation in space for which the channel responses at two antennas remain strongly correlated. Combating multipath fading therefore, requires spatial *diversity* arrays. Antenna elements are spaced sufficiently apart to ensure that the fading envelopes seen on each antenna are uncorrelated. Antenna separation distance [13] of greater than 10λ for base stations and $\lambda/2$ for handsets will usually ensure uncorrelated fading envelopes. Unlike beam-forming arrays, these widely spaced diversity arrays have no geometric interpretation in terms of the array response.

There are four principal types of space diversity combining techniques, which depend on the (1) complexity restrictions put on the communication system, and (2) the amount of channel state information (CSI) available at the receiver. The four classic methods are maximal ratio combining (MRC), equal-gain combining (EGC), selection combining (SC) and switch and stay combining (SSC) [55].

With the MRC method, all the paths are co-phased and summed with optimal weighting to maximize the output SNR. The MRC method is the optimal diversity combining scheme but comes at the expense of complexity since the MRC method requires the knowledge of all channel fading parameters.

The EGC method on the other hand have all the paths co-phased and summed with equal weighting. Although suboptimal, EGC is often an attractive solution since it does not require estimation of the fading amplitudes and hence results in reduced complexity relative to the optimum MRC scheme.

The two former space diversity combining techniques (MRC and EGC) require all or some of the CSI (fading amplitude, phase, and delay) from all the received signals. In addition, a separate receiver chain is needed for each diversity branch, which adds to the overall receiver complexity. On the other hand, the SC-type systems

process only one of the diversity branches. The SC combiner chooses the branch with the highest SNR. In addition, since the output of the SC combiner is equal to the signal on only one of the branches, the coherent sum of the individual of the individual sum of the individual branch signals is not required. SC requires simultaneous and continuous monitoring of all the diversity branches. The SC method is implemented in the form of switched or scanning diversity, in which rather than continually picking the best branch, the receiver selects a particular branch until its SNR drops below a predetermined threshold. When this happens the receiver switched to another branch.

The switch and stay combining (SSC) method in the simplest form, switches to and stays with, the other branch, regeardless of whether the SNR of that branch is above or below the predetermined threshold. SSC diversity is obviously the least complex diversity scheme to implement.

As earlier stated, the MRC is optimum from the standpoint of maximising the SNR at the combiner output. In addition to combating multipath fading, space diversity can also be used in cellular radio systems to reduce the relative power of co-channel interferers (CCI's). When operating in this scenario, the appropriate diversity scheme to employ is one that combines the branch outputs in such a way to maximise the SINR ratio at the combiner output. This scheme is referred to as *optimum combining* (OC)[56]. Optimum combining will achieve a larger output SINR than MRC and is thus highly desirable even when the number of interferers exceeds the number of antenna array elements.

Adaptive optimal combining approaches are similar to the adaptive beamforming approaches in that several of the algorithms have the same maximization criteria. The weights that maximize SNR are simply the maximal ratio combining (MRC) solution [57]. Other "optimal" solutions include MMSE [58], maximum SINR (optimum combining method of [56]), MVDR [37, 59] and ML methods [57, 10, 60].

2.3.2 Other Applications

Multiple antennas are also used for other uses than just improving the SNR or the SINR at the receiver output. They are also used for direction of arrival (DOA) estimation. An antenna array can determine the azimuth and elevation angles to

the sources, and possibly the range to the sources if they are located in the near-field of the array. Information on source velocity can be obtained by measuring frequency shifts, or angles and range rates of change [33]. Algorithms such as MUSIC [61] and ESPRIT[62] are examples of algorithms used to determine the direction of arrival of sources to the array.

Intelligent antennas in the wireless cellular framework can be applied to wireless position location. The Federal Communication Commission (FCC) in the United States have imposed on wireless service providers to provide 125 metre position location accuracy on all wireless emergency calls at least 67% of the time [63]. Intelligent antennas will be a crucial element in locating users in a hostile multipath and co-channel interference environment.

Another important use of multiple antenna is source separation. It can determine the signal waveforms transmitted by each source; the fact that the energy from each source arrives from different directions allows these waveforms to be separated even if they overlap in time and frequency. They can thus be used for signal enumeration. The work in Chapter 4 of this Thesis covers this particular application of multiple antennas.

Multiple antennas can also be used for channel estimation to determine the space-time propagation effects between the sources and the received antennas. Channel parameters such as the amplitude, delay and phase shift are crucial to the proper operation of receivers using coherent detection. The work in Chapter 5 of this Thesis for example covers the use of multiple antennas for channel estimation.

2.4 Smart Antenna Software Radio Platform

One of the key IMT-2000 technology facilitators [2] mentioned in Section 2.1 other than antenna technologies is software radios. This section will introduce the concept of software radio as they apply to smart antenna systems.

Practical implementation of smart antenna systems with adaptive spatial and time processing require weights that have adjustable gain and phase characteristics that must be continously adjusted by the adaptive processor [31]. This is traditionally done in the analog domain at radio (RF) or intermediate frequency (IF)

using continuosly variable gain amplifiers and phase shifters [31]. Since these must work at RF, they have a small error tolerance and the devices are very costly. The advent of low cost high speed digital signal processors (DSP) has made it possible to carry out space-time processing in the digital domain, where most of the signal processing is performed in software and reconfigurable digital hardware [64]. Digital space-time processing is based on the conversion of the RF signal at each antenna element into two streams of baseband signal samples representing the in-phase (I) and quadrature-phase (Q) channels which contain the amplitudes and phases of the signals received at each antenna. The key to digital space-time processing is the accurate translation of the analog signals into the digital domain using analog to digital converters (ADC). To minimize the impact of variation in analog components, it is therefore desirable to digitize the signal at the highest feasible intermediate frequency (IF). In the future, it may be possible to digitize the RF signal directly at the antenna in the the GHz range. By weighting and combining these digital signals within the DSP or computer according to the various criterion of optimality, the amplitude and phases of received signals are adjusted and added together to output the desired optimal result. The algorithms are implemented in software and downloaded into the DSP or computer hardware to run and operate on the digitized I and Q data. This leads to the concept of *software radios.*

Software radios implement key receiver functions digitally in software [8]. These functions include downconversion, IF and baseband processing. IF processing involves analogue to digital conversion, digital filtering and decimation to baseband. IF processing is computationally intensive and software on DSPs is still too slow to be used for down conversion [65, 66]. Dedicated but highly programmable filtering hardware called a digital down convertor (DDC), is used instead. It outputs the I and Q data at a rate that can be handled by software in DSP for baseband processing. Baseband processing involves demodulation, equalization, decoding and synchronization. For smart antenna applications, space-time processing will occur at baseband. A major advantage of the software radio approach is the *software-reconfigurable* functionality. The radio functions and space-time processing algorithms can be changed without any need for hardware changes. For this reason, software radios are considered one of the essential components of 3G systems as it

provides a more efficient approach toward the implementation of demanding multi-standard radios [66].

Space time processing algorithms developed in most research labs around world are simulated on a computer using programs such as Matlab under controlled conditions incorporating mathematical models that represent real world phenomenon [67, 68, 69, 70, 71, 72, 73, 74, 75, 76]. With a few exceptions [13, 77, 4, 64], most space-time algorithms are never field tested. Many algorithms can fail in the field because the assumptions made in the model or the mathematical models may not accurately represent the real conditions. The importance of testing algorithms in the field under real conditions even on a limited or reduced scale cannot be overemphasized. Chapter 3 of this Thesis covers the concept, architecture, development and demonstration of a Smart Antenna Software Radio Test System (SASRATS) platform to test the algorithm developed in Chapter 4. It extends the work of the author in [78]. The end result is a real platform with a flexible architecture capable of testing various signal enumeration, beamforming, diversity, modulation, demodulation and synchronization algorithms.

2.5 Literature Review

As already outlined in Section 1.4, this Thesis makes original contributions in three major areas: 1) smart antenna software radio test system; 2) signal enumeration algorithm using array antennas; and 3) a channel order estimation algorithm using multiple antennas. Here we provide a brief literature review discussing some of the previous work relevant to the areas of interest.

2.5.1 Smart Antenna Software Radio Test System

Software radio was first described as a military-related technology in 1992 by Mitola [79]. Mitola covered the architecture of a generic software radio architecture in [8]. He also introduced the fundamental concepts of the software radio using mathematical models [80] to characterize the emerging technology and provided insights into defining hardware and software components needed to implement software radios. The earliest software radio project, SPEAKeasy I [81] was funded by

the U.S. Defense Advanced Research Projects Agency (DARPA). The SPEAKeasy II [82] project was the catalyst that sparked commercial and worldwide interest in software radios leading to the formation of the Modular Multifunction Information Transfer System (MMITS) Forum in 1996. The MMITS Forum is now renamed the Software-Defined Radio (SDR) Forum, and signals a shift from military to commercial emphasis in open architecture standards for software radio. The European Community sponsored precompetitive software radio programs in its Research and Development in Advanced Communication in Europe (RACE) and Advanced Communication Technology and Services (ACTS) programs [83].

In defining the IMT-2000 standard for 3G wireless networks, the ITU in document ITU M.1036 [84] recommends amongst other methods, the use of smart antenna technology to achieve system performance and spectrum efficiency. In addition, because of the gradual implementation of 3G systems around the world, the ability to upgrade base stations from 2G to 3G, using software configuration has become a highly desirable feature. Work by Ana Perez-Neira *et al.* [64] analyses the requirements for the introduction of software radio techniques and array processing architectures in *multi-standard* scenarios. It basically summarizes the conclusions and results obtained within the ACTS project called Smart Universal Beamforming (SUNBEAM).

Bose *et al.* [85] describes a concept called " virtual radios". The concept is similar to the software radio concept except that the software processing is performed in a general purpose workstation rather than using DSPs'. It describes a hardware input/output subsystem that bridges the analog front end and the workstation internal bus using a new software operating system. Turletti *et al.* [86] focused on the design and performance of a library of software modules that can be used to implement the baseband portion of a GSM base station on a workstation using the "virtual radio" approach of [85].

The smart antenna architecture of Razavilar *et al.* [87] is based on the wideband IF down conversion approach. It covers some beamforming algorithms and their computational complexity . However, the performance of the beamforming algorithms is based on simulation only and not based on an actual system. The work of Gunn *et al.* [88] describes a software radio architecture based on a DSP

core-based application specific integrated circuit design (ASIC) for single antenna handsets and proposed the use of bandpass sampling technique.

Correal *et al.* [89] implemented a single antenna DSP-based direct sequence code division multiple access (DS-CDMA) multiuser receiver to test their interference cancellation algorithm. Seskar and Mandayam [90] also worked on interference cancellation in DS-CDMA using a software-defined radio platform based on a mix of field programmable gate arrays (FPGA) and DSPs. FPGAs allow the hardware to be electronically reconfigured by changing the FPGA configuration files. In contrast, DSPs are reconfigured through software using different DSP subroutines [83]. Recently, the work of Frigon and Daneshrad [91] on field measurements of an indoor high speed wireless system used a smart antenna test platform specially designed for quadrature amplitude modulation (QAM). The heart of their system is based on an application specific integrated circuit (ASIC) optimised for QAM. Separate field trials by Ericsson [92] and Lucent/AT&T [93] have demonstrated increased interference tolerance in an IS-136 system using a four-element adaptive array.

Chapter 3 covers a smart antenna test platform based on software radio principles incorporating some of the best aspects of previous works. The transmitter and receiver is software reconfigurable. The transmitter modulation, baud rate and pulse shaping filters are software configured in DSP. The receiver architecture incorporates digital intermediate frequency (IF), hybrid down conversion using bandpass sampling and a flexible data bus which will allow the complex digital baseband signals from multiple receivers to be processed by a pool of digital processors. The current pool of processors includes DSPs for real-time implementation of space-time algorithms and an off-line computer for batch processing. The computer can also go on-line in the pseudo-real time mode of operation. Dedicated ASICS and FPGAs can also be connected to the bus if needed. The bus architecture also allows for expandability up to 15 receivers. The software approach also allows the compensation of antenna mutual coupling effects to be easily accomplished during calibration. Most papers do not mention of the effects of antenna mutual coupling on their system performance and the need for calibration in their smart antenna systems. We also describe but do not test a method that uses only *one* cable to connect between multiple antennas and receivers.

2.5.2 Signal Enumeration

Many high resolution *parameter estimation* algorithms [94] used in array signal processing rely on *a priori* knowledge of the *number* of incident signals [95]. For example, algorithms for direction-of-arrival (DOA) estimation that use methods based on Maximum Likelihood [96], Eigenstructure [97, 61], Weighted Subspace Fitting (WSF) [98] or Estimation of Signal Parameters via the Rotational Invariance Technique (ESPRIT) [62] critically depend on knowing the number of signals present at the array output. Their performance is dependent on the exact knowledge of this number. Even recent work [10] on spatial diversity antennas for distinguishing cochannel signals by exploiting differences in the channel from each user requires the number of active users to be known. Under estimation of the actual number of signals can lead to catastrophic failure of the Viterbi algorithm used to estimate the channel in [10] and over estimation can increase the computational complexity of the algorithm exponentially. These methods assume that the number is known but in practice, the knowledge of the number of signals incident on an antenna array is not known a priori and must be determined. The topic of signal enumeration is the main subject covered in Chapter 4 of this Thesis. The chapter covers the theory and research carried out to find a robust signal enumeration algorithm that can be used as a first step prior to running parameter estimation algorithms.

One approach to this problem is based on the observation that the number of signals can be determined from the *eigenvalues* of the covariance matrix of the observation vector. An estimate of the number of signals is obtained from an estimate of the number of repeated smallest eigenvalues. Since in practice the input covariance matrix is formed using a finite set of samples, the smallest eigenvalues are not exactly equal. Various statistical methods have been proposed to test for the equality or closeness of eigenvalues, which can then be used to estimate the number of sources.

Bartlett [99] and Lawley [100] developed a procedure, based on a nested sequence of *hypothesis tests*, to implement this approach. Anderson [101] also developed a likelihood ratio statistic to test the closeness of the eigenvalues. For each hypothesis, the likelihood ratio statistic is computed and compared with a threshold. The hypothesis accepted is the first one that crosses the threshold. The problem

with these sequential hypothesis (SH) testing methods is the *subjective* judgement required for deciding on the threshold levels. Wax and Kaliath [102] proposed two other detection schemes based on the application of the Akaike information theoretic criteria (AIC) [103] and the Rissanen Minimum Descriptive Length (MDL) criteria [104]. These methods do not require a subjective threshold, and the number of the sources is determined as the value for which the AIC or MDL objective function is minimised. The method was further analysed by Zhang *et al.* [105] and Wang and Kaveh [106] and modified by Yin and Krishnaiah [107] and Wong *et al.* [108].

Wax and Kaliath [102] showed through simulations that the MDL criterion yields a consistent estimate of the number of signals, and the AIC yields an inconsistent estimate that tends, asymptotically, to overestimate the number of signals. To improve the performance of the AIC and MDL algorithms, Wu *et al.* [109] derived and applied a new estimator function called the Gerschgorin Likelihood Estimator (GLE) to the AIC and MDL criteria. It is shown in [109] that the Gershgorin AIC (GAIC) and Gershgorin MDL (GMDL) estimators are more consistent than the simple AIC and MDL estimators. However, they can detect only up to $M-2$ sources, as opposed to $M-1$ sources that can be detected using the regular AIC and MDL criteria where M is the number of antennas in the array.

All the source estimators discussed so far are based on the assumptions of Gaussian and spatially white noise. The AIC and MDL algorithms will not work with correlated sources. This is shown by simulation in Chapter 4. Correlated sources cause the AIC and MDL algorithms to underestimate the number of sources. The GAIC and GMDL algorithms will also not work as reported by Wu [109]. In practice, correlation of directional sources may exist due to multipath propagation [9]. Correlation tends to reduce the rank of the array correlation matrix. There are several pre-processing techniques, which try to restore this rank deficiency in the correlation matrix. Wax and Ziskind [110] modified the MDL principle and made it applicable to coherent sources but it requires the angle of arrival of the sources to be known or estimated first. It is further refined in [111] and [112] to improve performance.

Another pre-processing scheme is the spatial smoothing method of Shan *et al* [113]. In its basic form, it decorrelates the correlated signal arrivals by subdividing

the array into a number of smaller overlapping subarrays and then averaging the array correlation matrix obtained from each subarray. A decorrelation analysis of spatial smoothing by Yang and Tsai [114] shows that there exists an upper bound on the number of subarrays and the maximum distance between the subarrays depends on the fractional bandwidth of the signal. The use of subarrays also limits the effective aperture of the array as well as the number of degrees of freedom, and thus one needs a larger number of elements to process correlated arrivals than otherwise required.

An alternative scheme for estimating the number of sources present uses the eigenvectors instead of the eigenvalues of the array correlation matrix. This method is referred to as the eigenvector detection technique. The eigenvector detection technique of Lee and Li [115] is applicable to a cluster of sources whose approximate directions are known.

The matrix decomposition method of Di and Tian [116] and Di [117] offered a solution to the enumeration problem using rank sequences constructed from eigenvectors and submatrices of the array covariance matrix respectively. Cozzens and Sousa [12] improved on the matrix decomposition technique of Di [117] and provided a new set of stability rules for the rank sequences, although their technique is more computationally intensive.

The signal enumeration literature to date has concentrated on the techniques for source enumeration of uncorrelated sources and recently to correlated sources in white Gaussian noise environment using a *fixed* number of antennas in an array. To date there is no literature that looks at variable size arrays for signal enumeration. This thesis looks at using a variable number of antennas to reduce computational complexity and to maintain robust enumeration performance by dynamically adjusting the size of the array. The new technique works in a white Gaussian noise environment and also in a flat Rayleigh fading environment.

Chapter 4 develops a robust method to enumerate the incident signals impinging on a uniform but *variable* size linear array independant of the extent of their correlation in a Rayleigh flat fading channel environment. The method also self-optimizes by continously minimizing the required number of antennas for the number of signals present and adapts continously to maintain optimum performance

in a mobile environment where users (signals) come and go. The technique is a modification of the matrix decomposition method of Cozzens and Sousa [12]. A new set of stability, stopping and adaptive control criteria is presented. An algorithm is formulated and simulation results are presented. Field results of the algorithm using SASRATS are also presented.

2.5.3 Channel Order Estimation

We have seen in Section 2.2 that a transmitted signal undergo various impairments as it propagates through a wireless channel. To negate the effect of the channel, the channel must be estimated. In 2G modems, training sequences known at the receiver are periodically sent in the transmitted data stream to aid the equalizer to adaptively adjust the equalizer coefficients to negate the effects of the channel. Training sequences consume bandwidth as the effective date rate is increased since training symbols must be inserted with the information symbols. To obviate training and thus utilize bandwidth more efficiently, blind channel estimation algorithms based on the unique statistical properties of the transmitted signal have received attention in recent years. A common assumption in many of these blind channel identification algorithms [118] is that the order of the true channel is known. In practice the channel order must be estimated.

The AIC and MDL algorithms and its variations are commonly used for channel order estimation [118]. Here the AIC and MDL algorithm is used to estimate the rank of the autocorrelation matrix of the received signal. The AIC criterion strongly tends to overestimate the channel order [102] and MDL is often the prefered choice. Xu and Kaveh [119] show that in the presence of colored Gaussian noise, both the AIC and MDL approaches tend to overestimate the channel order with probability that increases with increasing the number of data samples. Liavas and Regalia [120] reported that both the AIC and MDL fail to estimate the order correctly at high SNR. Liavas *et al.* [118] proposed a new criterion based on the ratios of successive eigenvalues to overcome the problem of false estimation at high SNR. The method of [118] however suffers from poor performance at low SNR [121]. In another paper by Liavas *et al.* [122], it is noted that blind channel order estimation becomes a very hard problem if the channel impulse response contains small leading and/or trailing

coefficients.

The work in Chapter 5 presents a new robust channel order algorithm that will work over a wide SNR range. It is based on the application of linear prediction filter theory to channel order estimation. It is developed from a channel estimation algorithm of Karem Abed-Meraim *et al.* [123], which uses the prediction error method for blind identification. However the work of [123] uses the MDL algorithm to first estimate the channel order and thus suffers from channel order estimation errors at high SNR or when the channels are correlated. Our new algorithm overcomes this limitations by using an inherent property of the prediction error method being robust to an *over-estimation* of the channel order [124]. The new channel order estimation algorithm is superior to the MDL algorithm currently used in many channel estimation algorithms.

2.6 Summary

This Chapter has provided a summary of wireless system impairments and the general concept of intelligent antennas and software radio. We have also provided a brief literature review of the papers relevant to this Thesis in the subject of signal enumeration and channel order estimation.

Chapter 3

Smart Antenna Software Radio Test System

3.1 Introduction

Space time processing algorithms developed in most research labs around world are currently only simulated on a computer under controlled conditions incorporating mathematical models that represent real world phenomenon [67, 68, 69, 70, 71, 72, 73, 74, 75, 76]. There is abundant use of abstract mathematics and almost complete lack of experimentation with real-life data [11]. With few exceptions [91, 13, 77, 4, 64], most space-time algorithms are never field tested. Many algorithms may perform poorly or fail completely in the field because the assumptions made in the mathematical models do not accurately represent the real physics of the problem at hand. Sensitivity of the algorithm to deviations from the assumed mathematical model may also lead to instability [11].

For example, some research is based on analytical approaches using statistical channel models, while other works relies on simulations using either statistical models, measured channel impulse responses or ray-tracing techniques to model the wireless channel [91]. Although such studies are essential to the initial understanding and relative comparison of alternative systems and algorithms, they have in general neglected implementation issues such as antenna coupling, quantization noise and component non-linearity, just to name a few. Furthermore, the results are to some extent limited to the channel models used [54] and are difficult to generalise. Thus

the importance of testing the algorithms in the field under real conditions even on a limited or reduced scale is extremely important to system development.

This chapter covers the concept, architecture, development and demonstration of a Smart Antenna Software Radio Test System (SASRATS) to test the algorithm developed in Chapter 4. SASRATS was designed and developed as a functional and flexible system to facilitate the field testing of new space-time processing architectures and algorithms. A major objective is to provide correlation between simulated and measured performance of algorithms. The SASRATS architecture must also have the capability of real time implementation of a wide variety of signal processing algorithms.

3.2 SASRATS Architectural Requirements

Key architectural requirements of the system are as listed below:

- Flexible RF pass band operation to 1 GHz. Testing is in the approved 915 MHz Industrial, Scientific and Medical (ISM) band. The ISM band lies in between the 800 MHz and 900 MHz cellular bands. The channel characteristics will be similar to the cellular radio frequency channels. The system can be easily extended to operate up to the IMT-2000 3G frequencies (1.9 - 2.2 GHz) and the 2.4 GHz ISM band.

- Modular design of RF and IF sections. Modular design of the analogue section of the radio prior to digital IF processing accomodates architectural, RF characteristics and filter changes without major hardware modifications.

- Programmability on the fly. 'Software radio' programmability and flexibility. Digital IF processing allows radio characteristics such as filter selectivity and tuning resolution to be changed via software with no hardware changes needed. Baseband processing via digital signal processors (DSP) or computers allows algorithms to be be downloaded, tested, verified or modified almost instantaneously.

- Flexible TX data rates up to GSM (270 KSPS). Transmitter data symbol rates are currently programmable up to GSM rates of 270 KSPS. Data rates can be

extended via software changes.

. Flexible digital modulation and demodulation. Transmitter software allows selection of various digital modulation schemes such as binary phase shift keying (BPSK), quadrature phase shift keying (QPSK) and its variants such as $\pi/4$ differential QPSK and various types of quadrature amplitude modulation schemes. Other modulation schemes such as spread spectrum can be created in software and downloaded. Demodulation is done at baseband via software algorithms.

. Flexible data bus architecture for fast and timely transfer of data between receivers, the pool of digital processors and an off-line computer. This is critical for space-time processing as data from multiple radios must be sampled and processed at the same time instant. The system bus architecture must also be able to accomodate more radios in the future.

. Ruggedness for field environment testing. Requires the electronics to be housed in a solid chasis for ruggedness and reliability.

. System to be easily assembled and dismantled during field testing. Detachable subsytem components allows the system to be quickly assembled in the field or in a vehicle.

. Minimise electromagnetic interference (EMI). Use of proper cabling, filtering and balancing, grounding and shielding techniques to minimise EMI to subsystem components and nearby equipment.

. Low output transmit power ($\leq$ 100 mW). This will minimise interference to adjacent cellular radio bands during field tests. Ability to boost power to $\leq$ 1 W when required.

. Variable receiver antenna separation : $\lambda/2$ for beamforming and greater for diversity. Simple antenna structures to minimize tuning and maximize portability and ruggedness.

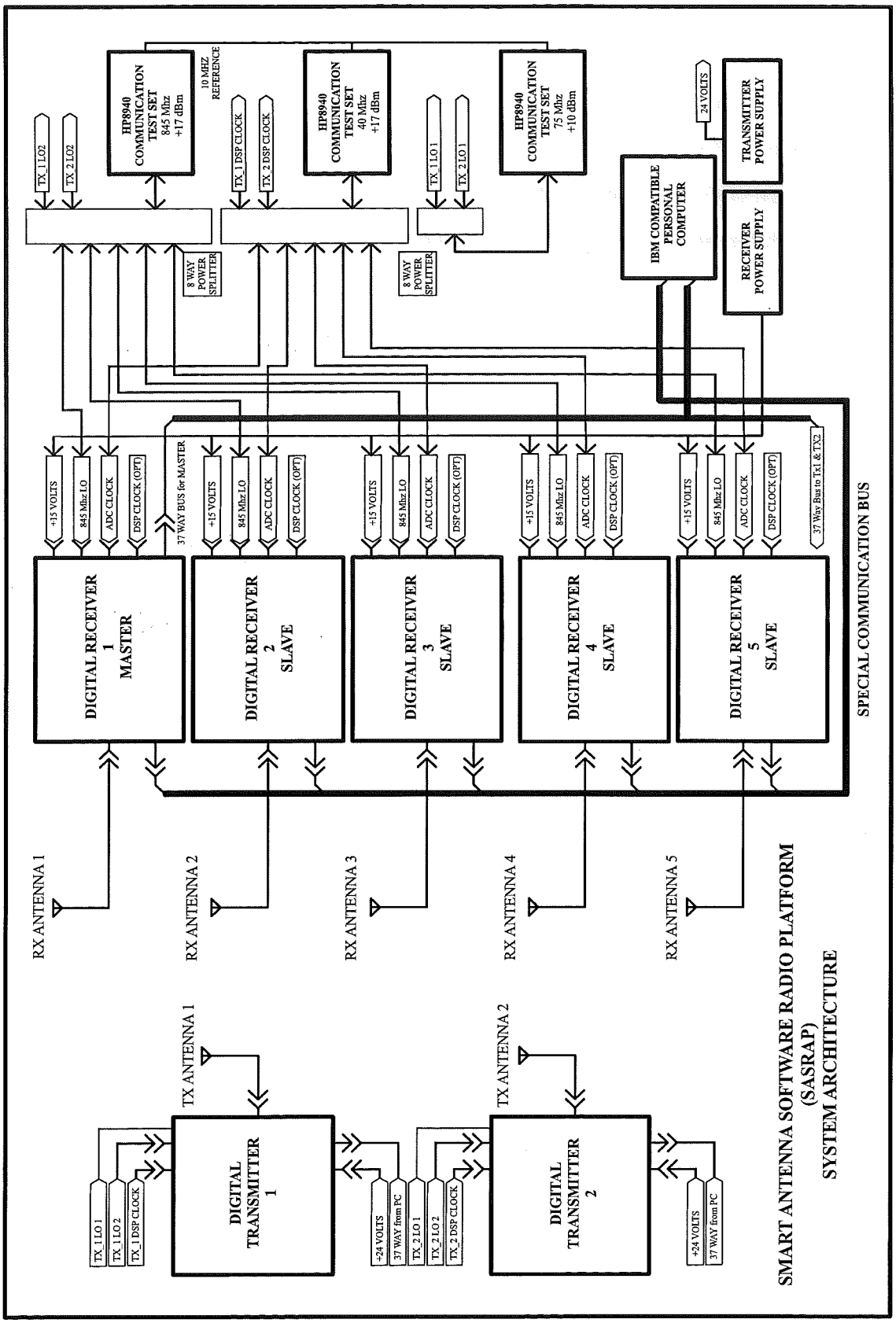

Figure 3.1: Smart Antenna Software Radio Test System (SASRATS) Architecture

3.3 SASRATS General System Architecture

The general system architecture of SASRATS is shown in Figure 3.1. The basic system consists of 5 digital receivers, 2 digital transmitters, 7 monopole antennas and auxilliary components such as power splitters, power supplies and oscillators. A personal computer is used for transmitter (TX) and receiver (RX) programming, DSP code assembly, data acquisition, storage and batch signal processing using Matlab. A 10 MHz reference output signal from one of the oscillators provides a commom 10 MHz reference signal to all oscillators in the system for the purpose of synchronization. Note that in this diagram, the RF subsystems are not specifically shown, but may be assumed to be associated with each antenna at both transmitter and receiver. The physical setup in the laboratory is shown in Figure 3.2. The picture shows the computer and five receivers on the left table and one transmitter with three Hewlett-Packard signal generators on the right table in the laboratory. For field measurements, the equipment is dismantled and reassembled in a vehicle and driven to the test site. Detailed specifications, circuit diagrams and operating instuctions for SASRATS can be found in *Smart Antenna Software Radio Test Sytem User Manual* [125], an internal technical report of the University of Canterbury.

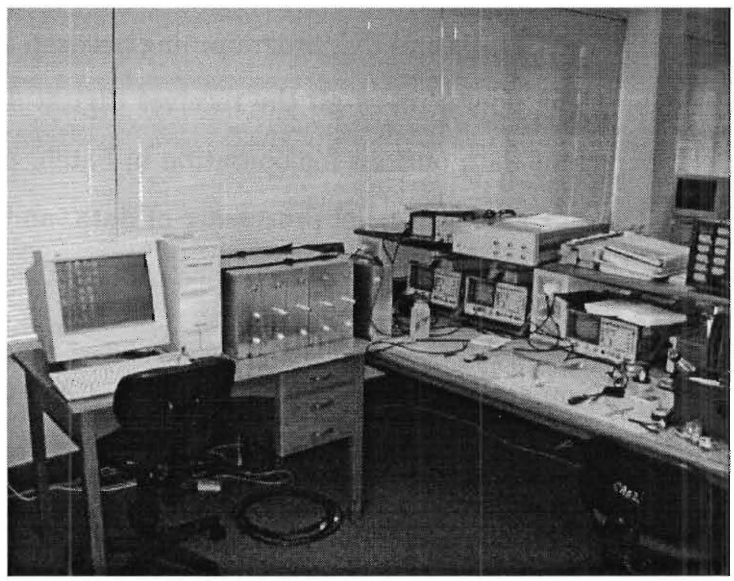

Figure 3.2: Smart Antenna Software Radio Test System (SASRATS) in the Lab

For much of the current experimental work, the transmitters and receivers

are hardwired in order to share a common clock for the purpose of synchronization. For beamforming experiments, a set of 5 monopole antennas spaced $\lambda/2$ apart are mounted on a large metal ground plane. For test purposes, the antennas are separated from the receivers by at least 20 metres of RF coaxial cables to minimize any interaction between the antenna array panel and the receivers. The transmit antenna cables are between 20 and 60 metres long. For distances greater than 60 metres, the TX can be configured to work independently using a separate PC, oscillator and power suppply but synchronization software in the receiver must then be used.

3.3.1 SASRATS Receiver System

The SASRATS receive system architecture of Figure 3.1 consists of 5 receivers; one *MASTER* and 4 *SLAVES*. The Master receiver has an extra dedicated DSP for selecting and programming all slave receivers plus running slower real time DSP algorithms. A fast DSP is also present for running space-time algorithms. Each of the 4 slaves has only a fast DSP for space-time processing algorithms. A critical portion of the RX architecture design is the Special Communication Bus (SCB). Designed with space-time processing in mind, the high speed bus allows for sharing of I and Q data among all radios, DSPs and PC, programming between master and slave radios and synchronizing the operation of all the receiver digital down converters. The bus offers flexible output data options for operation in batch, pseudo-real time or real time modes. The bus allows parallel processing of data, and also allows the slaves to work independently if required by an interface cable between the DSP and the SCB port.

The Special Communication Bus shown in Figure 3.3 has two ports to interface with various peripherals. The SCB-Serial port allows high speed serial data transfers between the receivers and a high speed National Instruments Data Acquisition (NIDAQ) card on the SASRATS PC and/or the enhanced synchronous serial interface (ESSI) ports available on most popular DSPs'. The NIDAQ card allows up to 15 receivers to be operated simultaneously. The SCB-Parallel port is available for wider bandwidth applications, allowing parallel transfer of data to PC or DSP. The parallel port behaves as a memory mapped external peripheral device.

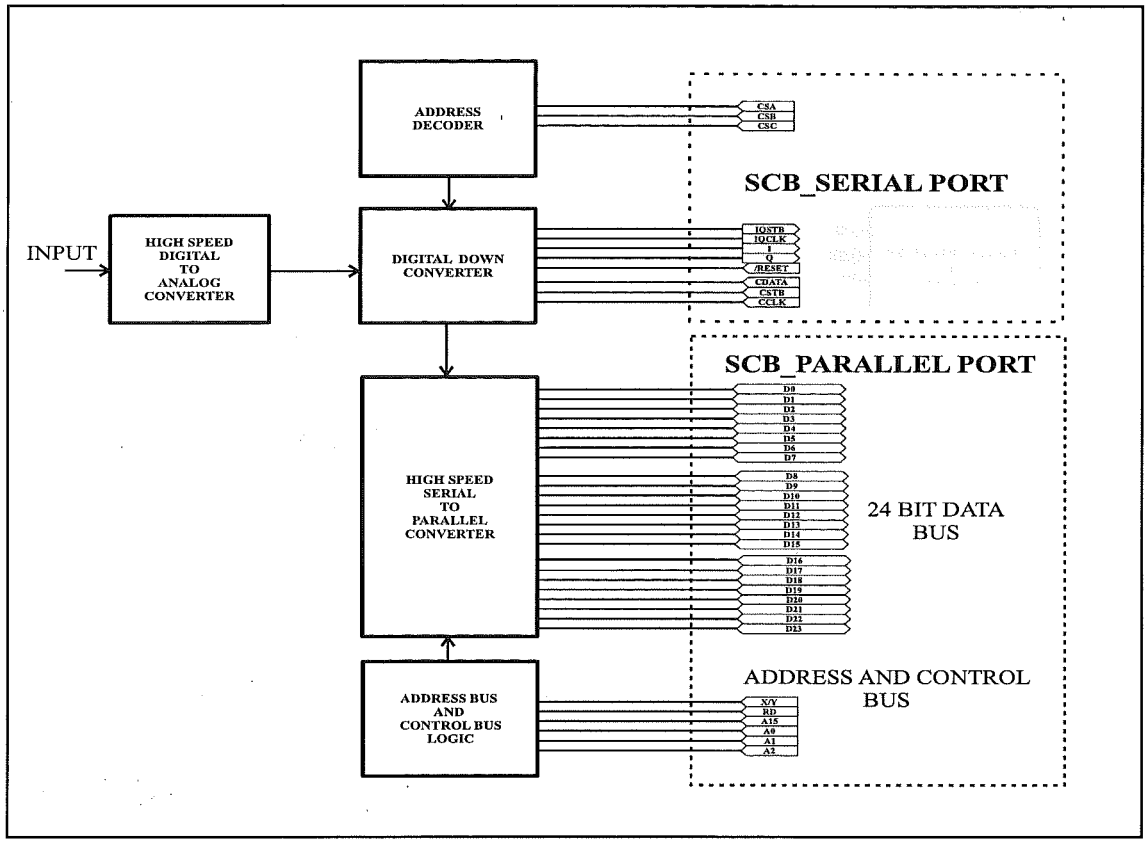

Figure 3.3: SASRATS Special Communication Bus - Serial and Parallel ports

In the batch and pseudo real-time modes shown in Figure 3.4, the serial in-phase (I) and quadrature phase (Q) data from all five receivers are read by a high speed digital input card. In batch mode, large amounts of data are stored on hard disk for delayed processing. In pseudo real-time processing mode, a Matlab program collects small batches of data for immediate processing. Pseudo real-time processing is extremely useful for calibration of amplitude and phase between the receivers and the testing of new algorithms running on Matlab.

Algorithms for space-time processing and synchronization can be performed in real time in the real-time mode of operation. Advanced field tests can use the real-time mode *after* algorithms are first verified to work on batch data collected in the batch or pseudo real-time modes using Matlab. Once verified, the time consuming process of rewriting the algorithm in DSP assembler language can then proceed. Development tools from the Texas instruments TMS320C6XX family and Motorola Star*Core family of DSPs', allow algorithms written in the C language to be compiled and optimized directly to machine code [17]. This cuts down on the

development time for real-time implementations.

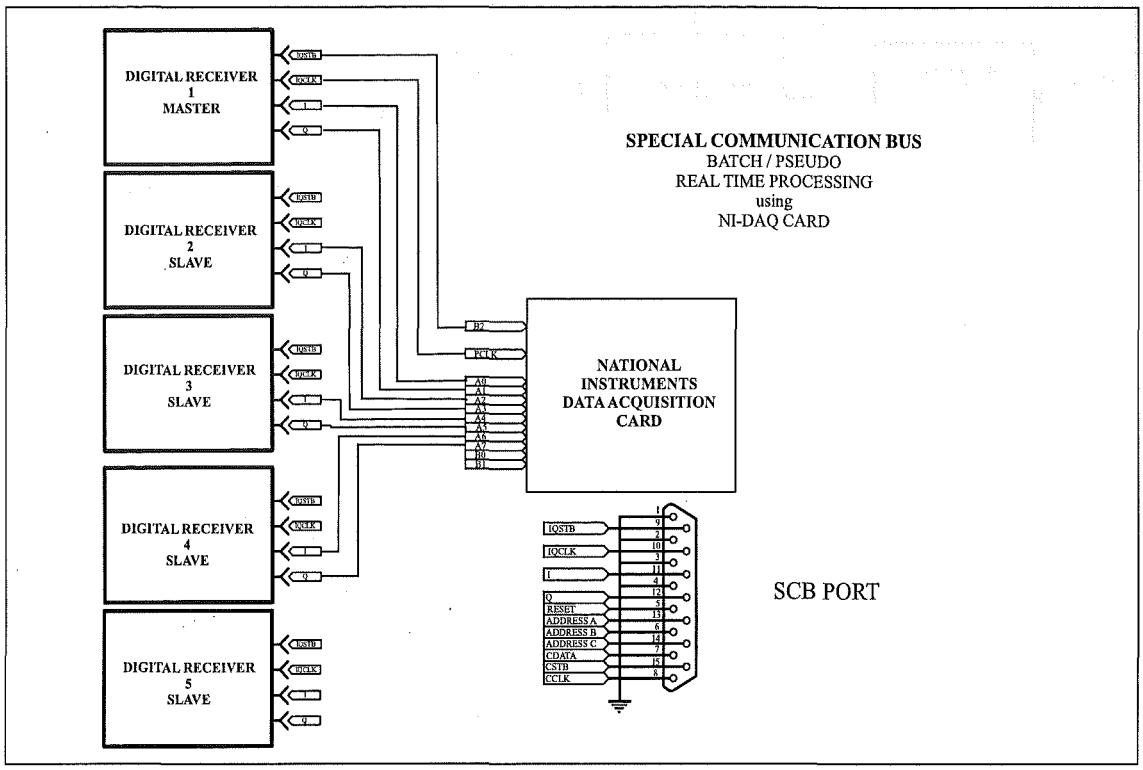

Figure 3.4: SASRATS SCB Batch / Pseudo Real-Time Processing Configuration

In the real time mode shown in Figure 3.5, serial I and Q data from all receivers are programmed in *time division multiplexed mode* on the SCB-Serial port. The data is picked up by the appropriate DSP in each receiver for processing at the proper time slot. In Figure 3.5, an extra DSP is shown connected to the common bus. In fact a pool of processors can be connected to the bus for parallel processing of data. The time division multiplexed mode has limitations. For a constant output clock rate, each receiver's bandwidth must be reduced as more receivers are added and take up more time slots. Thus for wider bandwidth operation and/or as more receivers are added to the system, the SCB-Parallel port is used instead. Detailed information can be found in the *Smart Antenna Software Radio Test Sytem User Manual* [125].

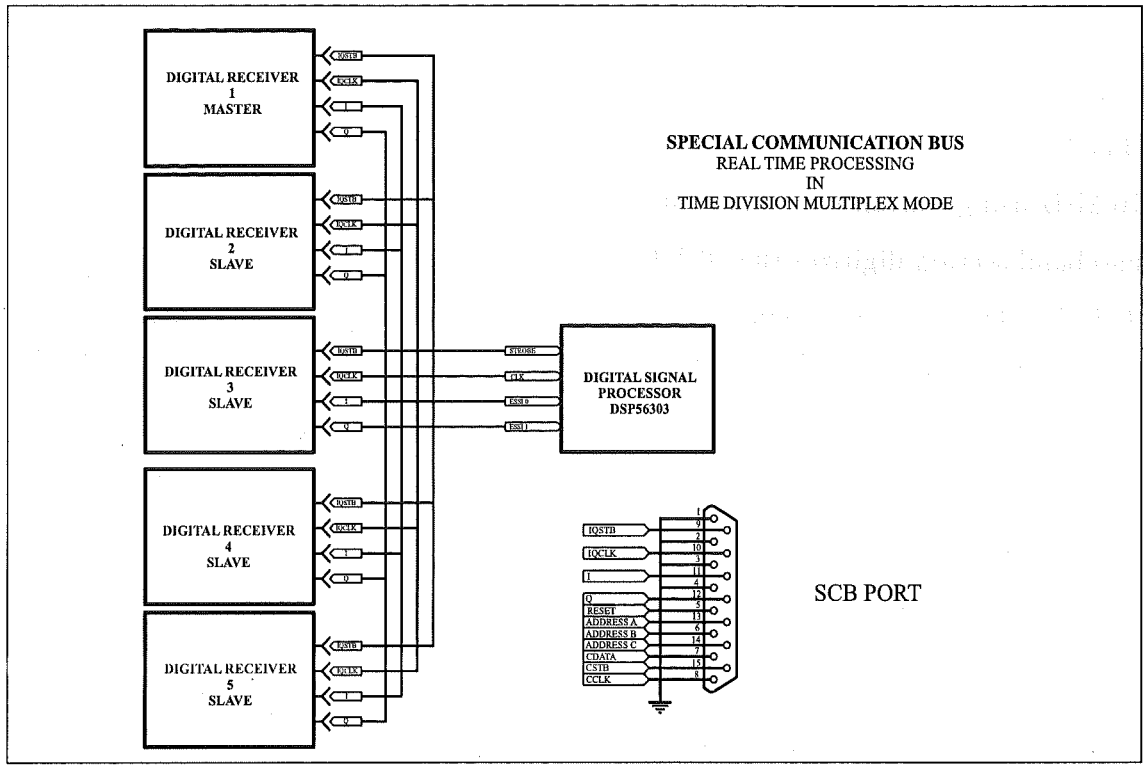

Figure 3.5: SASRATS SCB Real-Time Processing Configuration

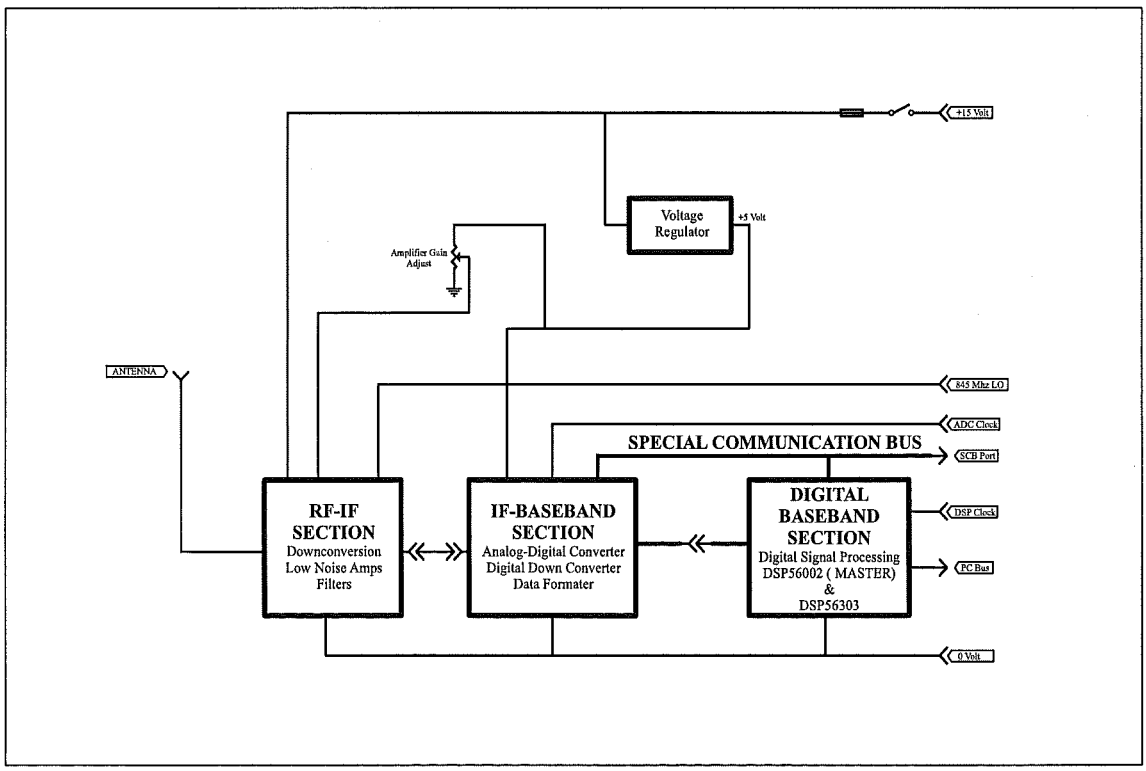

Figure 3.6: SASRATS RX unit System Architecture

The RX architecture consist of 5 sections and is shown in Figure 3.6. The sections are RF-IF, IF-Baseband, baseband, the PC and the Special Communication Bus (SCB). The RF-IF section downconverts the 915 MHz received signal to an IF of 70 MHz using conventional analogue low noise amplifiers, mixer and filters. The IF-baseband section digitizes the 70 Mhz IF signal. The digital down converter (DDC) digitally downconverts, decimates and filters the samples and serially outputs digital I and Q baseband samples. The baseband section performs real time processing of complex baseband data using the DSP. The PC is used for DSP programming, batch data storage or pseudo real-time processing using Matlab via the NIDAQ card.

A key RX design feature is digital down conversion from IF to baseband. Traditional analog down conversion from IF to baseband consists of an analogue mixer based on diodes and transformers or active mixer designs. The I and Q mixers require tight phase matching with equal group delay and a 90 degree phase shift network for the local oscillator to drive the mixers [31]. The output of the I and Q mixers are phase matched at a particular input carrier and local oscillator frequency. The mixers must also have the same group delay response (i.e. the change of phase over frequency characteristics) over the bandwidth of operation. Analogue filters are used for image filtering. For sharp attenuation of out of channel components, a costly surface acoustic wave (SAW) filter is often used. Only then can the baseband processing effectively extract the desired signals.

Digital IF downconversion requires that the signal is digitized by an ADC before processing. The functional blocks remain the same as the analog approach but the processing is done digitally. The digital signal is multiplied by the sine/cosine terms of a numerical controlled oscillator which is functionally equivalent to an analogue mixer and local oscillator. Digital synthesis vastly improves tuning resolution with very fast tuning speeds and generates sine/cosine signals with *exact* 90 degree phase balance. Digital filtering is used to select the band of interest and reject unwanted signals. Digital filtering allows the implementation of highly selective almost "brick wall filters" with linear phase characteristics which is impossible to achieve with analog filters. Analog filter characteristics change due to temperature variations and aging. They are also susceptible to mechanical shock and vibration. Digital filters on the other hand, do not vary with temperature or time. Other advantages of

digital IF processing include flexibility of design, reliability and programmability on the fly.

There are two types of processing for digital IF down conversion; narrow band and wide band. In narrow band processing, only the portion of the spectrum which contains the required signal channel is down converted for processing. Wide band processing involves the down conversion of several channels, simultaneously, before individual information channels are separated. For example, the entire 25 MHz receive GSM cellular band (890-915 MHz) may be down converted and digitised using the wide band processing approach prior to the separation or demultiplexing of individual signalling channels. This is in contrast to down converting and digitising a single 200 KHz GSM channel bandwidth using the narrow band processing approach.

In narrow band processing, the desired signal is bandpass filtered at RF to remove all of the unwanted spectrum outside the desired RF bandwidth before it is down converted to the first IF. At the first IF, the signal is again filtered to remove any unwanted spectrum outside the desired *channel or information* bandwidth and amplified. The resulting IF spectrum is then digitized, down converted to DC and the receiver outputs the I and Q base band samples.

SASRATS receivers use a *hybrid* approach to digital IF conversion. The bandwidth of the first IF filter (10 MHz) is usually much wider than the transmitted information bandwidth (typically 200 KHz). This feature gives the receiver the flexibility in the future to work with symbol rates higher than the maximum symbol rate of the current transmitters. This feature also allows multiple information channels (as in the wide band approach) instead of just one information channel (as used in the narrow band approach) to be digitised.

The SASRATS IF is 70 MHz. The 1 dB bandwidth of the 70 MHz IF bandpass filters used in SASRATS limits the IF signal bandwidth to 10 MHz. The IF is then band pass sampled at 40 MHz. The band pass sampling approach will be discussed in detail in the next section. The digital down convertor is programmed to digitally tune to the centre of the desired information channel and the down converted data stream is decimated, low pass filtered and outputs the I and Q base band samples.

Bandpass sampling

Basic to the SASRATS RX architecture is the use of bandpass sampling. Bandpass sampling is also known as undersampling, subsampling and aliasing sampling but in this Thesis, the term bandpass sampling will be used throughout. Numerous papers have been written on the theory [126, 127] and application [128, 129] of bandpass sampling.

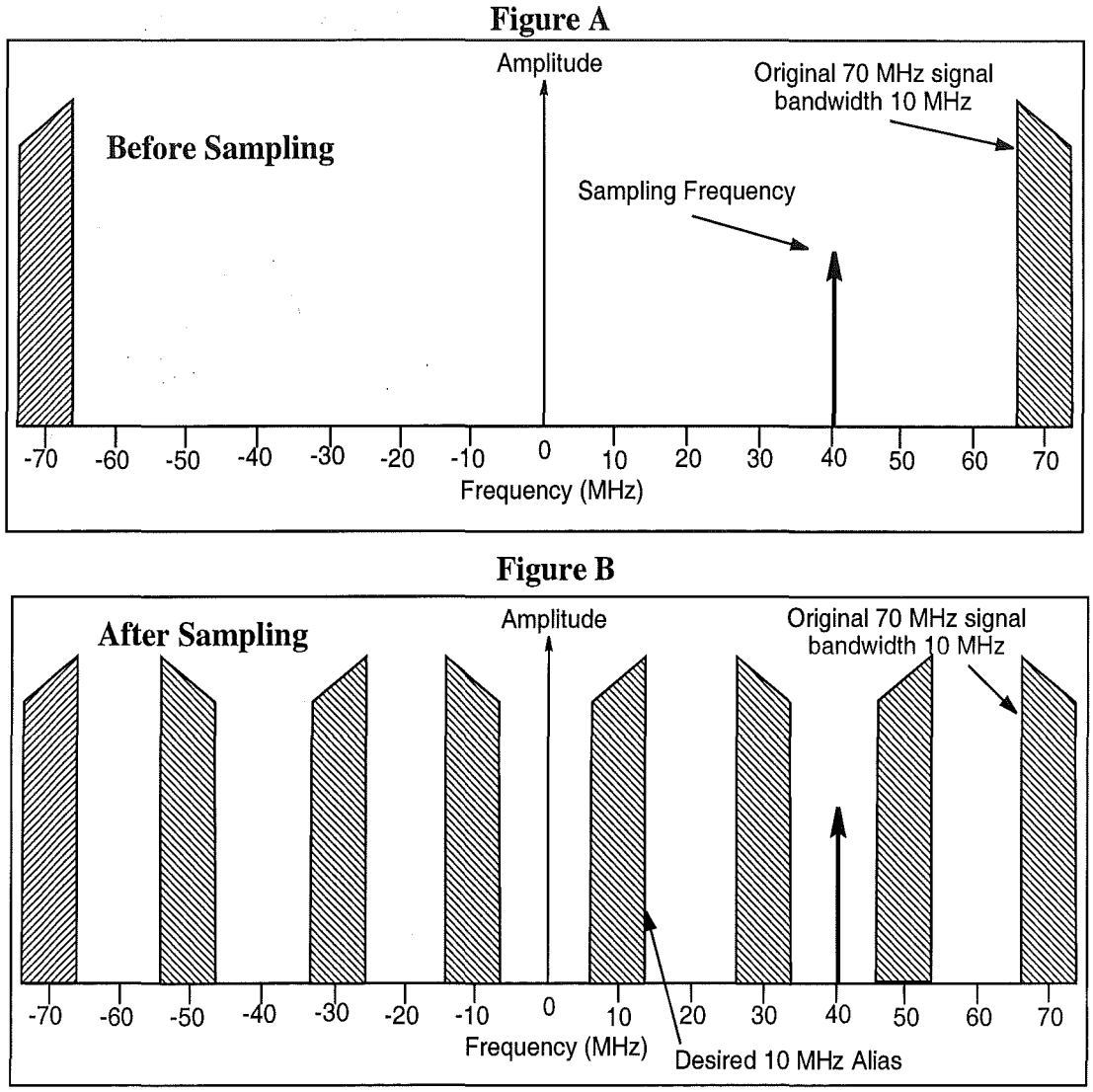

Figure 3.7: Bandpass Sampling

The concept is best illustrated in Figure 3.7. Figure 3.7A illustrates the spectrum of the desired signal spectrum, centred at f_{IF} and of bandwidth BW before bandpass sampling occurs at the ADC. Since the highest frequency component is

$f_{IF} + \frac{BW}{2}$, conventional Nyquist sampling dictates a sampling frequency of at least $2(f_{IF} + \frac{BW}{2})$. If f_{IF} = 70MHz and BW = 10 MHz, the conventional Nyquist sampling frequency, f_S must be at least 150 MHz. Using bandpass sampling, the signal can be sampled at a much *lower* rate and still allow the recovery of the desired signal. The desired signal is sampled at a rate that meets the Nyquist criterion for the signal's *bandwidth* but not for its absolute frequency. In other words, the sampling rate is at least twice the bandwidth of interest but *not* twice the highest absolute frequency. Figure 3.7B shows the resulting spectrum with the ADC sampling the signal at f_S of 40 MHz. The bandpass sampling technique in the ADC generates multiple images of the original signal. The images are spaced at f_S. The desired image used in the SASRATS receiver is centered at 10 MHz which actually is a lower sideband alias. The bandpass sampled data is then fed into the digital down converter. Here a numerical controlled oscillator internal to the DDC is programmed to generate the sine and cosine frequencies of a 10 MHz signal. The bandpass sampled data is then multiplied by the two 10 MHz (sine and cosine) signals using two digital mixers. The resultant inphase and quadrature phase baseband signals are then low pass filtered and finally decimated to the Nyquist rate for the bandwidth BW using two separate sets of low pass and decimation filters internal to the DDC.

However, proper bandpass sampling has restrictions. The sampling frequency f_S must satisfy inequality 3.1 or the spectrum of the images will overlap, i.e aliasing occurs and the affected spectrum cannot be recovered. Aliasing is exploited by carefully filtering the IF signal, then bandpass sampling it at an appropriate rate. The acceptable range of sampling frequencies is [129] defined by

$$\frac{2f_{IF} - BW}{n} > f_S > \frac{2f_{IF} + BW}{n+1} \tag{3.1}$$

where n is any positive integer. If f_{IF} = 70 MHz and BW = 10 MHz, the range for various n is shown in Table 3.1. There are six possible ranges of allowable frequencies. The bandpass sampling frequency chosen for SASRATS is 40 MHz ($n = 3$). For a chosen n, the guardband is defined as the difference between the chosen sampling frequency and the two limits in equation 3.1, whichever is smaller. The SASRATS system thus has a minimum guardband of 2.5 MHz. Note that as the value of n gets

larger, the range of allowable sampling frequencies gets smaller. Bandpass sampling allows both the ADC and the digital down converter to process the signal at much lower data rates thus providing the option of using a less expensive ADC.

The SASRATS architecture uses external programmable oscillators as local oscillators for down conversion from 915 MHz to 70 MHz IF and to provide the 40 MHZ ADC sampling clock. All oscillators are be synchronized through a 10 MHz reference. The use of programmable oscillators provide flexible operation at RF and the ability to easily change sampling frequencies.

Table 3.1

Range of allowable bandpass sampling frequencies for various n with $f_{IF} = 70MHz$ and $BW = 10MHz$

n	Minimum f_S $\frac{2f_{IF}-BW}{n+1}$	Maximum f_S $\frac{2f_{IF}-BW}{n}$
1	75	130
2	50	65
3	37.5	43.33
⋮	⋮	⋮
6	21.428	21.666

Although bandpass sampling allows the desired bandpass signal to be sampled at a lower rate and allows the use of cheaper ADCs', the disadvantage is that there is a degradation of the signal to noise ratio of the sampled signal. Whenever a bandpass signal is reproduced at a baseband position by sampling, the noise from all the aliased bands is combined into the baseband. Even with a ideal anti-aliasing filter, the signal to noise ratio is *not* preserved owing to post filter thermal noise contributions from the aliased spectra. This degradation is quantified by [126] the signal to noise ratio

$$SNR_S \approx \frac{S}{N_{in} + (n-1)N_{out}} \tag{3.2}$$

where S is the bandpass signal spectral power density, N_{in} the in-band noise power density, N_{out} the out-of-band noise power density and n is defined as

$$1 \leq n \leq I_g\left[\frac{f_{IF} + \frac{BW}{2}}{BW}\right] \tag{3.3}$$

and the function $I_g[x]$ is the floor function of the largest integer within x . Under most circumstances, $N_{in} >> N_{out}$ and the SNR is established before sampling. If $N_{in} = N_{out}$ and assuming $n >> 1$, the degradation of the SNR in decibels is given by [126]

$$D_{SNR} \approx 10\log_{10}(n) \tag{3.4}$$

In SASRATS case, with $n = 3$, $D \approx 4.7$ dB. Despite the degradation in the SNR of the sampled signal, previous work by the author in [78], which involves the investigation of performance trade-offs of bandpass samping techniques on receiver sensitivity and immunity to intermodulation distortion, shows that with proper selectivity of the IF filters and low values of n, excellent receiver performance is achievable.

Software radio programmability

Another key SASRATS receiver design feature is its flexible 'software radio' programming features. In the past, digital IF solutions consisted of multi-board implementations of high-speed, low-level, mathematical building blocks such as multipliers. As a consequence, a digital IF was widely used in only cost-insensitive military radios, but rarely used in commercial products where the classical analog superheterodyne implementations were the solutions of choice. Today, semiconductor technology has evolved to support the levels of integration and processing speed required to implement digital IF processing. Many additional features for tuning, phase correction, output bandwidth and resolution have been added. This is made possible by the availability of high performance VLSI chips from Intersil [130] and Analog Devices. The SASRAT receivers make full use of these VLSI chips to achieve the 'software radio' functionality mentioned in Section 3.2.

3.3.2 SASRATS Transmitter System

A key TX design feature is real time baseband processing of I and Q samples. Flexible software allows for programmable modulation, pulse shaping and baud rate options. It is simple to use. The required TX options are chosen, the DSP code assembled and loaded into the DSP and run. The TX system architecture is shown in Figure 3.8.

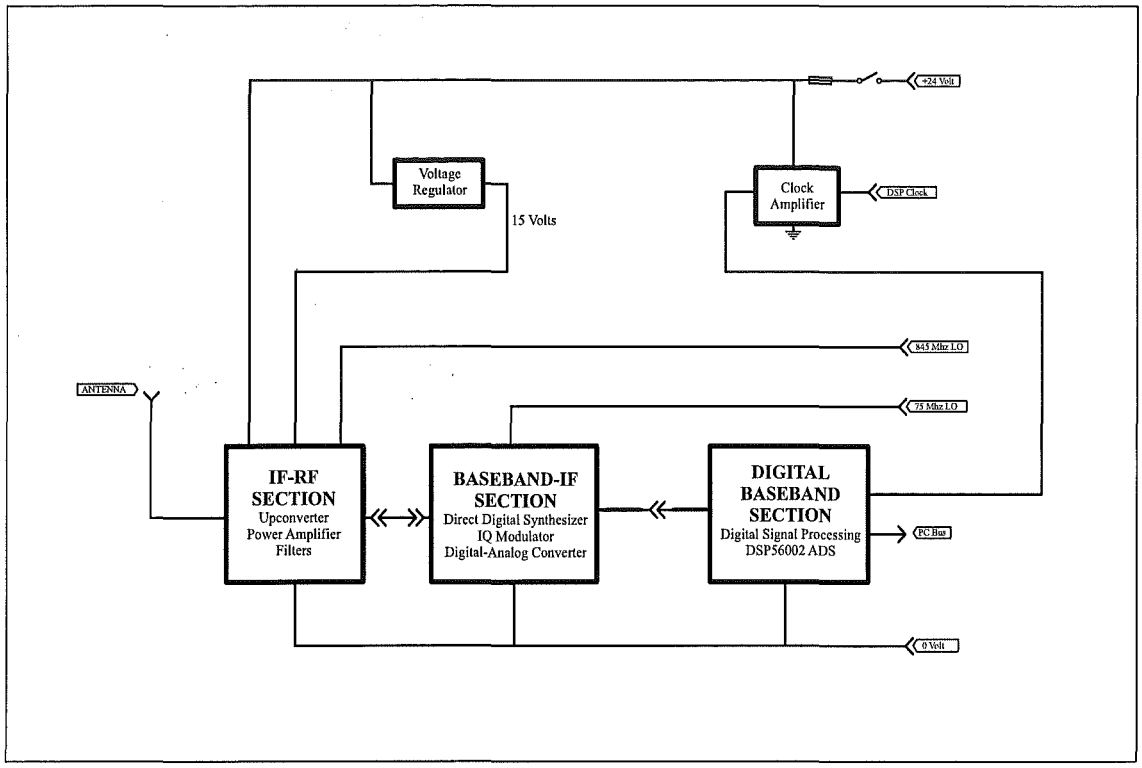

Figure 3.8: SASRATS TX System Architecture

The TX architecture consist of 3 sections; digital baseband, baseband-IF and IF-RF sections. A PC is used for programming and assembling of DSP code. The code is then loaded into the DSP board in the digital baseband section. The digital baseband section is where real-time processing is done. This is where the random bits are generated, mapped into the required modulation and filtered. In the baseband-IF section, the filtered I and Q samples from the DSP in the baseband section, digitally modulate the output of a direct digital synthesizer (DDS). The output of the DDS is a real analog IF signal centered at 5 MHz. The IF-RF section consist of conventional analogue upconversion circuits, linear preamplifier, power amplifier

and filters to output the RF energy at 915 MHz into the antenna. Detailed circuit diagrams and specification of the transmitter can be found in [78] and also in *Smart Antenna Software Radio Test Sytem User Manual* [125].

3.4 SASRATS in the field

Critical in beamforming algorithms is the accuracy and precision (stability) of *phase* measurements of the transmitted signal picked up by the 5 monopole antennas at the receivers. Multipath propagation makes *indoor* laboratory measurements useless unless done in a special radio frequency (RF) anechoic chamber which absorbs and prevents reflections of RF energy off walls. The facility is not available at the University. One option is to use the RF anechoic chamber at Industrial Research Limited in Wellington. To avoid the hassle of relocating the whole system to Wellington, we chose to remain in Canterbury. The only option then is to go outdoors.

Initial locations were not perfect due to the limited field size and close proximity to nearby objects. Finally an almost ideal location was found at Ilam Fields (a large athletic field) where the wide open unobstructed field provides better channel characteristics (relatively free from multipath) for the received signal. The Sports Pavillion at Ilam Fields was used for storage of the antenna array and to provide power to our equipment. The SASRATS equipment was set up in a station wagon and driven to the test site daily. The first five field tests were mainly tests to characterize and calibrate the SASRATS system. The oscillators used throughout the SASRATS field tests are the Hewlett Packard 8920A RF Communication Test Sets. Many unsuspected problems were encountered in the field relating to phase measurements and calibration. Considerable time was spent to understand these problems and compensate for them. They will be discussed in the following subsections.

3.4.1 Effect of the environment on phase measurements

One major field problem observed is the significant drift in absolute phase with changes in ambient temperature. The 5-antenna linear receive antenna array panel is generally placed 20 metres away from the receivers and connected via 5 x 20m coaxial cables. One sunny winter's afternoon when a cloud suddenly covered the

setup, the ambient temperature quickly cooled down the panel and the coax cables, causing the absolute measured phase of an unmodulated 915 Mhz carrier from a transmitter placed 30 metres away, to decrease significantly by as much as 120 degrees over a 5 minute period. The observed 120 degree shift is not caused by the Hewlett Packard oscillators but by the 20m coaxial cable between the antenna and the receiver. Temperature changes cause the phase characteristic of the cable to change over temperature. This made *absolute* phase measurements difficult as it is impossible to control the environment(sun, wind, cloud cover) which can cause the cable temperature and thus absolute phase to change significantly. The solution is to measure *differential* phase of two adjacent antennas on the panel. With 5 antennas, 4 distinct differential phases can be computed. This is based on the assumption that all antennas and coax cables 'see' or undergo the same variation with temperature. This assumption is found to be true empirically and we managed to get phase variations down to less than 1 degree over the most adverse field conditions encountered.

Based on the field experiments, we propose for future systems, an architecture that we suggest can minimise the phase sensitivity problem, improve receiver sensitivity and reduce the number of cables between antenna arrays and receivers. It is depicted in Figure 3.9. As cited in [2],

Intelligent antenna systems will require a significant increase in the number of signals that pass between the base station and radiating elements, driving the need for a new interface to replace existing large coaxial cables which frequently exceed one inch in diameter

Here we look at the possibility of reducing the number of cables on the receiver side. The architecture requires frequency synthesizers, mixer and RF amplifier to be mounted near the receiving antennas. This will require the integration of passive antenna elements with active circuitry.

It is envisioned that widespread use of intelligent antenna arrays will eventually force the acceptance of integrated active and passive electronics. It will also require the electronics to be robust to harsh environmental conditions. Rather than deal with the environmental issues, it is also a known fact [2] that many wireless service providers prefer to lose 2-5 dB of sensitivity and RF power output due to losses in the coaxial antenna cables. The simple addition of low-noise preamplifiers

at the tower top can regain the receiver sensitivity loss and permit the use of smaller, lower-cost antenna cables.

In our proposed architecture, the signal from each element of the antenna array is first amplified with a low noise amplifier (LNA) and then mixed with a local oscillator with small offsets in frequency Δf. The second element LO frequency is offset at LO $+\Delta f$ and the N^{th} element LO oscillator at LO $+(N-1)\Delta f$. Δf is assumed wide enough to carry the desired signal bandwidth plus a guardband. The output of the mixers are summed and will contain the signals of the first, second and N^{th} antenna exactly at IF, IF $-\Delta f$ and IF $-(N-1)\Delta f$ respectively. In this way, the signals from the antennas are channelized and sent to the base station via only *one* (long) coaxial cable. At the base station, the signal is amplified by a single high performance high gain linear IF amplifier and provides the correct drive level into one high performance ADC. This architecture eliminates the use of many expensive IF amplifiers and ADCs' but require accurate LOs'. The digitized data output is then fed into N digital down converters and each DDC is tuned to the various channels and the complex baseband signals from the respective antennas are recovered. The data is then sent along the Special Communication Bus for processing via the various modes of operation. By careful allociation of spectrum, the coaxial cable serves a bi-directional function. It not only carries the IF signal from the antennas to the basestation but also DC from the basestation to power the active devices used at the antennas. The basestation also provides the reference signal for the synthesizers. A small portion of the spectrum can be used to send up synthesizer programming data.

In our proposed one-cable architecture, phase calibration is minimised as there is no longer the need to carefully match all cables from antennas to receivers. Note that all field measurements in this Thesis are based on the multi-cable architecture of Figure 3.1.

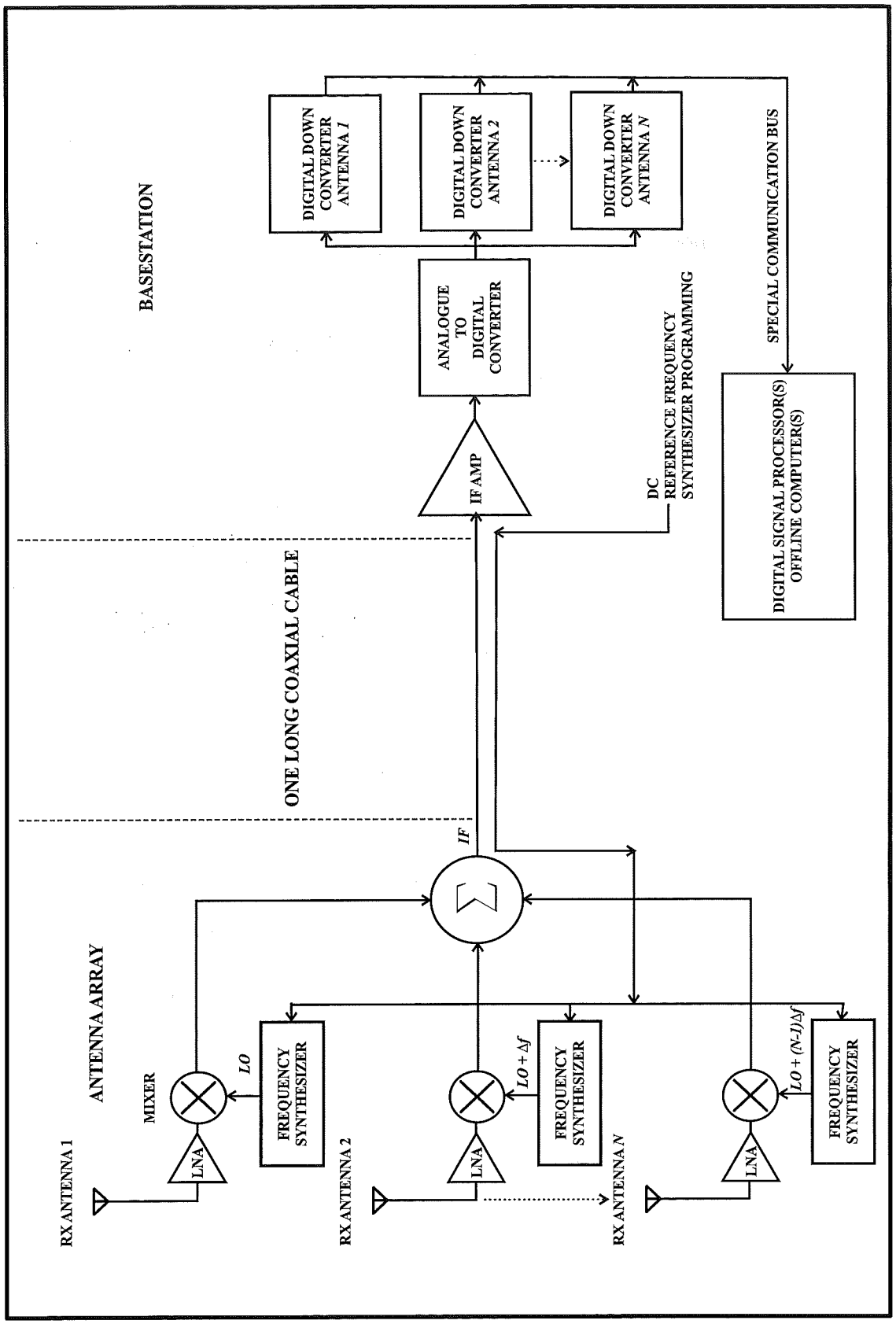

Figure 3.9: One Cable Smart Antenna Array Architecture

3.4.2 Antenna mutual coupling: problem description and compensation

A second observed field problem was the significant phase difference between adjacent antennas in the array as the angle of arrival of the transmitter departed from normal to the line of the array. Theoretically, the phase difference between any two adjacent antennas along a linear array of antennas should be identical for a particular angle of arrival of the transmitted signal. Almost all signal processing papers [77, 131, 132, 12, 116, 117, 9] on linear antennas assume this is so, but a real antenna system departs significantly from this ideal behaviour. This departure is caused by interaction between neighbouring antennas, and is called mutual coupling. The impedance of an antenna is changed by the electromagnetic coupling of neighbouring antennas which change its impedance and therefore amplitude and phase. The degree of mutual coupling is also dependent on the type of antenna element, their placement position on the array and the distance separating them. Antennas at the ends of the array see the least interaction because there are antennas only to the left or right but not both.

The received signal at the kth element of an M-element linear array of antennas as depicted in Figure 3.10 can be written as

$$v_k(\varphi) = c_{kk}E_k f(\varphi) + \sum_{l,k\neq l}^{M} c_{kl}E_l f(\varphi) \qquad k = 1, \cdots, M. \tag{3.5}$$

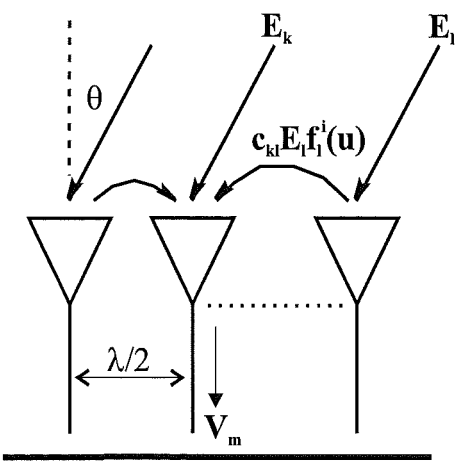

Figure 3.10: Antenna mutual coupling

The incident field E_k at element k impresses an aperture current amplitude $E_k f(\varphi)$ where $f(\varphi)$ is the isolated element pattern and $\varphi = sin(\theta)$ where the angle θ is measured from the normal to the line of the array. This current generates a voltage $c_{kk}E_k f(\varphi)$, where c_{kk} is the coupling from the aperture to the output transmission line. Similarly, neighbouring elements couple into element k through the coupling coefficients c_{kl}. If we let $E_l f(\varphi)$ be the desired, mutual coupling free signal received by a single element at the array aperture, then for our uniformly spaced array of identical elements

$$E_l f(\varphi) = E_0 e^{jl\kappa d\varphi} f(\varphi) = v_l^d(\varphi) \tag{3.6}$$

where κ is the wavenumber, d the spacing between the array elements and E_0 is the amplitude of the incident plane wave from direction θ. Substituting (3.6) into (3.5), we may write a vector of received signals over the array as

$$\begin{bmatrix} v_1(\varphi) \\ \vdots \\ v_M(\varphi) \end{bmatrix} = \begin{bmatrix} c_{mn} \end{bmatrix} \begin{bmatrix} v_1^d(\varphi) \\ \vdots \\ v_M^d(\varphi) \end{bmatrix} \tag{3.7}$$

Or, more compactly

$$\boldsymbol{V} = \boldsymbol{C}\boldsymbol{V^d} \tag{3.8}$$

The effects of mutual coupling can then be compensated by multiplying the received signal by the inverse of the coupling matrix $\boldsymbol{C}^{-1}$ such that

$$\boldsymbol{V^d} = \boldsymbol{C^{-1}}\boldsymbol{V} \tag{3.9}$$

provided that $\boldsymbol{C}$ is full rank. This can be shown to always be true. Moreover, it can be shown that the mutual coupling compensation is *independent* of the direction of arrival of the incoming wave for parallel wire antennas [133, 134]. The antenna used in SASRATS consists of 5 parallel monopoles, and can be compensated using the technique above. As SASRATS is a digital system, compensation using the $\boldsymbol{C}^{-1}$ matrix is an easy DSP process once the coupling coefficients are determined. Compensation is done prior to beamforming and enables subsequent calculations to use ideal element signals essentially free from mutual coupling effects.

The mutual coupling coefficients can be determined in 2 ways - one by Fourier decomposition of the measured array element patterns and another by coupling measurements between the array ports [133]. Although the latter method is adopted, the Fourier decomposition will be described and its disadvantage mentioned for sake of completeness. In the Fourier decomposition method, the complex voltage patterns $g_m(\varphi)$ of the elements in the array are computed using

$$g_m(\varphi) = \frac{v_m(\varphi)}{E_0} = f(\varphi) \sum_n c_{mn} e^{jl\kappa d\varphi} \qquad m = 1, \cdots, M. \tag{3.10}$$

Recognizing that c_{mn} are the Fourier coefficients of these patterns, the coefficients can be numerically determined according to

$$c_{mn} = \frac{1}{2\lambda} \int_{-\lambda/\kappa d}^{\lambda/\kappa d} \frac{g_m(\varphi)}{f(\varphi)} e^{-jl\kappa d\varphi} d\varphi \tag{3.11}$$

To evaluate (3.11), $f(\varphi)$ must not have a null in the integration interval. Another restriction on (3.11) is that the element spacing be larger than $\lambda/2$. Otherwise the integration interval extends beyond visible space, i.e. beyond the interval $-1 < \varphi < 1$ where $g_m(\varphi)$ and $f(\varphi)$ are known. For the case of element spacings $d \leq \lambda/2$, we can still perform a spectral analysis of

$$\frac{g_m(\varphi)}{f(\varphi)} = \sum_n c_{mn} e^{jl\kappa d\varphi} \qquad m = 1, \cdots, M. \tag{3.12}$$

to determine the coefficients c_{mn}, but the convenient orthogonality of the harmonic functions is lost and accuracy becomes a major issue. The Fourier decomposition method is not adopted because SASRAT is intended for flexible testing conditions with the possibility of testing an array of antennas with $d < \lambda/2$. To avoid accuracy issues with antennas separated by $d < \lambda/2$, the mutual impedance coupling measurement method between the elements is adopted for the SASRATS system.

The relationship between the various currents and voltages of the element in an array of M elements are given by the set of equations

$$\begin{array}{lcccccc}
V_1 & = & I_1 Z_{11} + & \cdots & +I_k Z_{1k} + & \cdots & +I_M Z_{1M} \\
\vdots & & \vdots & & \vdots & & \vdots \\
V_k & = & I_k Z_{k1} + & \cdots & +I_k Z_{kk} + & \cdots & +I_M Z_{kM} \\
\vdots & & \vdots & & \vdots & & \vdots \\
V_M & = & I_1 Z_{M1} + & \cdots & +I_k Z_{Mk} + & \cdots & +I_M Z_{MM}
\end{array} \tag{3.13}$$

where Z_{kk} is the self impedance of the kth element when all other elements are open circuited and Z_{kl} represents the mutual impedance between the array elements k and l. The *mutual impedance* Z_{kl} is the ratio of the open circuit voltage produced at the first terminal pair to the current in the second when all other terminals are open circuited, that is

$$Z_{kl} = \left.\frac{V_k}{I_l}\right|_{I_i=0} \qquad \text{for all } i \text{ except } i = k \tag{3.14}$$

and the *active impedance* of an element is the input impedance of that element when all other elements are excited. For example, from (3.13), the active impedance of element 1 is

$$Z_{1,in} = \frac{V_1}{I_1} = Z_{11} + \frac{I_2}{I_1}Z_{12} + \ldots \frac{I_M}{I_1}Z_{1M}. \tag{3.15}$$

For a two element array, it can be shown that

$$Z_{1,in} = \frac{V_1}{I_1} = Z_{11} - \frac{(Z_{12})^2}{Z_{22} + Z_2} \tag{3.16}$$

where the input impedance is expressed in terms of two self-impedances Z_{11} and Z_{22}, the mutual impedance Z_{12} and the load Z_2 at the unexcited terminals of antenna 2.

In general, the mutual impedance between two antennas can be determined by performing three measurements as listed below [135]:

1. With antenna 2 either removed or open circuited, measure Z_{11} at the terminals of antenna 1.

2. Measure Z_{22} the same way as for Z_{11}.

3. Measure $Z_{1,in}$ when antenna 2 is shorted. From (3.16), we can calculate [135]

$$Z_{12} = \sqrt{Z_{22}(Z_{11} - Z_{1,in})} \tag{3.17}$$

Knowing Z_{12}, the active impedance can be calculated from (3.15) and the voltage neccessary to establish the current required for a proper array radiation pattern can be determined. Using the system of equations of (3.13) and the various conditions outlined above, a general impedance coupling matrix $\boldsymbol{C}$ can be created for an array

of M elements as

$$\boldsymbol{C} = \begin{bmatrix} 1+\frac{Z_{11}}{Z_L} & \frac{Z_{12}}{Z_L} & \dots & \frac{Z_{1M}}{Z_L} \\ \frac{Z_{21}}{Z_L} & 1+\frac{Z_{22}}{Z_L} & \dots & \frac{Z_{2M}}{Z_L} \\ \vdots & \vdots & \ddots & \\ \frac{Z_{M1}}{Z_L} & \frac{Z_{M2}}{Z_L} & \dots & 1+\frac{Z_{MM}}{Z_L} \end{bmatrix} \tag{3.18}$$

where Z_L is the 50 Ω input impedance of the SASRAT receivers and the characteristic impedance of the coaxial cables connecting the antennas and the receivers. A 5×5 impedance coupling matrix is needed for the SASRATS 5 element linear array. By extending the method used for two antennas, the self and active impedances were measured and the various mutual coupling impedances computed [135, 136].

Considerable time was spent modelling, characterizing and measuring the antenna mutual coupling effect. The 5 element array was first reduced to 2 elements to simplify analysis, modelling and experimentation. A two element array model based on equations 3.13 to 3.18 was first evaluated. The effect of mutual coupling as the angle of arrival departs from normal was modelled using $Z_{11} = Z_{22} = 50\Omega$ at various values of active impedances ($Z_{1,in} = Z_{2,in} = 30, 40, 50, 60, 70\Omega$). We mounted two SASRATS monopoles on a groundplane spaced $\lambda/2$ apart and measured the self and active impedances. The mutual coupling impedances were computed and we modelled the response of a pair of SASRAT monopoles antennas. The results are seen in Figure 3.11.

An active impedance of 50Ω implies no mutual coupling and therefore a straight line with no deviation from the true angle of arrival. However we see an inverted S-curve for active impedances less than 50Ω. The S-curve is more pronounced at a lower active impedance of 30Ω as the mutual coupling increases. For active impedances greater than 50Ω, we see a double S-curve effect. We can conclude from the Figure 3.11 that with mutual coupling, we can expect a deviation from the true angle of arrival as it departs from normal. From the shape of the curves, we can also predict the extent of mutual coupling and whether the active impedance $Z_{1,in}, Z_{2,in}$ is above or below Z_{11}, Z_{22}. The response from the SASRAT monopoles indicates the presence of mutual coupling . The amount of coupling however is small compared to the other simulated plots and the active impedance is slightly below 50Ω.

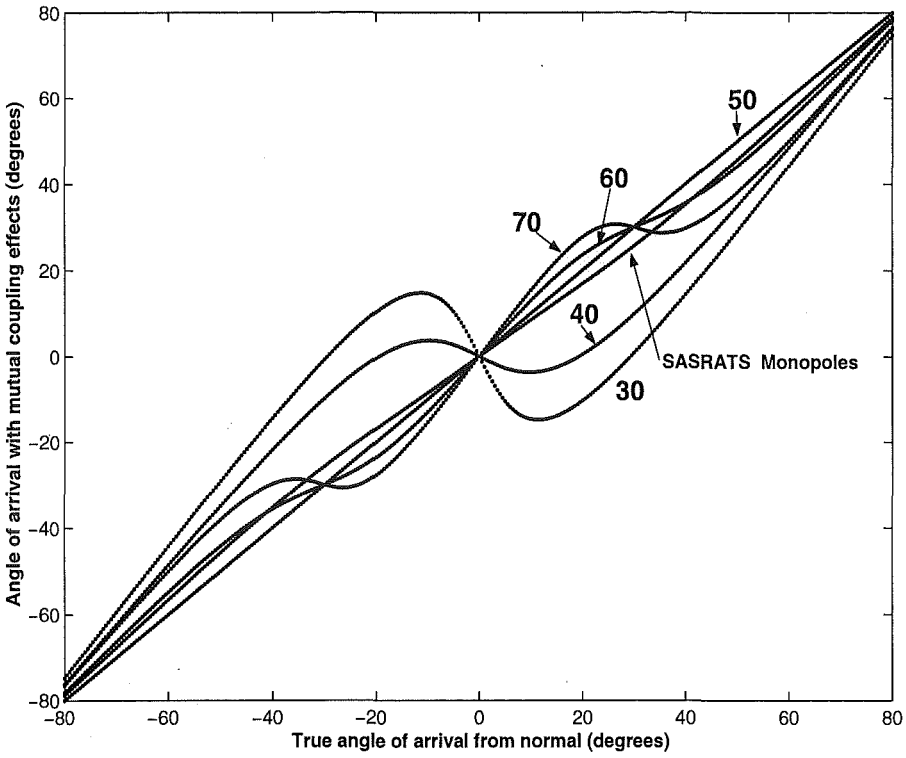

Figure 3.11: Effect of mutual coupling on a 2 Element Linear Antenna Array Model at various active impedances

The modelled response of the SASRATS antennas is compared with actual field measurements. The two monopoles were mounted on a rectangular groundplane and rotated by a heavy duty stepper motor under the control of the SASRATS computer. It receives a signal from a transmitter placed 20 metres away. The plot of the modelled response versus actual field measurements (average of 5 plots) is shown in Figure 3.12.

From Figure 3.12, we can see that the modelled response matches the actual response very well for angles of arrival between -45 and +45 degrees from normal. The model progressively departs from the actual measured response at angles of arrival exceeding ± 45 degrees and is worst at ± 90 degrees. This may be due to scattering effects on the ground plane when it is rotated past ± 45 towards ± 90 degrees respecctively. These effects are not modelled and is beyond the scope of this thesis. We choose to restrict our future measurements to ± 45 degrees knowing that the model based on impedance measurements can accurately predict the measured field response to within ± 1 degree and thus validates the compensation method.

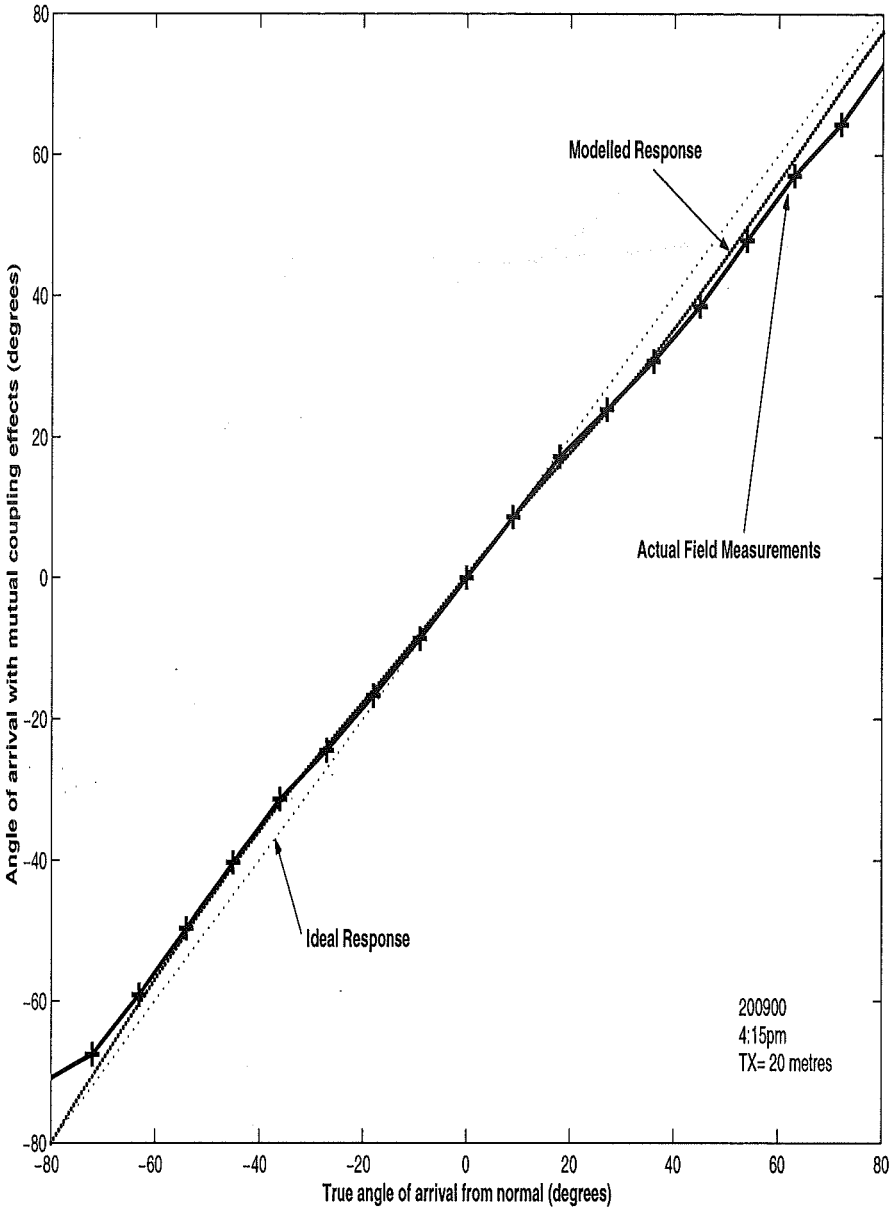

Figure 3.12: Effects of mutual coupling: Plot of modelled versus measured response of a 2 Element SASRATS array

The effect of mutual coupling compensation method on the angle of arrival of a signal on a 2 element SASRATS linear array is shown in Figure 3.13. Without mutual coupling compensation, there is a characteristic inverted S-curve on the error plot as the angle of arrival departs from normal (0 degrees). The error peaks at arrival angles of approximately ± 40 degrees from normal with a maximum error of 9 degrees from the true angle of arrival.

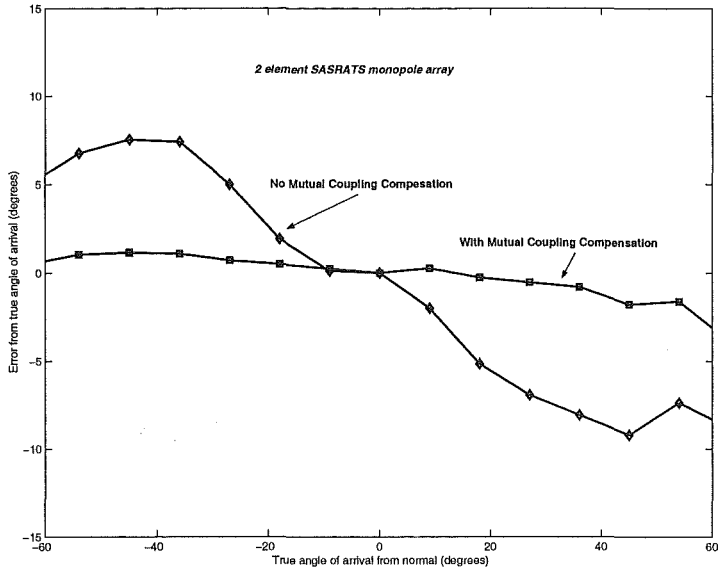

Figure 3.13: Effect of mutual coupling on a 2 Element SASRATS Linear Antenna Array

With compensation, the S-curve flattens out and the error is reduced to less than ± 1 degree throughout the ± 40 degree range from normal. The characterization was extended to 5 antennas. The angle of arrival measurements were carried out on 4 antenna pairs; 1-2, 2-3, 3-4 and 4-5 and compared with the true angle of arrival. This is done in 5 degree steps between -45 and 45 degrees from antenna normal.

Figure 3.14A shows the error between measured and actual angle of arrivals for the four pairs of antenna with no mutual coupling compensation. The error range of the 4 antenna pairs broadens as the angle of arrival departs from normal and can exceed 10 degrees. Figure 3.14B shows a much narrower error spread after mutual coupling compensation is used. This validates the compensation method.

3.4.3 Phase stability over time

A significant field problem is a slow drift in absolute phase measurements over time. This problem was traced to the signal generators which provide the clock and local oscillator signals to the system. Even though the generators are driven from the same reference 10 MHz clock, there is observable phase drift (2 degrees per minute) at startup from cold. The signal generators on the HP8920A RF communication test sets take several hours to stabilize and were left on at all times. This substan-

tially reduced the problem. The temperature compensated oscillator (TCXO) in the HP8920A is specified at 1 part per million (ppm) over a temperature range from 0 to 55 degrees Centigrade. At an operating frequency of 915 MHz, this translate to a possible change of 915 Hz in frequency over the temperature range. Also the frequency stability is specified at ±2 ppm of the final frequency after 30 secs of warm-up time. This translates to ±1830 Hz at an operating frequency of 915 MHz.

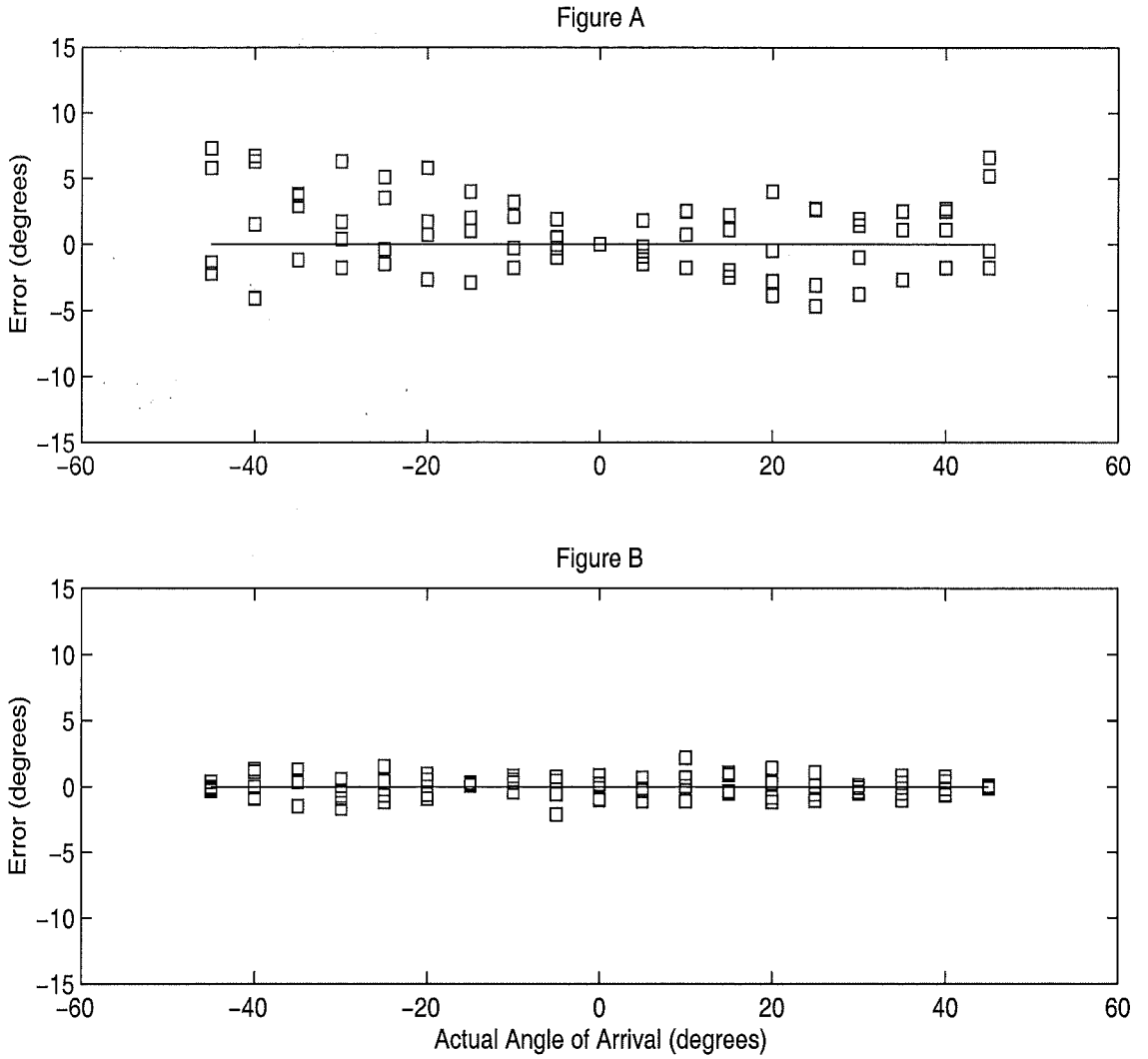

Figure 3.14: Effect of mutual coupling on a 5 Element SASRATS Linear Antenna Array (A) Uncompensated and (B) Compensated

After a 24 hour warmup, the drift in absolute phase is less than 10 degrees per hour. A similar problem at 2.4 GHz reported in [137] was resolved using high stability rubidium oscillators. Although the absolute phase drift is substantial, the differential

phase error performance between two receivers, which is *critical* to beamforming experiments is excellent at better than ±0.3 degree. This shows that the effect of absolute phase drift in the receivers is effectively cancelled when differential measurements are made. All HP8920A signal generators are connected to the same reference 10 Mhz TCXO and any drift in the TCXO stability affects all generators the same way and the drift is effectively cancelled when the difference between phase(frequency)of the receivers is measured. In experiments where the absolute phase measurement is critical, calibration and measurements must be done within a short period of time (< 5 minutes) or a very stable (rubidium) reference source for the oscillators must be used.

Another system problem is a substantial very low frequency (< 1 Hz) sinusiodal variation in *differential* phase error between pairs of receivers over time. Large errors (as much as 8 degrees) are observed if the signal level into the analogue to digital convertor (ADC) is more than 25dB below full scale levels. The solution is to ensure that signal levels into the ADC are centred in the dynamic range of the ADC. This is achieved by adjusting the gain of the intermediate frequency amplifier and/or the transmit power. The frequency of the sinusoidal variation is a function of the signal generator's temperature status. The period of the sinusoid is shorter at start-up, lengthening over time as the signal generators warm up. This is related to the problem of slow drift in phase over time.

3.4.4 Array factor of SASRATS linear array

The array factor of an antenna array represents the far-field radiation pattern of an array of isotropically radiating elements [31]. The normalized array factor for an ideal M element, uniformly excited, equally spaced linear array with no mutual coupling effect is given by [31] as

$$F(\theta) = W_0 + W_1 e^{j\kappa d sin\theta} + W_2 e^{j2\kappa d sin\theta} + \cdots = \sum_{k=0}^{M-1} W_k e^{j2\kappa k d sin\theta} \tag{3.19}$$

where W_k is a complex weight applied to antenna element k, $\kappa = \frac{2\pi}{\lambda}$, λ = wavelength and θ is the angle of arrival of a plane wave with respect to the array *normal*. If

$W_k = A_k e^{jk\gamma}$, the array factor becomes

$$F(\theta) = \sum_{k=0}^{M-1} A_k e^{j2\kappa k d sin\theta + k\gamma} \tag{3.20}$$

and if $\gamma = -\kappa d sin\theta_0$, a maximum response of $F(\theta)$ will result at the angle θ_0. This means that the antenna is steered towards the wave source coming from θ_0.

The theoretical array factor of a 5 element linear antenna array [135] steered towards the boresight ($\theta_0 = 0$) is shown in Figure 3.15. The directivity pattern, i.e. the relative sensitivity of the response to signals from various directions is plotted in this figure in a plane over an angular range of $-\pi$ to π. The pattern is symmetrical about the horizontal line at 0 degrees. The main lobe is thus centered at 0 degrees. Figure 3.16 shows the measured response of the 5 element linear antenna array used in SASRATS after calibration. This figure is a linear plot of the directivity pattern of the SASRATS antenna array (after mutual coupling compensation) between $\theta = -\pi/4$ and $\pi/4$ versus theoretical. Good correlation between measured and theoretical values is achieved.

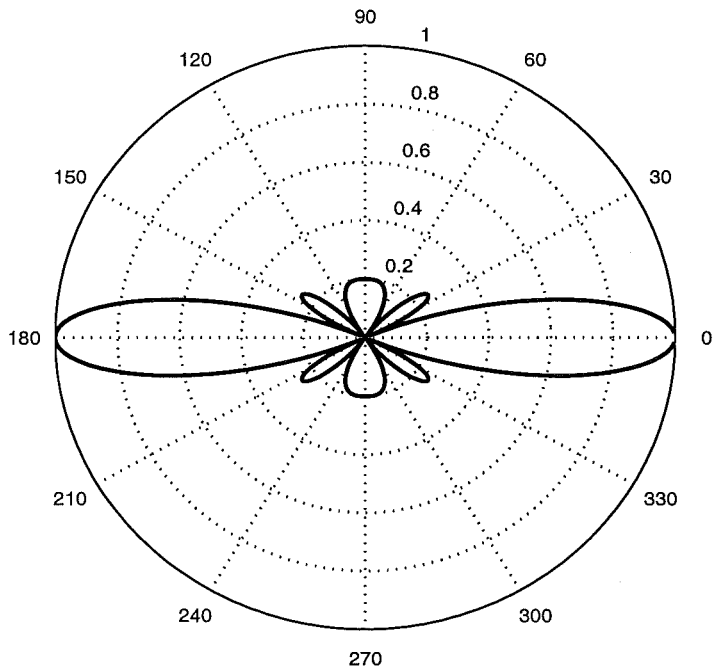

Figure 3.15: Theoretical Polar Response of a 5 Element Linear Array

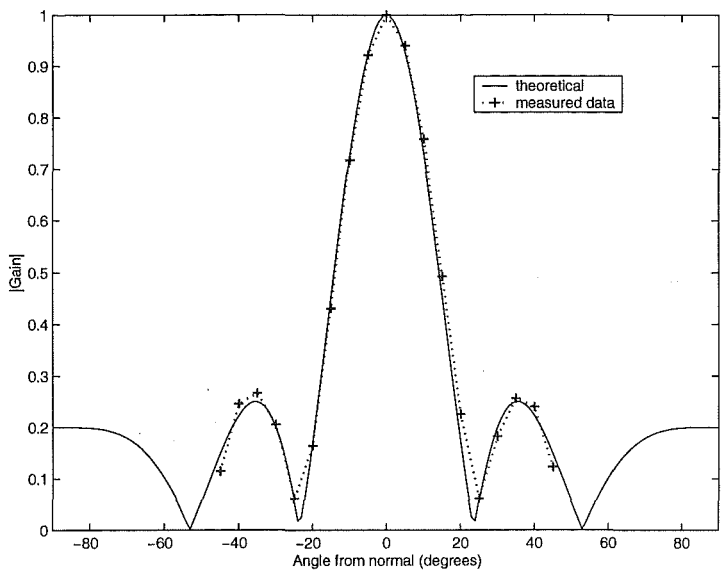

Figure 3.16: Measured versus Theoretical response of the SASRATS 5 Element Linear Array

3.5 Demonstration of adaptive cyclostationary beamforming on SASRATS

This section demostrates an adaptive beamforming algorithm developed in [132] and verified by SASRATS. The method is based on the property of cyclostationary signals to generate spectral lines when they pass through certain nonlinear transformations [138]. The frequencies where spectral lines appear correspond to the fluctuation frequencies of their statistical parameters. These are termed *higher order* periodicities since they do not appear in the signal power spectral density but are revealed after the nonlinearity. The beamforming algorithm is limited to the zero-memory nonlinearity of a signal raised to an integer power $p \geq 2$.

A signal will only generate spectral lines if it has a nonzero p^{th} *order cyclic moment* defined as [132]

$$m_{px}^{\alpha} = \langle x^p(t) e^{-j2\pi\alpha t} \rangle = \lim_{T\to\infty} \frac{1}{T} \int_{-T/2}^{T/2} x^p(t) e^{-j2\pi\alpha t} dt \tag{3.21}$$

where $x(t)$ is the zero-mean complex signal, α is the frequency of the spectral line after passing through the nonlinearity $(.)^p$ and $\langle . \rangle$ denotes a time average operation.

The cyclic moment m_{px}^{α} is the amplitude of the spectral line at frequency α contained in the power spectrum of $x^p(t)$. For a linear modulation, we can write

$$u(t) = \Big(\sum_n g(t - nT)s(k)\Big)e^{j2\pi f_c t} \tag{3.22}$$

where $g(t)$ denotes the continuous-time pulse shape that includes the effects of the transmitting and receiving filters, $s(k)$ denotes the transmitted symbols, T denotes the symbol period and f_c is the carrier frequency. It is shown in [139] that the spectral lines generated by the envelope of $s(t)$ appear at multiples of the symbol rate. They will be centered around the frequency $\alpha = pf_c$ for the $(.)^p$ nonlinearity used. Thus if $p = 2$, the spectral lines are obtained at $\alpha = 2f_c$ and $\alpha = 2f_c \pm kf_s$, $k = 1, 2, ...$ where $f_s = \frac{1}{T}$

The coefficients $\boldsymbol{w}$ of the antenna array are chosen to minimize the cost function

$$J = \langle |e^{j2\pi\alpha t} - y^p(t)|^2 \rangle \tag{3.23}$$

where $y(t) = \boldsymbol{w}^H \boldsymbol{x}(t)$ is the complex-valued output of the array. The values of p and α are chosen according to the order and the frequency of the spectral line generated by the signal to be extracted. Although the cost function is non-convex and may have more than one minimum point, it has been shown in [132] that if the signal of interest (SOI) is the only signal in the environment that generates a spectral line at the reference frequency, the minimization of the cost function J results in the minimization of Gaussian noise power, interferences are cancelled, and ISI is removed by combining the multipath signals. An important condition to remove ISI is that the number of sensors is larger than the length of the ISI [140]. J can be adaptively minimized using the method of steepest descent where

$$\boldsymbol{w}(n+1) = \boldsymbol{w}(n) - \mu \nabla_{\boldsymbol{w}} J(n) \tag{3.24}$$

where μ is the step size and $\nabla_{\boldsymbol{w}} J(n)$ is the complex gradient of J with respect to $\boldsymbol{w}$ at the point $\boldsymbol{w}(n)$. It is shown in [132] that

$$\nabla_{\boldsymbol{w}} J(n) = -p\langle e^*(n) y^{p-1}(n) \boldsymbol{x}(n) \rangle \tag{3.25}$$

where $e(n) = e^{j2\pi\alpha n} - y^p(n)$ is the error signal. The time-averaging process is replaced by its instantaneous estimate and the resultant stochastic gradient-based adaptive

algorithm takes the form

$$\boldsymbol{w}(n+1) = \boldsymbol{w}(n) + \mu e^*(n) y^{p-1} \boldsymbol{x}(n). \tag{3.26}$$

The algorithm is simple and robust compared to the SCORE algorithm of Gardner[23] which requires the use of singular value decompositions. The primary virtue of this beamforming approach is that the optimal extraction of the signal of interest(SOI) requires only the *a priori* knowledge of the frequency α or any one of its harmonics.

3.5.1 Simulation and Field Results

Simulations were carried out prior to field testing to establish the performance of the algorithm. As the SASRATS linear array is a 5-element design, simulations were carried out using 5 elements. The sensors were assumed ideal without mutual coupling effects. The desired signal is BPSK with 100 percent excess bandwidth at a normalised carrier frequency of $f_c = 0.1$. The sampling rate is 5 times faster than the symbol rate of $f_s = \frac{1}{T} = 0.200$. When the signal is squared, three spectral lines appear in the power spectral density: the dominant at $2f_c = 0.2$ and two others at $2f_c \pm f_s$ at -16 dB below the dominant signal. The algorithm parameters were chosen to select the signal at $2f_c$ with $p = 2$ and $\alpha = 0.2$.

Example 1:Simulations were carried out with the SOI arriving at +30 degrees from array normal and an unmodulated carrier at 0 degree. The SINR was set at 0 dB. The output was initially set for an omnidirectional antenna response by setting all weight vector elements to zero except one. The algorithm step size was set to $\mu = 0.0001$. Castedo-Vidal [132] used $\mu = 0.0001$ to simulate their algorithm and the same μ value was thus used to verify their algorithm. In the field, two transmit sources were also set up at +30 and 0 degrees with BPSK and unmodulated carrier respectively at 915 MHz and power levels were adjusted for 0 dB SINR during the calibration process. SASRATS is operated in the pseudo real-time mode and the results after 6000 simulated and measured samples are shown in Figure 3.17.

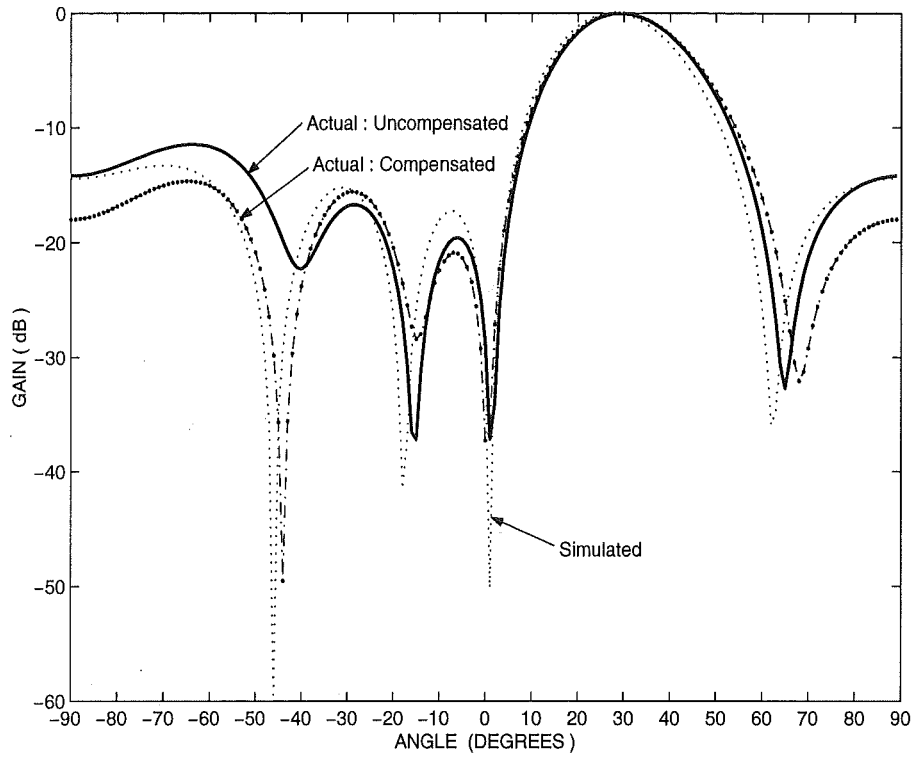

Figure 3.17: Actual versus simulated response of algorithm to SOI at 30 and SNOI at 0 degrees with respect to array normal

There are three plots. The plot labelled 'Actual : Uncompensated' is the plot of the beamformer based on actual field data collected on SASRATS without mutual coupling compensation. The plot labelled 'Actual : Compensated' is the plot of the beamformer based on actual field data collected on SASRATS with mutual coupling compensation. The last plot is the beamformer plot and is based purely on simulation under ideal conditions. It can be seen that all plots show maximum gain to the SOI arriving at +30 degrees and a commom null at 0 degree to remove the interference. The nulls at 0 degree are at about -35 dB for both the compensated and uncompensated case with the best performance from the ideal simulated case at -50 dB. However, the location of the other three nulls do not coincide exactly and spread over a few degrees. This is not critical as the main objective of the beamformer is to cancel the main interference at 0 degrees and maximimize the gain for the SOI coming from +30 degrees. It can be seen that the overall shape of the compensated plot in Figure 3.17 is *closer* to the simulated plot. The reason for showing the compensated and uncompensated plot is to show that mutual coupling compensation

can be ignored for the adaptive algorithm investigated. Without mutual coupling compensation, the algorithm will not match the simulated performance as well as the compensated case but still meets the major performance objectives.

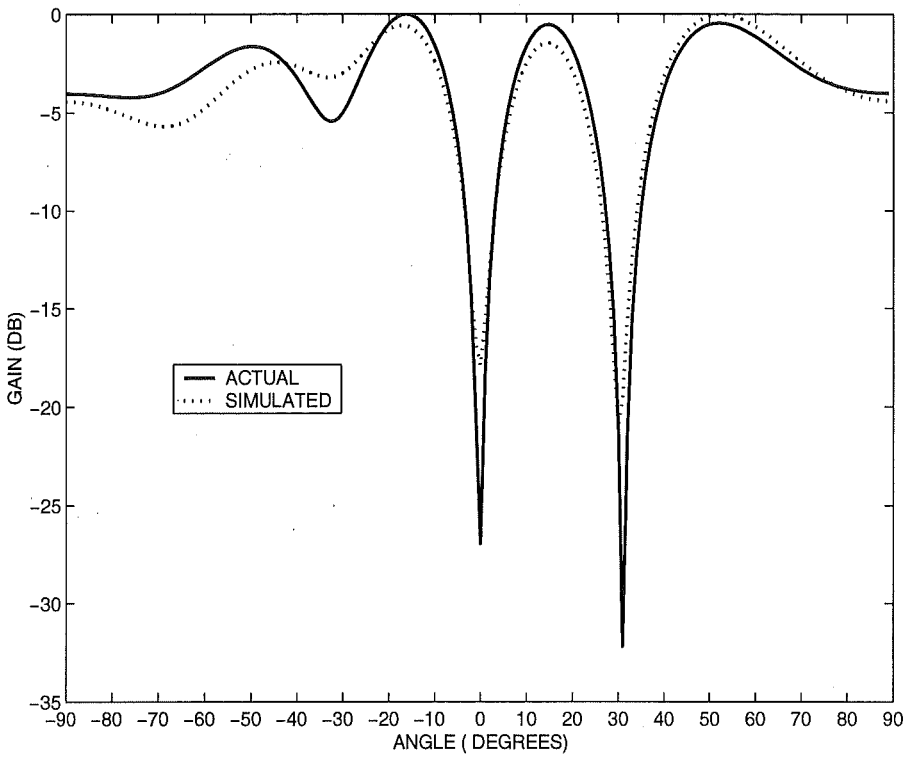

Figure 3.18: Actual versus simulated response of algorithm to 2 SNOI at 30 and 0 degrees

Example 2: The simulation and field measurements are repeated with two unmodulated carriers at 0 and 30 degrees. There is no SOI in this example. Here the algorithm is expected to null out both signals and this is clearly evident in Figure 3.18. The plot labelled 'Actual' represent the measured data after mutual coupling compensation is carried out. There are two distinct nulls at 0 and 30 degrees. The nulling performance of the actual signal is better than the simulated. This is a random occurrence because the noise for the two cases are not exactly the same at any particular iteration of the algorithm. In practice, the depth of the nulls will vary over time.

3.6 Summary

This Chapter has described a wireless test platform called SASRATS, which has been designed and developed to test space and/or time processing and software radio algorithms. SASRATS is fully functional and has been successfully used to demonstrate and verify an adaptive cyclostationary beamforming algorithm. SASRATS will be used in later chapters to test and verify other algorithms.

Chapter 4

Signal Enumeration

4.1 Introduction

Many high resolution parameter estimation algorithms used in modern array processing rely on prior knowledge of the number of incident signals [95, 9]. For example, algorithms for direction-of-arrival (DOA) estimation that use methods based on Eigenstructure [97, 61], Weighted Subspace Fitting (WSF) [98] or Estimation of Signal Parameters via the Rotational Invariance Technique (ESPRIT) [62] critically depend on knowing the number of signals present at the array output. Their performance is dependent on the exact knowledge of this number. This is because the number of "large" (signal) eigenvalues of the array covariance matrix must equal the number of signals in order for the algorithms to produce valid estimates of the desired signal parameters. Correctly determining the number of signal eigenvalues is a formidable task if any of the following occur:

- The signal-to-noise ratio (SNR) is low.
- The number of data records used to approximate the array covariance matrix is small.
- The extent of correlation of the incident signals is high.

Even recent work [10] on diversity antennas for distinguishing cochannel signals by exploiting differences in the channel from each user requires the number of active users to be known. Under estimation of the actual number of signals can

lead to catastrophic failure of the Viterbi algorithm used to estimate the channel in [10] and over estimation can increase the computational complexity of the algorithm exponentially.

In a mobile communication environment, the signals that arrive at the base station antenna consist of a mix of uncorrelated and correlated signals, all subjected to some degree of fading. Correlated signals refer to the multipath scenario, where several replicas of the signal arrive through different paths. The ability to detect and correctly enumerate the incident signals independent of the extent of their correlation in a fading channel environment is crucial *to the proper operation of these algorithms.*

The early signal enumeration method of Bartlett [99, 141] and Lawley [100] used a sequence of hypothesis tests which needed subjective judgement in the selection of threshold levels for different tests. This was replaced by the information-theoretic techniques of Wax-Kailath [102] which are based on either the Akaike information-theoretic criterion (AIC) [103] or the minimum description length (MDL) criterion of Rissanen [104]. These information-theoretic techniques look at the detection problem as a model selection problem and apply information theoretic criteria for model selection.

The matrix decomposition method of Di [117] made it possible for enumeration algorithms to work in a correlated signal environment. The algorithms of Di and others such as Cadzow [142],the smoothed rank profile method of Shan et al. [143] and the modified rank sequence method of Cozzens and Sousa [12] use the decorrelation technique known as spatial smoothing. In contrast to these approaches, Cadzow [131] has developed an algorithm based on a multidimensional search, and Wax and Ziskind [110] have extended the MDL method so that it is now applicable to correlated signals. Recently Shrimpton and Schell [144] have extended the information theoretic criteria to correlated cyclostationary signals. This chapter summarizes the enumeration method based on the AIC, MDL and modified rank sequence methods. These methods are then used with a new stopping criterion to develop a new, modified algorithm that will enumerature all incident signals independent of the extent of their correlation in a fading channel environment. The algorithm also minimizes the required number of antennas with respect to the number of signals and adapts continuously to maintain performance in a mobile environment where users (signals)

come and go. It ensures that the amount of computation is kept to a minimum and in a practical system, switches off or puts on standby; RF, IF and digital circuits which are not needed, thereby allowing the reallocation of DSP workload for other applications. One immediate benefit of minimizing the number of antennas is to reduce the overall power consumption of the system.

The off load DSP can be software reconfigured to process non-critical batch data that was stored for off-line processing. In a large software radio system as envisioned by Mitola [8], the offload DSP's can be used to trial new or enhanced space-time (e.g. beamformer, diversity and equalizer) or decoder algorithms. These enhancements may be prototyped and linked into other processing algorithms, allowing one to debug the algorithm(s), to experiment with parameter settings, and to determine service value(e.g., in improved subscriber density) and resources impact (e.g. on processing resources, I/O bandwidth, and time delays).

The new algorithm is also robust and accurate over a large range of SNR. The AIC and MDL methods tend to overestimate the number of signals when the SNR is high.

The chapter is organized as follows. Section 4.2 reviews the standard narrowband model. Methods for enumerating signals are discussed in Section 4.3. Section 4.3.1 looks at enumeration of uncorrelated signals. Section 4.3.2 looks at enumeration of fully correlated signals. Section 4.4 describes the dynamic signal enumeration algorithm. Section 4.5 covers the simulation results and Section 4.7 summarizes the chapter.

4.2 Problem formulaton

Consider a linear antenna array composed of M elements. Assume that K narrowband sources, centered at a known frequency, ω_0, impinge on the array from directions-of-arrival $\phi_1, \cdots, \phi_K$.

Using complex envelope representation, the $M \times 1$ vector signal received by the array can be expressed as

$$\boldsymbol{x}(t) = \sum_{k=1}^{K} \boldsymbol{a}(\phi_k) s_k(t) + \boldsymbol{n}(t) \tag{4.1}$$

where $\boldsymbol{a}(\phi)$ is the "steering vector" of the array in the direction ϕ,

$$\boldsymbol{a}(\phi) = \left[a_1(\phi)e^{-j\omega_0\tau_1(\phi)}, \cdots, a_M(\phi)e^{-j\omega_0\tau_M(\phi)}\right]^T \tag{4.2}$$

and

- $a_k(\phi)$ is the gain of the k-th element in the direction ϕ,
- $\tau_k(\phi)$ is the propagation delay between the array reference point and the k-th sensor to a wavefront impinging from direction ϕ,
- $s_k(t)$ is the signal of the k-th source as received at the reference point,
- $n_k(t)$ is the additive white Gaussian noise at the k-th element.

In matrix notation, the signal $\boldsymbol{x}(t)$ is an $M \times 1$ complex vector signal given by

$$\boldsymbol{x}(t) = \boldsymbol{A}(\phi^{(K)})\boldsymbol{s}(t) + \boldsymbol{n}(t) \tag{4.3}$$

where $\boldsymbol{A}(\phi^{(K)})$ is an $M \times K$ matrix of steering vectors such that

$$\boldsymbol{A}(\phi^{(K)}) = [\boldsymbol{a}(\phi_1), \boldsymbol{a}(\phi_2), \boldsymbol{a}(\phi_3), \cdots, \boldsymbol{a}(\phi_K)] \tag{4.4}$$

with $\boldsymbol{a}(\phi_k)$ an $M \times 1$ complex vector characterized by unknown angle ϕ_k associated with the k^{th} signal and

$$\boldsymbol{s}(t) = [s_1(t), s_2(t), \cdots, s_K(t)]^T \tag{4.5}$$

is the $K \times 1$ signal vector with $\boldsymbol{s_k}(t)$ being a complex waveform representing the k^{th} signal and $\boldsymbol{n}(t)$ is the $M \times 1$ complex noise vector. Now assume that $K < M$, that the K signals are narrow-band ergodic Gaussian processes with zero mean and that the covariance matrix of $\boldsymbol{s}(t)$ is *positive definite.* $\boldsymbol{n}(t)$ is an stationary Gaussian process with zero mean and covariance matrix $\sigma_n^2\boldsymbol{I}$ where σ_n^2 is an unknown constant and $\boldsymbol{I}$ is the identity matrix. Also assume that the matrix $\boldsymbol{A}$ is a *full* column rank matrix, i.e., the column vectors $\boldsymbol{a}(\phi_K)$, $k = 1, ..., K$ are all *linearly independent.* Then the covariance matrix of $\boldsymbol{x}(t)$ is given by

$$\boldsymbol{R}_x \triangleq E[\boldsymbol{x}(t)\boldsymbol{x}^H(t)] = \boldsymbol{A}\boldsymbol{R}_s\boldsymbol{A}^H + \sigma_n^2\boldsymbol{I} \tag{4.6}$$

where $\boldsymbol{R_s}$ is the covariance matrix of $\boldsymbol{s}(t)$.

The rank of $\boldsymbol{A}\boldsymbol{R}_s\boldsymbol{A}^{\boldsymbol{H}}$ is thus K. Denoting the ordered eigenvalues of $\boldsymbol{R}_{\boldsymbol{x}}$ by $\lambda_1 \geq \lambda_2 \geq \cdots \geq \lambda_M$, it follows that the smallest $M-K$of its eigenvalues must all be equal to σ_n^2, i.e.,

$$\lambda_{K+1} = \lambda_{K+2} = \cdots = \lambda_M = \sigma_n^2 \tag{4.7}$$

The number of signals K can then in principle be determined from the multiplicity of the smallest eigenvalue of $\boldsymbol{R}_{\boldsymbol{x}}$. In practice, the received vector signal $\boldsymbol{x}(\boldsymbol{t})$ is sampled at N discrete times, t_j, $j = 1, ..., N$. $\boldsymbol{R}_{\boldsymbol{x}}$ is then approximated by the sample covariance matrix given by

$$\hat{\boldsymbol{R}}_{\boldsymbol{x}} = 1/N \sum_{j=1}^{N} \boldsymbol{x}(t_j)\boldsymbol{x}(t_j)^H \tag{4.8}$$

The actual value of K and hence the rank of both $\boldsymbol{A}$ and $\boldsymbol{s}$ are unknown, as is the value of σ_n^2. The problem is, given the data $\boldsymbol{x}(t_j)$, $j = 1, ..., N$, determine the number of sources K.

4.3 Enumeration of signals

4.3.1 Enumeration of uncorrelated signals using information theoretic techniques

The information theoretic criteria for model selection introduced by Akaike [103] and Rissanen [104] address the problem of selecting the model that best fits the observed data from a set of N observations $\boldsymbol{X} = \{\boldsymbol{x}(1), \cdots, \boldsymbol{x}(N)\}$, parameter vector $\boldsymbol{\Theta}$ and a family of models, that is, a parameterized family of probability densities $(\boldsymbol{X}|\boldsymbol{\Theta})$.

Using the information-theoretic criteria of Akaike and Rissanen, the best model is the one which either minimizes the AIC defined by

$$C_{AIC} = -2 \log f(\boldsymbol{X}|\hat{\boldsymbol{\Theta}}) + 2k \tag{4.9}$$

or minimizes the MDL criterion defined by

$$C_{MDL} = -\log f(\boldsymbol{X}|\hat{\boldsymbol{\Theta}}) + \frac{1}{2} k \log N \tag{4.10}$$

where $f(\boldsymbol{X}|\hat{\boldsymbol{\Theta}})$ is the conditional probability density function, $\boldsymbol{X}$ is the matrix composed of N observed data vectors, $\hat{\boldsymbol{\Theta}}$ is the maximum likelihood estimate of

the parameter vector Θ, defining the model, and k is the number of free adjusted parameters in Θ. The first term is the well-known log-likelihood of the maximum likelihood estimator of the parameters of the model. The second term is a bias correction term. In equation 4.9, the second term is inserted so as to make the AIC an unbiased estimate of the mean Kulback-Liebler distance between the modelled density $f(\boldsymbol{X}|\Theta)$ and the estimated density $f(\boldsymbol{X}|\hat{\Theta})$. The Kulback Leibler distance [145] is a measure of the inefficiency of assuming that the distribution is $f(\boldsymbol{X}|\hat{\Theta})$ when the true distribution is $f(\boldsymbol{X}|\Theta)$. Rissanen on the other hand, proposed to select the model that minimizes the MDL criterion and apart from a factor of 2, the first term is identical to the corresponding one in the AIC, while the second term has an extra factor of $\frac{1}{2}\log N$. It is shown in [102] that as the sample size increases to infinity, the AIC yields an inconsistent estimate that tends, asymptotically, to overestimate the number of signals while the MDL yields a consistent estimate. The MDL is therefore the preferred choice.

To apply these information theoretic criteria to detect the number of signals, Wax and Kailath assume that the observation vectors $\boldsymbol{x}(1), \cdots, \boldsymbol{x}(N)$ are statistically independent and identically distributed complex Gaussian random vectors of zero mean. Using the results obtained by Anderson [101], Wax and Kailath obtained the maximum likelihood estimates of the parameters in $\boldsymbol{\Theta(k)}$ as

$$\hat{\lambda_i} = l_i, i = 1, \cdots, k \tag{4.11}$$

$$\hat{\sigma_v^2} = \frac{1}{M-k}\sum_{i=k+1}^{M} l_i \tag{4.12}$$

and

$$\hat{\boldsymbol{v_i}} = \boldsymbol{u_i}, i = 1, \cdots, k \tag{4.13}$$

where λ_i and $\boldsymbol{u}_i$ are the ordered eigenvalues and eigenvectors of the sample covariance matrix, $\hat{\boldsymbol{R}}_{\boldsymbol{x}}$ respectively. $\hat{\sigma_v^2}$ is an unknown constant. The number of free parameters in $\boldsymbol{\Theta(k)}$ is obtained by counting the number of degrees of freedom of the space spanned by $\boldsymbol{\Theta(k)}$. It is shown in [102] that as the eigenvalues of a complex covariance are real but the eigenvectors are complex, it follows that $\boldsymbol{\Theta(k)}$ has $k + 1 + 2pk$ parameters. The factor two is due to complex eigenvectors. However, not all of these

parameters are freely adjustable. The normality and the mutual orthogonality of the eigenvectors imposes constraints on the elements of the vectors. This amounts to a reduction of $2k$ degrees of freedom due to the normalization and $2\frac{1}{2}k(k-1)$ degrees of freedom due to mutual orthogonalization. Thus the number of free adjusted parameters is $k(2p-k)+1$. Wax and Kaliath thus reduced the number of degrees of freedom and simplified the AIC and MDL criteria to

$$C_{AIC}(k) = -L_I(\tilde{\Theta}(k)) + 2k(2M-k) \tag{4.14}$$

and

$$C_{MDL} = -L_I(\tilde{\Theta}(k)) + \frac{1}{2}k(2M-k)\log N \tag{4.15}$$

where

$$L_I(\tilde{\Theta}(k)) = \log\left[\frac{\prod_{i=k+1}^{M} l_i^{\frac{1}{M-k}}}{(\frac{1}{M-k}\sum_{i=k+1}^{M} l_i)}\right]^{(M-k)N} \tag{4.16}$$

The estimated number of signals $\hat{K}$ is determined as the value of $k \in \{0, 1, \cdots, M-1\}$ which minimizes the AIC or the MDL functions of Eq.(4.14) and Eq.(4.15).

Simulation

The effectiveness of the AIC/MDL criteria in emumerating source(s) subjected to independent flat Rayleigh fading channel(s) was tested in a simulation using Matlab. A linear array with ten sensors ($M = 10$), equally separated by $\lambda/2$ receives up to 6 source signals. The first source is at an angle of $-20°$ to the array normal and each subsequent source is separated by an angle step of $10°$. The maximum signal-to-noise ratio SNR, defined as the maximum power of each signal to the spatially white Gaussian noise power σ_n^2, is initially set at -5 dB and repeated at levels of $0, 5, 10, 15$ dB for 1,3 and 6 independent Rayleigh faded sources. To simulate a real environment scenario where sources will appear as a mixture of both correlated and uncorrelated signals, a mixed source consisting of 3 independent Rayleigh faded sources and 3 coherent sources was also evaluated. The number of snapshots (N) per trial is 100 and 100 Monte Carlo trials were conducted.

The coherent signals refer to signals of the form $s_k(t) = a_k e^{2\pi j f_k t + \phi_k}$ with $a_k = 1, \phi_k = 0$ and also f_k is set to the same value for all k.

Rayleigh faded signals refer to signals $s_k(t) = \alpha_R(t) a_k e^{2\pi j f_k t + \phi_k}$ with $a_k = 1, \phi_k = 0$ and also f_k set to the same value for all k. Here $\alpha_R(t)$ is a complex variable taken from a look-up table of k independent Rayleigh sources. At the start of the each experiment consisting of 100 trials with 100 runs per trial, k independent sets of Rayleigh faded samples ($k \times 100 \times 100$ samples in total) representing k independent Rayleigh sources are calculated and stored. These samples representing $\alpha_R(t)$ are used in the trials.

Thus all coherent sources have the same power in a given trial with a preset SNR. A Rayleigh faded source is always changing over time and changes at each sample but cannot exceed the preset SNR.

Correlated signals refer to the multipath scenario where several replicas of the signal arrive through different directions. The signal is assumed to be unmodulated and the received multipaths will just be phase shifted versions of the signal with different attenuation characteristics. In simulations using 3 correlated signals, $\chi_k = 0, 0.2, 0.3$, $a_k = 1, 0.9, 0.8$ and $\phi_k = -45, -15, +15$ respectively for $k = 1, 2, 3$.

In this simulation, the performance of the AIC/MDL enumeration algorithm is tested at various SNR and different source types. Table 4.1 shows enumeration performance using 1 ($\phi_1 = -20°$), 3 ($\phi_1 = -20°, \phi_2 = -10°, \phi_3 = 0°$), 6 ($\phi_1 = -20°, \phi_2 = -10°, \phi_3 = 0°, \phi_4 = 10°, \phi_5 = 20°, \phi_6 = 30°$) independent Rayleigh source(s) and the mixed mode consist of 3 coherent sources ($\phi_1 = -20°, \phi_3 = 0°, \phi_5 = 20°$) and 3 independent Rayleigh sources ($\phi_2 = -10°, \phi_4 = 10°, \phi_6 = 30°$).

Note that whenever the signals are uncorrelated with one another, the sample covariance matrix $\boldsymbol{R_s}$ is diagonal and hence, nonsingular . The signals are considered partially correlated whenever $\boldsymbol{R_s}$ is nonsingular but not diagonal. $\boldsymbol{R_s}$ is singular (rank deficient) when the signals are correlated. The signals are coherent whenever the rank of $\boldsymbol{R_s}$ equals one.

The simulation results are summarized in Table 4.1 and show that the AIC/MDL based algorithm works well in enumerating sources subjected to independent flat fading signals. Higher SNR is needed as more signals are present. The method, however, fails when some or all of the sources are correlated. In the above mixed source scenario, the estimated number of signals is 3 instead of 6 indicating that it correctly estimated the 3 independent Rayleigh faded sources but was unable to

detect the other 3 coherent signals. This is because the covariance matrix of $\boldsymbol{s}(t)$ is no longer *positive definite* but becomes *nonnegative definite* for the coherent signals, and therefore, its rank is strictly less than K. The AIC/MDL approach however, remains useful in determining the number of uncorrelated sources in a mixed signal environment. It will be used later to determine the rank of decorrelated matrices.

Table 4.1

Performance of AIC/MDL enumeration algorithm at various SNR and source types

Number of Sources	Probability of correct enumeration over SNR (dB)				
	-5	0	5	10	15
1	0.77	0.93	0.99	1	1
3	0.39	0.90	0.97	0.99	1
6	0.05	0.56	0.94	0.99	0.99
Mixed	0	0	0	0	0

4.3.2 Enumeration of correlated signals

In this section, the generalised matrix decomposition method of [12] will be detailed followed by a new stopping criterion and adaptive selection of antennas. The dynamic signal enumeration algorithm is described in detail and simulation results are presented.

Generalised Matrix Decomposition

The matrix decomposition method of [12] adds reverse conjugate sampling to the original matrix decomposition method of Di [117]. The method is outlined below. From Eq.(4.6), let $\boldsymbol{B}_0$ be the noise free part of $\boldsymbol{R}_x$ defined as

$$\boldsymbol{B}_0 = \boldsymbol{A}\boldsymbol{R}_s\boldsymbol{A}^H = \boldsymbol{R}_x - \sigma_n^2\boldsymbol{I} \tag{4.17}$$

and for $k = 0, 1, 2, \cdots, M - p$ denote $\mathbf{B}_0^{(k)}$ as the $p \times M$ matrix consisting of p successive row vectors of $\mathbf{B}_0 = (b_{i,j})$ starting with the $(k+1)$st,

$$\mathbf{B}_0^{(k)} = \begin{pmatrix} b_{1+k,1} & b_{1+k,2} & \cdots & b_{1+k,M} \\ b_{2+k,1} & b_{2+k,2} & \cdots & b_{2+k,M} \\ \vdots & \vdots & \ddots & \vdots \\ b_{p+k,1} & b_{p+k,2} & \cdots & b_{p+k,M} \end{pmatrix} \tag{4.18}$$

For $n > 0$, let $\boldsymbol{J}_n$ be the $n \times n$ "exchange matrix"

$$\mathbf{J}_n = \begin{pmatrix} 0 & 0 & \ldots & 0 & 1 \\ 0 & 0 & \ldots & 1 & 0 \\ \vdots & \vdots & \ddots & \vdots & \vdots \\ 0 & 1 & \ldots & 0 & 0 \\ 1 & 0 & \ldots & 0 & 0 \end{pmatrix} \tag{4.19}$$

and set $\varepsilon(\boldsymbol{B}_0) = [\boldsymbol{B}_0, \boldsymbol{J}_M \overline{\boldsymbol{B}_0} \boldsymbol{J}_M]$where $[\boldsymbol{B}_0, \boldsymbol{J}_M \overline{\boldsymbol{B}_0} \boldsymbol{J}_M]$denotes the *augmentation* of matrix $\boldsymbol{B}_0$ with matrix $\boldsymbol{J}_M \overline{\boldsymbol{B}_0} \boldsymbol{J}_M$ and $\overline{\boldsymbol{B}_o}$ denotes the element-wise conjugate of $\boldsymbol{B}_o$ and $\boldsymbol{J}_M \overline{\boldsymbol{B}_0} \boldsymbol{J}_M$ is an $M \times M$ matrix. Pre-multiplying $\overline{\boldsymbol{B}_0}$ by $\boldsymbol{J}_M$ creates an intermediate matrix with reversed order of rows of $\overline{\boldsymbol{B}_0}$. Post-multiplying this intermediate matrix by $\boldsymbol{J}_M$ then reverses the order of the columns. Finally, for $2 \leq p \leq M$ and $0 \leq m \leq M - p$, we define the set of $p \times 2M$ matrices

$$\varepsilon(\boldsymbol{B}_0)^{(m)} = [\boldsymbol{B}_0^{(m)}, \boldsymbol{J}_p \overline{\boldsymbol{B}_0}^{(M-p-m)} \boldsymbol{J}_M] \tag{4.20}$$

We then define the $p \times 2(m+1)M$ matrix

$$\boldsymbol{Y}(m, p) = [\varepsilon(\boldsymbol{B}_o)^{(0)}, \varepsilon(\boldsymbol{B}_o)^{(1)}, \ldots, \varepsilon(\boldsymbol{B}_o)^{(m)}] \tag{4.21}$$

The collection of matrices $\boldsymbol{Y}(m, p)$ is called the generalized matrix decomposition of the array covariance matrix $\boldsymbol{B}_o$ (induced by m and p).

To extract useful information , we study the ranks of the matrices $\boldsymbol{Y}(m, p)$ obtained from the matrix decomposition process outlined above. For $2 \leq p \leq M$, there exists a set of rank sequences defined as

$$\{\text{rank } \boldsymbol{Y}(m, p) : 0 \leq m \leq M - p\} \tag{4.22}$$

The rank of the matrices in all such sequences are nondecreasing and bounded above by K [12].

Di's theorem [117] states that there is a value of k denoted $k_0 < m - p$ such that

$$\text{rank } \boldsymbol{Y}(k_0 + j, p) = \text{rank } \boldsymbol{Y}(k_0, p) = K < p \tag{4.23}$$

where

$$j = 1, 2, \cdots, M - p - k_0 \tag{4.24}$$

Then the number of sources is K. Thus, rank $\boldsymbol{Y}(k, p)$ will increase as k increases until rank $\boldsymbol{Y}(k, p) = K$ for some k. Also if:

$$\text{rank } \boldsymbol{Y}(M - p - 1, p) < \text{rank } \boldsymbol{Y}(M - p, p) = p \tag{4.25}$$

then the theorem cannot give the exact answer to the number of signals, but only tells us that the number of signals is not less than p.

If $K < p$, then the rank sequence will strictly increase until it reaches K, and the point at which a rank sequence levels off (two successive terms have the same value) can be used to estimate the number of signals K. The value of p must be carefully chosen. A large value of p may not give the rank sequence enough room to unfold the signal subspace especially when the signals are coherent as the linear relations induced by correlated signals collapse the signal subspace. A small value of p will mean that there will be an increase in the number of terms in the rank sequence before it stabilizes. The consequence will be an increase in computational complexity.

In a real environment, the array covariance matrix which is used in the matrix decomposition and ranking process is not known and one must use the sample covariance matrix of (4.8) instead. Thus, the word "rank" is replaced by "effective rank". The MDL algorithm is used to calculate the effective rank of the decorrelated matrices.

In a realistic situation, the number of signals will vary with time. Users come in and out frequently in a mobile cellular environment and the number of users may increase significantly during peak hours. It is thus desirable to make the operation dynamic to optimize the number of antennas in use with respect to the number of users needing service. This reduces the amount of computation needed especially when the number of antennas is large and fixed.

4.4 The Dynamic Signal Enumeration Algorithm

We develop here a different stopping criterion to enumerate the number of signals present in a fading channel environment and an algorithm which will dynamically adjust the number of antennas needed with respect to the number of signals present.

It was observed during simulation, using a mix of Rayleigh faded and coherent signals, that the rank sequence can weakly stabilize at more than one point (eg. multiple stabilization points). The algorithm of [117], which stops after two successive terms have the same rank value, can result in false estimation of the actual number of signals. The dynamic algorithm of this chapter is based on calculating the effective ranks in $\boldsymbol{Y}(M-p-1,p)$ and $\boldsymbol{Y}(M-p,p)$ and selecting K based on the highest frequency of occurrence, namely, the *mode* of the calculated effective ranks. Table 4.2 shows the probability of correct estimation versus SNR using various statistics to estimate the ranks. The simulation results in Table 4.2 are based on three correlated signals which are coherent signals and the three uncorrelated signals refer to 3 independent Rayleigh faded sources. Both types of signals are defined in subsection 4.3.1 . The angle of arrivals for the 3 correlated sources are $-45°, -15°, 15°$ and the 3 independent Rayleigh sources are $-30°, 0°, 30°$.

The number of snapshots (N) is 100 and 100 trials were conducted. The mode of the effective ranks gave the best performance down to 0dB SNR compared to using the rounded mean or rounded median. The mode of the effective ranks is thus used throughout this chapter.

At initialization, an estimate of the number of uncorrelated sources, $\hat{u}$ is calculated using the MDL algorithm. Then a collection of effective ranks in $\boldsymbol{Y}(M-p-1,p)$ and $\boldsymbol{Y}(M-p,p)$ are calculated for values of $p=\hat{u},\hat{u}+1,...M-1$. Based on the assumption that the total number of signals K consists of a mix of uncorrelated and correlated sources such that $K \geq \hat{u}$, all values of effective ranks less than $\hat{u}$ invalidate the assumption and are removed from the collection. The algorithm then counts the number of valid estimates, L, and also calculates the frequency of occurrence of the estimates. The rank sequence is considered stable only when there exists a unique rank, r', which occurs with the highest frequency in the collection of valid estimates. If the frequencies of occurrence of all estimates are equi-probable,

then no unique rank exists and according to Di's inequality 4.25, there are insufficient rows in $\boldsymbol{B}_0$, and therefore, M must be increased. The algorithm increases M by one and the process repeats using $p = \hat{u}, \hat{u}+1, ...M$. The algorithm will continuously increase M by 1 until the rank stabilizes.

Table 4.2

Probability of correct estimation vs SNR using various statistical modes of 3 uncorrelated and 3 correlated signals impinging from $-45°, -30°, -15°, 0°, 15°$ and $30°$

SNR	Probability of correct enumeration		
	rounded mean	rounded median	mode
0	0.93	0.82	0.95
1	0.95	0.98	0.96
2	0.97	0.94	0.97
5	0.96	0.96	0.98
10	1	1	1
15	1	1	1
20	1	1	1

If stabilization is achieved , then r' is taken as the estimate of K, i.e. the number of signals. The *next* sample covariance matrix is then calculated but this time the effective ranks in $\boldsymbol{Y}(M-p-1,p)$ and $\boldsymbol{Y}(M-p,p)$ are calculated for values of $p = r', r'+1, ..., M-1$. Di's inequality in general states that if $p > K$, then the induced rank sequence will strictly increase until it stabilizes at K, thus the validating the use of $p = r' = \hat{K}$ for subsequent processing.

The number of valid rank estimates, L for p to $M-p$, is compared with a constant, Z, which sets the desired estimation performance of the algorithm as shown in Table 4.3. From Table 4.3, it can be seen that at low SNR, a higher probability of correct estimation of K is obtained using higher values of Z. Z is the basis for the adaptive control criterion which decides whether the number of the antennas to be used in the next cycle is increased, decreased or maintained. The adaptive control criterion states

1. $L < Z$, $M_{next} = M_{current} + 1$

2. $L > Z$, $M_{next} = M_{current} - 1$

3. $L = Z$, $M_{next} = M_{current}$

The algorithm as simulated uses $Z = 6$ to give a higher level of confidence in estimating K at low SNR. This value was chosen as a compromise between enumeration performance and computational complexity.

Table 4.3

Probability of correct estimation vs SNR for various values of Z based on 3 uncorrelated and 3 correlated signals impinging from $-45°$, $-30°$, $-15°$, $0°$, $15°$ and $30°$

SNR	Probability of correct enumeration over Z values		
	Z=6	Z=4	Z=2
0	0.95	0.79	0.81
1	0.96	0.96	0.91
2	0.97	0.96	0.91
5	0.98	0.93	0.94
10	1	1	0.98
15	1	0.98	0.96
20	1	1	1

The first condition of criterion applies when the actual number of signals K increases. When K increases, the induced rank sequence which uses p and M based on the *lower* (previous) estimation of K will have fewer valid estimates therefore reducing the number of valid estimates L. To restore L back to Z, M must be increased.

Conversely when K is reduced, the induced rank sequence based on a *higher* (previous) estimate of K will have more valid estimates thus increasing the value of L. This implies that there are more rows in $\boldsymbol{B}_0$ than is necessary and the second condition applies to reduce M until $L = Z$.

When the number of signals K remains unchanged, the induced rank sequence based on the previous estimate of K stabilizes at the same point and the third condition applies and M is maintained for the next cycle.

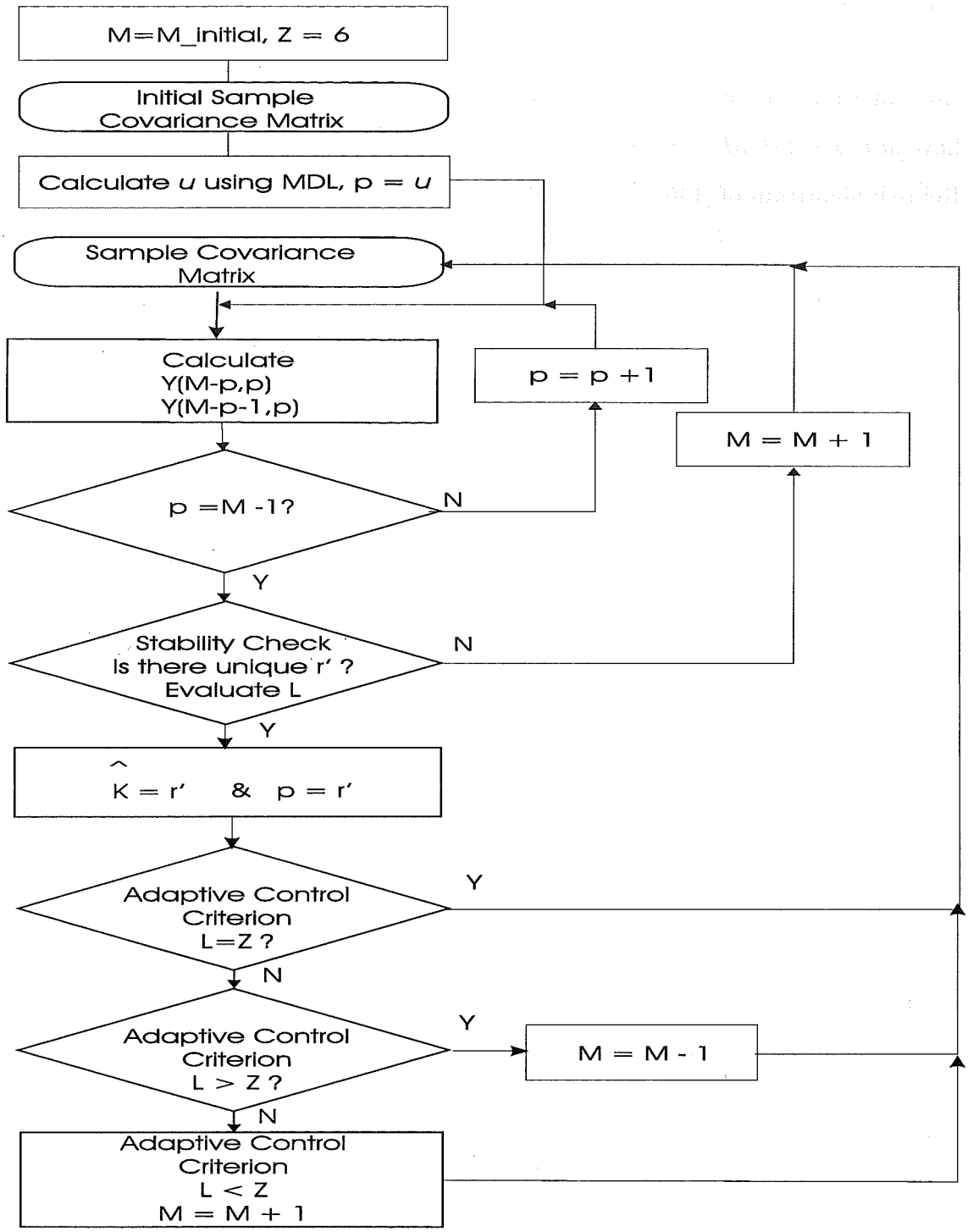

Figure 4.1: Flowchart of the algorithm

Simulation results show that the algorithm tends to maintain a buffer of size $\frac{Z}{2}$ between the number of antennas present for the next cycle and the current estimate of K. Note that it is a necessary condition for M to be greater than K by at least one [44]. The detailed structure of the dynamic signal enumeration algorithm is

depicted in the flowchart of Figure 4.1.

The major drawback of the rank sequence engine is the need to compute the singular values of large matrices. The $\boldsymbol{Y}(M-p-1,p)$ and $\boldsymbol{Y}(M-p,p)$ matrices have size $p \times 2M(M-p)$ and $p \times 2M(M-p+1)$ respectively. Using the Golub-Reinsch algorithm of [146], the singular values of a $m \times n$ matrix can be computed in roughly $2nm^2 - \frac{2}{3}m^3$ flops [12]. This present work however will highlight the computation savings obtained using the dynamic signal algorithm versus the same algorithm using a fixed number of antennas via simulation.

4.5 Simulation Results

Example 1: The dynamic behaviour of the algorithm is simulated using a linear array with the initial number of antennas $M_{initial}$ set to 10. They are equally separated at a distance of $\lambda/2$ and receive 3 independent sources and 3 coherent sources arriving at $-45°, -30°, -15°, 0°, 15°$ and $30°$. The frequencies of the signals are all equal to simulate the arrival of the main and strong reflected signals and also cochannel signals. The number of sources varies at *random* between 3 and 6 but remains in one particular state over 4 trials. The number of snapshots (N) per trial is 100 and 100 trials were conducted. The maximum signal-to-noise ratio SNR is defined as the maximum power of each signal to the spatially white Gaussian noise power σ_n^2. The results are shown in Figure 4.2.

Figure 4.2 contain four plots showing the responses at different SNRs. In each plot, the top trace indicates the number of antenna elements in use, the middle trace shows the actual number of sources and the bottom trace is the error between the estimate and the actual number of sources. The algorithm gives perfect estimation at 10 dB SNR and higher and the number of antennas tracks the number of actual signals impinging on the antennas. At 5 dB SNR, the probability of correct estimation drops to 0.98. In general, a larger number of antennas are used at lower SNR because the algorithm tends to increase the number of antennas to find a stable point in the rank sequence.

The computational complexity of the dynamic algorithm comparing the dynamic versus fixed approach will be described next. Table 4.4 shows the average

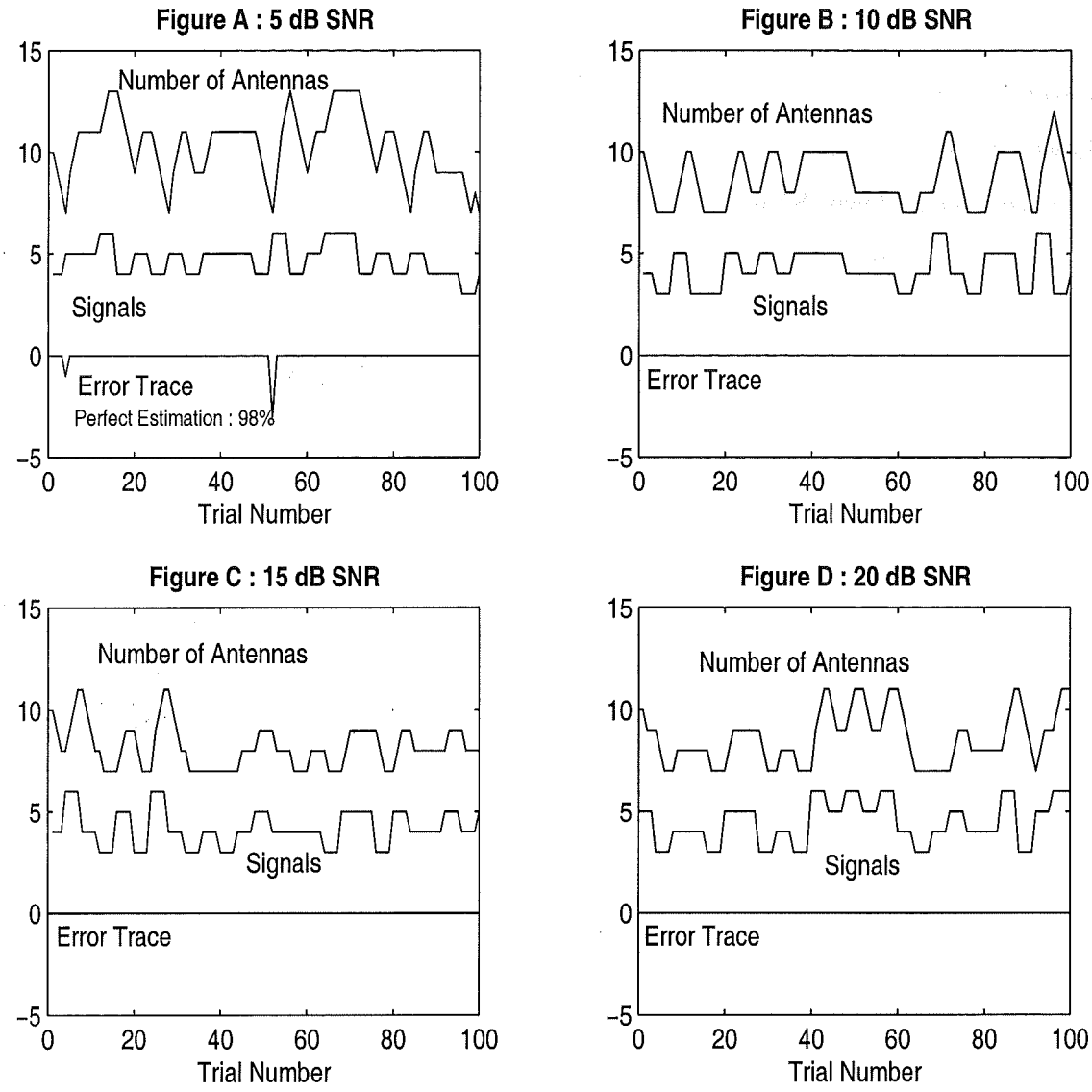

Figure 4.2: Performance of algorithm to random number of signals at various SNRs based on 3 uncorrelated signals and 3 correlated signals impinging from $-45°, -30°, -15°, 0°, 15°$ and $30°$.

computational complexity of the algorithm collected over 100 trials at various SNR values with probability of correct estimation of 1 or otherwise stated in brackets. Complexity is measured in millions of floating-point operations (Mflops) per trial. There are 4 sets of results based on a fixed number of antennas ($M = 8, 10, 12, 14$) and 3 sets based on the dynamic approach using $Z = 2, 4, 6$ per the adaptive control criterion. As expected, the complexity increases substantially when the number of fixed antennas is increased from $M = 8$ to $M = 14$. The complexity is independent of SNR for the fixed antenna case. The dynamic approach on the other hand op-

erates at a much lower complexity with its highest complexity at 5 dB SNR. This happens because more antennas are added to the rank sequence at low SNR to help resolve the uncertainly in establishing a correct estimate of the number of signals. Lower values of Z ensure lower complexity but at the expense of poorer estimation performance at lower SNR. The dynamic algorithm in general works at a *lower* average level of complexity compared to the fixed antenna systems consisting of 10 or more antennas.

Table 4.4

Average complexity of the algorithm vs SNR for fixed and dynamic control of number of antennas based on *random* signals using 3 uncorrelated and 3 correlated signals impinging from $-45°$, $-30°$, $-15°$, $0°$, $15°$ and $30°$.

Mode	Average Complexity (Mflops) over SNR (dB)		
	5	10	20
Fixed $M = 8$	0.96(0.98)	0.96	0.96
Fixed $M = 10$	1.72	1.71	1.73
Fixed $M = 12$	3.09	3.08	3.11
Fixed $M = 14$	5.45	5.44	5.48
Dynamic $Z = 2$	1.32(0.94)	0.92	0.917
Dynamic $Z = 4$	1.41(0.93)	1.15	0.93
Dynamic $Z = 6$	2.132	1.29	1.26

The dynamic complexity of the algorithm responding to a random number of signals is shown in Figure 4.3. There is a trace between the error and the actual signal traces which shows the complexity of the algorithm at each trial. It can be seen that worst case complexity occurs during antenna ramp up and during periods of high antenna usage especially at low SNR as more computations of large matrices are required.

Example 2: The dynamic behaviour of the algorithm with *Rayleigh* fading sources is investigated next. Conditions remain the same as in *Example 1* except that there are 3 independent *Rayleigh* fading sources and 3 coherent sources impinging on the antenna array. The SNR is initially set at 0 dB and the experiment is repeated at 5, 10, 20, 30 and 40 dB. Tables 4.5 and 4.6 show the probability of correct estimation

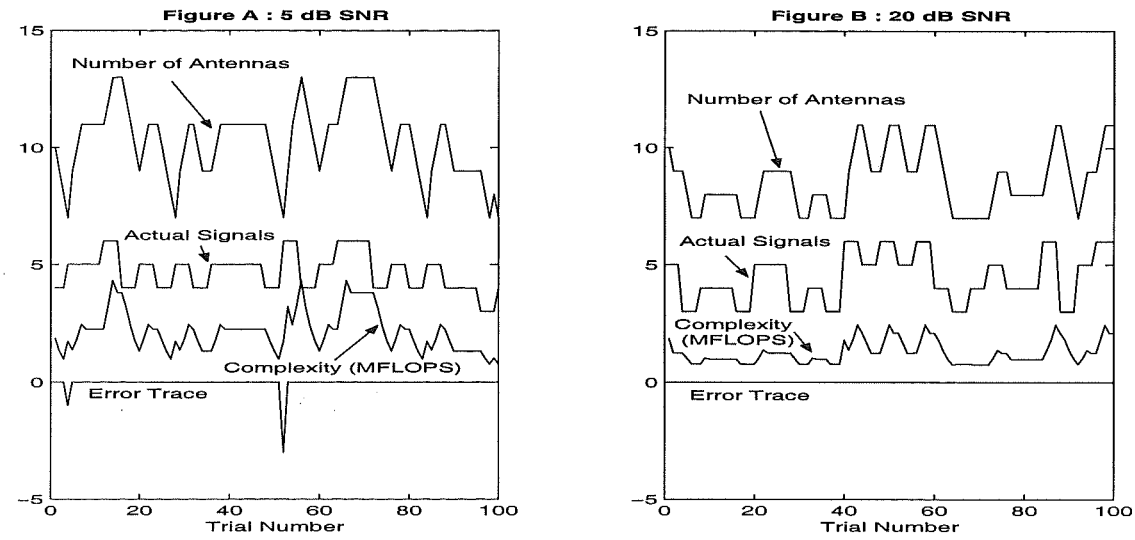

Figure 4.3: Dynamic complexity of algorithm to random number of signals at various SNRs based on 3 uncorrelated signals and 3 correlated signals impinging from $-45°, -30°, -15°, 0°, 15°$ and $30°$.

and the average computational complexity of the algorithm respectively. Figure 4.4 contain four plots showing the responses at 10, 20, 30 and 40 dB SNR.

Table 4.5

Probability of correct estimation vs SNR for fixed and dynamic control of number of antennas based on *random* signals using 3 Rayleigh fading signals and 3 correlated signals impinging from $-45°$, $-30°$, $-15°$, $0°$, $15°$ and $30°$.

Mode	Probability of correct enumeration over SNR (dB)					
	0	5	10	20	30	40
Fixed $M = 8$	0.15	0.66	0.91	0.89	0.98	0.93
Fixed $M = 10$	0.36	0.89	0.97	0.99	0.98	1
Fixed $M = 12$	0.42	0.91	0.97	0.99	1	1
Fixed $M = 14$	0.51	0.88	0.97	1	1	1
Dynamic $Z = 6$	0.49	0.87	0.93	0.97	0.99	1

Table 4.6

Average complexity of the algorithm vs SNR for fixed and dynamic control of number of antennas based on *random* signals using 3 Rayleigh fading signals and 3 correlated signals impinging from $-45°$, $-30°$, $-15°$, $0°$, $15°$ and $30°$.

Mode	Average Complexity (Mflops) over SNR (dB)					
	0	5	10	20	30	40
Fixed $M = 8$	0.46	0.4	0.39	0.38	0.39	0.38
Fixed $M = 10$	1.04	0.94	0.95	0.95	0.94	0.94
Fixed $M = 12$	2.19	2.08	2.05	2.07	2.09	2.05
Fixed $M = 14$	4.3	4.18	4.14	4.16	4.19	4.15
Dynamic $Z = 6$	4.2	1.31	0.71	0.52	0.48	0.49

Table 4.5 shows that the algorithm for both fixed and dynamic modes of operation requires a much higher average SNR in Rayleigh fading conditions compared to *Example 1* to achieve the equivalent level of enumeration performance. This is expected as Rayleigh faded signals can have amplitude variations of as much as 30 dB and the algorithm will not detect a presence of the signal below the receiver noise threshold. At low SNR, there is a higher probability for the Rayleigh signals to dissappear below the noise and thus go undetected. The algorithm will therefore underestimate the number of signals at low SNR as shown in Figure 4.4. The dynamic algorithm has an enumeration performance almost equivalent to a 14 element fixed antenna system but with a significant reduction ($8\times$) in complexity at high SNR.

Example 3: In this experiment, the performance of the algorithm is determined at various angles of separation. Conditions remain as in *Example 1* except that the first source arrives at $-45°$ and the angle of the next and subsequent signals increase in steps of $10°$. The maximum signal-to-noise ratio SNR is fixed at 20 dB. The incoming signals are now closer to each other compared to the $15°$ angle step used in *Example 1*. The experiment is then repeated for an angle step of $5°$. Table 4.7 shows the limitation of the algorithm when the angle of arrival of signals are too close to each other. At 20 db SNR and with $15°$ separation between signals,

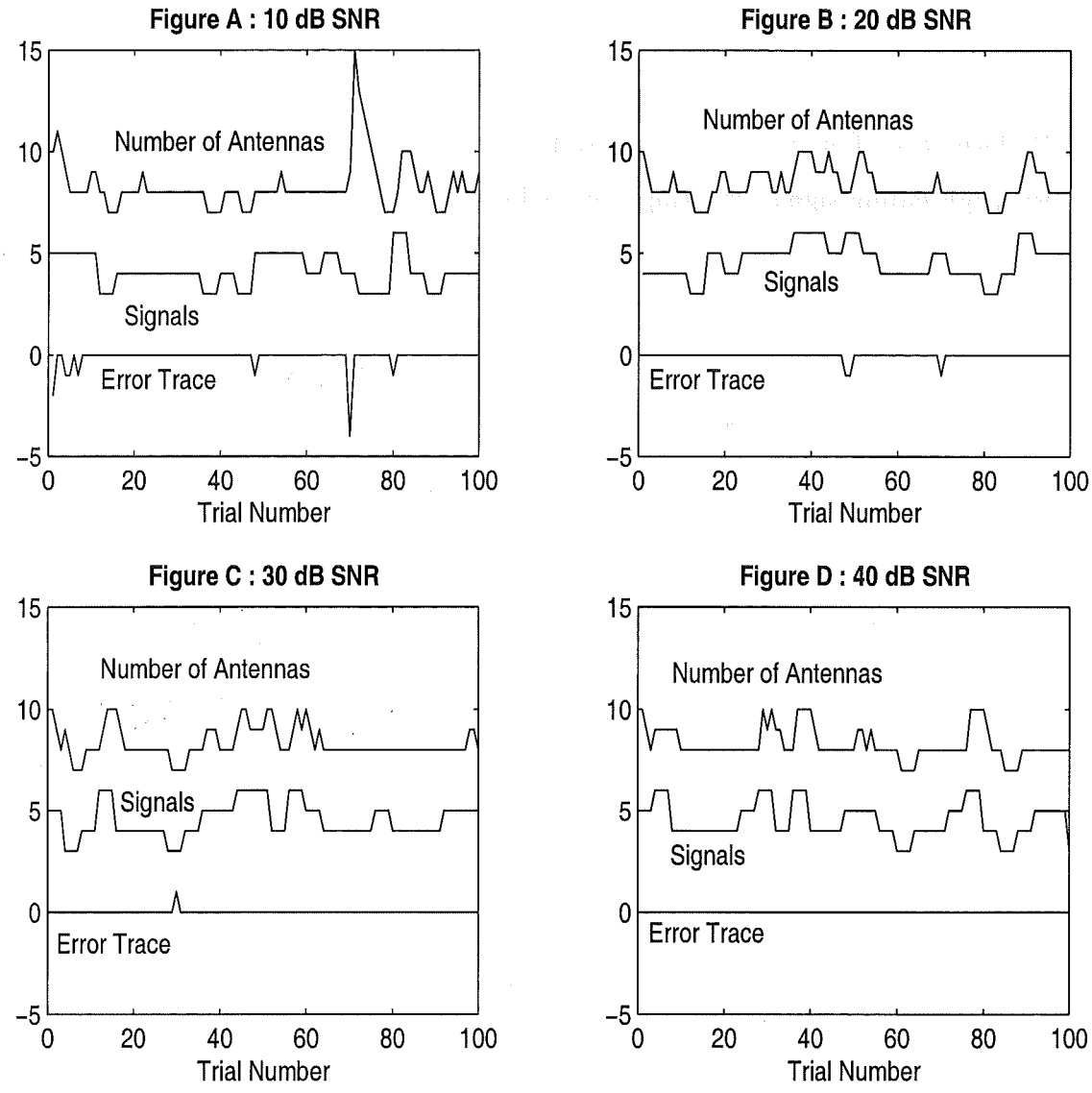

Figure 4.4: Performance of algorithm to random number of signals at various SNRs based on 3 *Rayleigh* fading signals and 3 correlated signals impinging from $-45°, -30°, -15°, 0°, 15°$ and $30°$.

the estimate was 100 percent correct. This degrades to 87 percent and 33 percent when the angle of separation is reduced to $10°$ and $5°$ respectively. The algorithm is unable to resolve the signals and this leads to an under-estimation of the number of sources. It is an indication that the resolution capacity of the antenna array has been exceeded. The term "resolution capacity" is defined by Bresler and Macovski [147] as the maximum number of direction of arrivals (DOA) that may be resolved using a given sensor array. If the covariance matrix of a uniform linear narrow-band array is *positive definite*, the resolution capacity is one less than the number of

sensors [147, 9].

Table 4.7

Performance of enumeration algorithm using 3 uncorrelated and 3 correlated Rayleigh fading signals starting from -45 with different angles of separation. $M_{initial} = 5$

Angle of Separation	Probability of correct enumeration over 100 trials at 20 dB SNR			
	3	4	5	6
15°	0	0	0	100
10°	0	0	13	87
5°	10	45	12	33

Example 4: A comparison between the dynamic signal algorithm and the algorithm of Cozzens and Sousa [12] is made in this example. For comparison purposes, the number of antennas used in the algorithm of Cozzen and Souza and the maximum allowable number of antennas in the dynamic signal algorithm is set to 14. The testing conditions of *Example 2* still apply. Table 4.8 shows that the enumeration performance of the two algorithms is almost identical. The major difference is shown in the complexity table in Table 4.9 where the dynamic algorithm performs better above 5 dB. Above 20dB SNR, the dynamic signal algorithm is about half as complex as the algorithm of [12].

Table 4.8

Comparison between the dynamic signal algorithm and algorithm of Cozzen and Sousa

Mode	Probability of correct enumeration over SNR (dB)					
	0	5	10	20	30	40
Dynamic Algorithm	0.53	0.87	0.96	0.97	0.99	0.99
Cozzen Sousa	0.47	0.89	0.95	0.98	0.99	0.96

Table 4.9

Comparison between the dynamic signal algorithm and algorithm of Cozzen and Sousa

Mode	Average Complexity (Mflops) over SNR (dB)					
	0	5	10	20	30	40
Dynamic Algorithm	4.2	1.03	0.73	0.49	0.49	0.49
Cozzen Sousa	1.269	1.05	0.99	0.98	0.98	0.97

4.6 Field Results

The algorithm was also experimentally verified using SASRATS at 915 MHz. The 5 element antenna array receives 2 *coherent* sources arriving at $-15°$ and $15°$. The number of signals varies at *random* from 0 to 2 users. The number of samples (N) per trial is 100.

To set the SNR in the field, an unmodulated test carrier signal is turned on at the transmitter and the output power is adjusted until the level at the output of the IF test port at the receiver is about 1 dB below the ADC's full scale input power. This is to ensure that the ADC is not overdriven. 4 sets of 8192 I and Q samples are recorded and processed in a Matlab program using SASRAT in pseudo-real time mode. The power spectral density (PSD) is calculated in Matlab by averaging the squared values of 4 Hanning-windowed 4096 point FFT's. To obtain the estimate of the signal power, the largest 16 FFT bins were summed. The estimate of the noise power spectral density (PSD) is obtained by averaging the remaining FFT bins. The power of the carrier signal computed this way is actually the power of the signal *plus* noise. As the estimate of the noise power is known, the SNR can be calculated from the signal + noise-to-noise ratio using the relationship $SNR = 10\log_{10}(10^{(\frac{S+N}{N}-1)})$. The Matlab program running SASRAT in pseudo-real time mode, continuously samples the received signal and computes the SNR. The transmitter power is adjusted until the desired SNR is reached.

The upper trace of Figure 4.5 shows the actual number of transmitted signals.

The middle trace is the number of signals enumerated by the algorithm at the receiver and the lower trace is the error. The enumeration accuracy over 420 trials at 10 db SNR is 99 percent with 1 percent over-estimation. There is no under-estimation. Performance is better than simulated because the sources experience only mild Rayleigh fading in the field experiments.

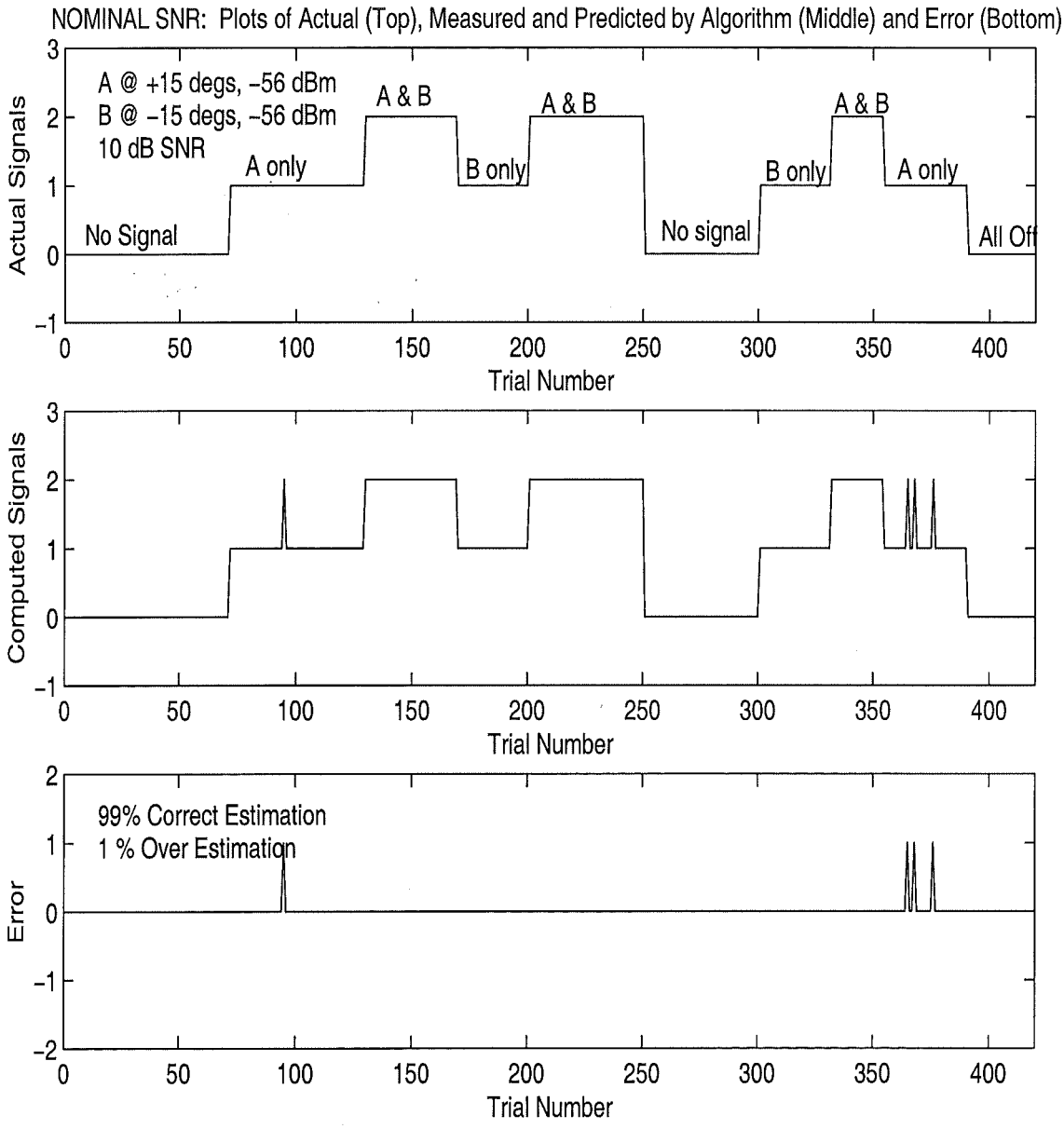

Figure 4.5: Field performance of algorithm using SASRATS at 915 MHz and 10 dB SNR

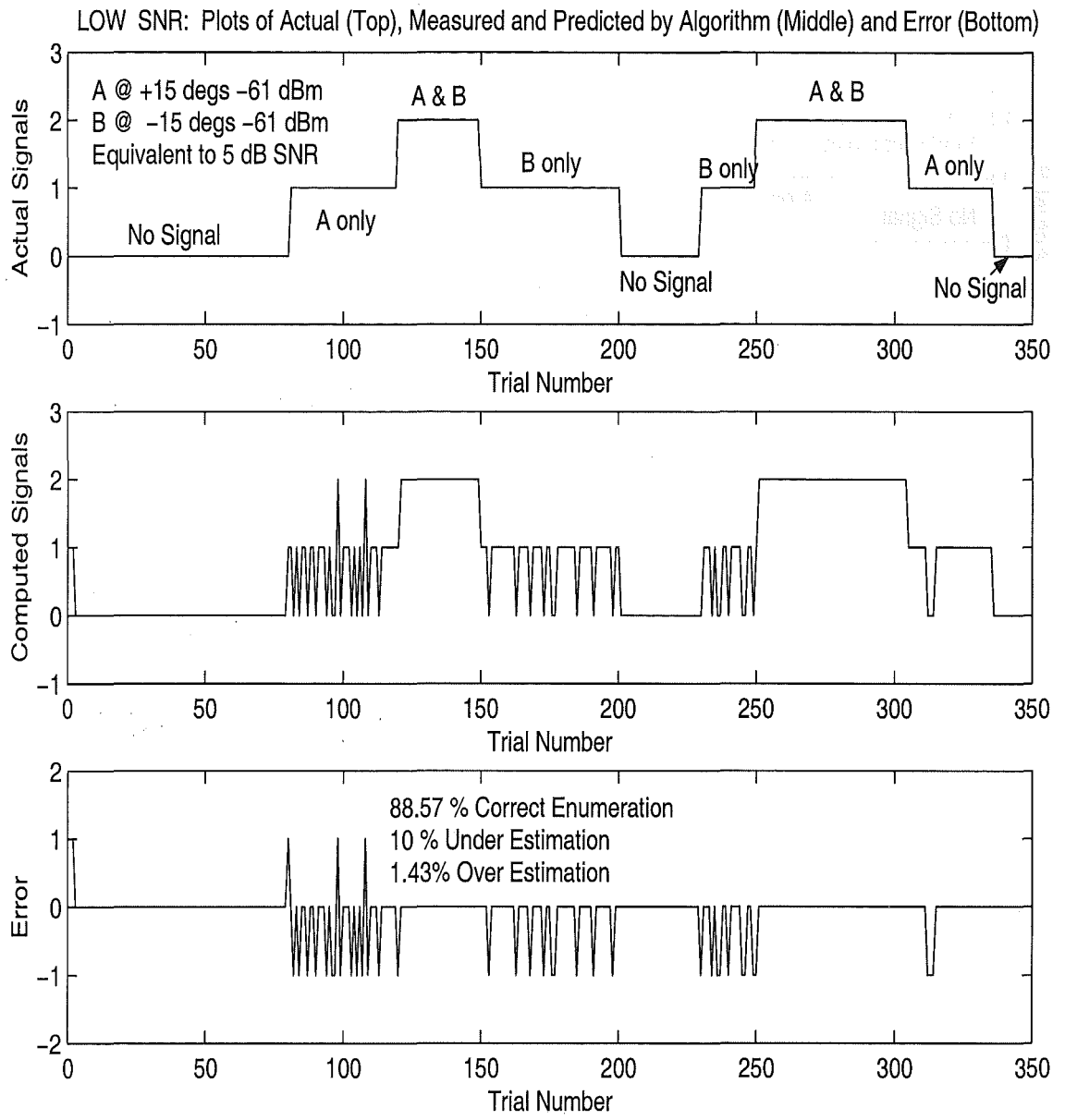

Figure 4.6: Field performance of algorithm using SASRATS at 915 MHz and 5 db SNR

At 5 dB SNR, the performance degrades as expected. This is shown in Figure 4.6. Perfect enumeration occurs at 88.57 percent of the trials with 10 percent under-estimated and 1.43 percent over-estimated. Under similar conditions, simulation predicted perfect enumeration at 86 percent with 14 percent under-estimations. No over-estimations were predicted.

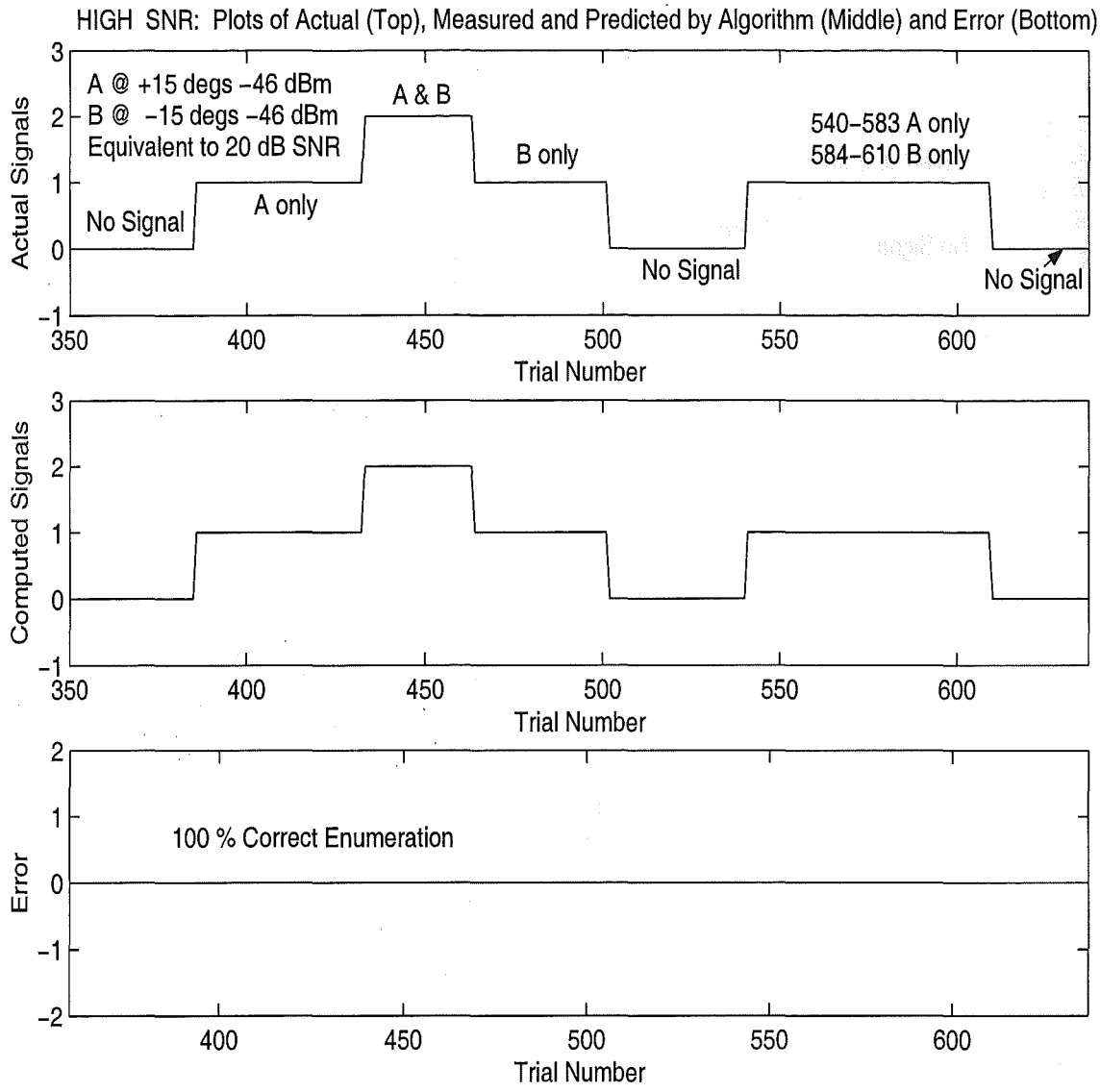

Figure 4.7: Field performance of algorithm using SASRATS at 915 MHz and 20 dB SNR

Best performance is achieved at 20 dB SNR and higher. Figure 4.7 shows perfect enumeration as expected. Field results show that the algorithms works very well with performance close to simulation.

4.7 Summary

The dynamic enumeration algorithm works well in the presence of uncorrelated and correlated signals for signals at above 5 dB SNR per the conditions outlined in *Example 1.* Under Rayleigh fading channel conditions, the algorithm works well

above 10 dB SNR. Compared with the algorithm of [12], the dynamic enumeration algorithm is significantly less complex above 20dB SNR. The dynamic nature of the algorithm ensures that the number of antennas needed is minimized for the number of signals present and will adjust appropriately when additional signals arrive or depart as will happen in a real mobile environment. It ensures that the amount of computation is kept to a minimum and in a practical system, switches off or puts on standby RF, IF and digital circuits which are not needed and allows the reallocation of DSP workload for other applications.

The algorithm has also been verified in field experiments using SASRATS. Limited by mild Rayleigh fading conditions in the field, the field performance was slightly better than simulated performance.

When the resolution capacity of the antenna array is exceeded, the algorithm underestimates the number of signals present. To correctly enumerate closely spaced signals, a different approach will be needed and is outside the scope of this Thesis.

Chapter 5

Channel Order Estimation

5.1 Introduction

The transmission of high data rate signals through a dispersive communication channel will usually introduce intersymbol interference (ISI) to the received signal due to the required bandwidth. Equalization is used to compensate for the ISI due to the channel so as to obtain more reliable estimates of the transmitted symbols. Training sequences known at the receiver are periodically sent in the transmitted data stream to aid the equalizer to adaptively adjust the equalizer coefficients to negate the effects of the channel. The drawback of this approach is that the effective data rate is reduced as training symbols cannot be used for information symbols. This drawback can be reduced or avoided by using blind channel estimation methods which do not rely on training symbols but on unique statistical properties of the transmitted signal.

Blind channel estimation methods work using one of three general techiniques [121]: the application of a stochastic gradient technique to minimize a specified error performance function; the use of higher order statistics (HOS); the use of second order cyclostationary properties of the received signal. A common assumption in many of these blind channel identification methods [118] is that the order of the true channel is known. In practice the channel order must be estimated. Often this is done by applying a rank detection procedure to the received signal covariance matrix. The use of information theoretic criteria, eg Akaike information-theoretic criterion (AIC) or minimum description length (MDL) has become the standard first

step of the many of the methods that address the blind channel estimation problem.

The AIC or MDL criteria is based on the assumption that successive data samples are i.i.d (independent, identically distributed) zero mean Gaussian random samples. Also the noise is assumed white Gaussian and uncorrelated with the signal. However, in blind channel identification, the successive data samples are *not* statistically independent because the data covariance matrix is built from autocovariance coefficients calculated from the expectation of the product of the data samples with time shifted versions of itself[118]. Hence, in the context of blind channel identification, the assumptions on which the information theoretic criteria are based do not hold true. It is also found in this work and also that by Liavas *et al.*[118] that the information theoretic criteria based algorithms are sensitive to variations in SNR and are not robust enough for realistic applications. To overcome the shortcomings of the information theoretic criteria, we propose a different approach based on forward linear prediction methods. The proposed algorithm estimates the channel order using the linear prediction filter approach first investigated by Slock[124] and later by Karim *et al.*[123]. The algorithm exploits the fact that the linear prediction approach to channel estimation is robust to the over-determination of the channel order. The proposed channel order estimation algorithm developed here is robust over a wide SNR range and is independent of correlation in the received channels.

5.2 Signal Model

This section describes the signal model of a single user with a single transmit antenna to a base station which uses multiple antennas. It is also known as a single input multiple output (SIMO) system. Let us consider an M-element array. The received noiseless complex baseband signal received at the ith antenna can be written as

$$x_i(t) = \sum_{k=-\infty}^{\infty} h_i(t - kT)s(k) \tag{5.1}$$

where $h_i(t)$ represents the composite baseband impulse response of the channel for the user's transmitter to the output of the the ith sensor, $s(k)$ denotes the transmitted symbols and T denote the baud (or symbol) period. The transmitted symbol sequence $\{s(k)\}$, is assumed to be a zero-mean, unit-variance process. The com-

posite impulse response includes the transmit pulse shaping filter, the propagation channel and the receiving filters. This impulse response $h_i(t)$ has a finite effective duration called the channel length. We assume that the channel remains *constant* over the time interval during which we collect data, and therefore, we treat $h_i(t)$ as time invariant. If $h_i(t)$ is sampled at the symbol rate, we get $h_i(n) = h_i(t)|_{t=t_0+nT}$ where t_0 is the initial sampling instant. The symbol-rate sampled received signal at the output of the ith antenna element can then be expressed as

$$x_i(k) = \sum_{n=0}^{N-1} h_i(n)s(k-n), \qquad i = 1, \ldots, M. \tag{5.2}$$

where we have assumed that the impulse response corresponding to each antenna spans N symbol periods (corresponding to a channel length of NT). If we define the array output as $\boldsymbol{x}(k) = [x_1(k) \ldots x_M(k)]^T$, we can be rewrite (5.2) as

$$\boldsymbol{x}(k) = \sum_{n=0}^{N-1} \boldsymbol{h}(n)s(k-n), \tag{5.3}$$

where $\boldsymbol{h}(n) = \boldsymbol{h}(t)|_{t=t_0+nT}$. If H is defined as

$$H = [\boldsymbol{h}(0) \ldots \boldsymbol{h}(N-1)], \tag{5.4}$$

(an $M \times N$ channel matrix), then (5.3) can be rewritten as

$$\boldsymbol{x}(k) = H\boldsymbol{s}(k), \tag{5.5}$$

where

$$\boldsymbol{s}(k) = \begin{bmatrix} s(k) \\ \vdots \\ s(k-N+1) \end{bmatrix} \tag{5.6}$$

In practice, noise is always present at the antennas' inputs and we can incorporate noise into (5.5) as

$$\boldsymbol{x}(k) = H\boldsymbol{s}(k) + \boldsymbol{n}(k), \tag{5.7}$$

where $\boldsymbol{n}(k)$ is a zero-mean process, uncorrelated with the transmitted symbols and antenna elements.

If $h_i(t)$ is sampled at a rate greater than the symbol rate, then the signal model can be easily modified to incorporate this oversampling. If we let $T_s = T/P$

be the fractional sampling interval and P is an integer, we can define the pth phase, $p = 1, 2, \ldots, P$, of the fractionally space channel response corresponding to the ith antenna as

$$\boldsymbol{h}_p(n) = \boldsymbol{h}_t|_{t=t_0+nT+\frac{p-1}{P}T}. \tag{5.8}$$

The new vector channel impulse response now becomes a matrix of size $MP \times 1$ and is redefined as

$$\boldsymbol{h}(n) = \begin{bmatrix} \boldsymbol{h}_1(n) \\ \vdots \\ \boldsymbol{h}_P(n) \end{bmatrix}. \tag{5.9}$$

The pth phase of the vector received signal $\boldsymbol{x}_p(k)$ assuming that the impulse response of each phase spans N symbol periods is redefined as

$$\boldsymbol{x}_p(n) = \sum_{n=0}^{N-1} \boldsymbol{h}_p(n)s(k-n), \tag{5.10}$$

H is now a $MP \times N$ matrix with the number of subchannels as MP and each channel length as N. H obeys the definition (5.4) with $\boldsymbol{h}$ given in (5.9). The channel model remains unchanged as

$$\boldsymbol{x}(k) = H\boldsymbol{s}(k), \tag{5.11}$$

with $\boldsymbol{x}(k) = [\boldsymbol{x}_1^T(k) \ldots \boldsymbol{x}_P^T(k)]^T$.

It can be shown[148] that $x(t)$ defined in (5.1) is cyclostationary if the channel $h_i(t)$ is time invariant over the symbol duration. By sampling at the symbol rate $\frac{1}{T}$, the discrete sequence $\{x_i\}$ is wide-sense stationary[149, 150]. If the sequence is oversampled at a rate higher than 1/T (temporal oversampling) or at 1/T but using multiple antenna elements (spatial oversampling), the discrete sequence is cyclostationary. The cyclostationary signal consists of a number of *phases*, each of which is stationary. A phase corresponds to a shift in the sampling point in temporal oversampling and different antenna element in spatial oversampling. This information can be exploited to identify the channel. As we wish to estimate the channel, what conditions must the received signal statistics have to provide blind channel identification?

If we let $H(z) = \sum_{i=1}^{mP} z^{-i} H(z^{mP})$ represent the z-transform of the interleaved channel response, a condition for blind channel identification derived by Tong *et al.* [151, 152] is that the polynomials of $H(z), i = 1, \cdots, mP - 1$ corresponding to the different rows of H must have *no* common roots. However, if the oversampling factor P is too large, the components of the filter $H(z)$ may be almost identical. Hence, they may posses approximately common roots, leading possibly to poor performance of second-order schemes. In order to overcome this drawback, it is possible to use spatial oversampling (multiple antennas) to take benefit of the spatial diversity of the channels [123].

The linear prediction (LP) method to identify $H(z)$ is first investigated by Slock in [124] in the case where M is known and the degree N of $H(z)$ is known. The work of [123] generalised the results of Slock. It shows that the linear prediction approach to channel estimation is robust to an overdetermination of the order N. Their work relies on the MDL algorithm to first estimate the order of N. Their work also focussed on temporal oversampling of the channel and using the cyclostationary properties of the received signal to identify $H(z)$. The present work exploits the duality between temporal and spatial oversampling, and uses the LP method in the spatial context.

The objective is to find a robust channel order and channel estimator that will work at any antenna spacing. In practice, when the antennas are close together , there is a high degree of correlation between the received signals and the LP method of [123] applied in the spatial context fails. The LP method of [123] fails because the MDL algorithm as discussed in Chapter 4 underestimates the order N when there is a high degree of correlation between the received signals. The MDL algorithm also severely overestimates under high SNR conditions.

This work presents an algorithm based on the LP method to estimate the channel order. The algorithm compares the estimated channel coefficients with a set threshold under the assumption that the coefficients in the channel estimates are significant (eg have significant power over the noise power). The iterative algorithm works on the LP method by increasing the channel order until the coefficients of the channel estimates fall below the threshold. We also assume that all channels have the same channel order. The next sections will describe the theory and algorithm

in detail.

5.3 Linear Prediction Method

This section covers the basic concept of the linear prediction method for blind channel identification. In linear prediction, we try to estimate the sample $x(n)$ based on the previous samples of x at times $x(n-1), x(n-2), \ldots, x(n-N)$. This is also referred to as *forward* linear prediction.

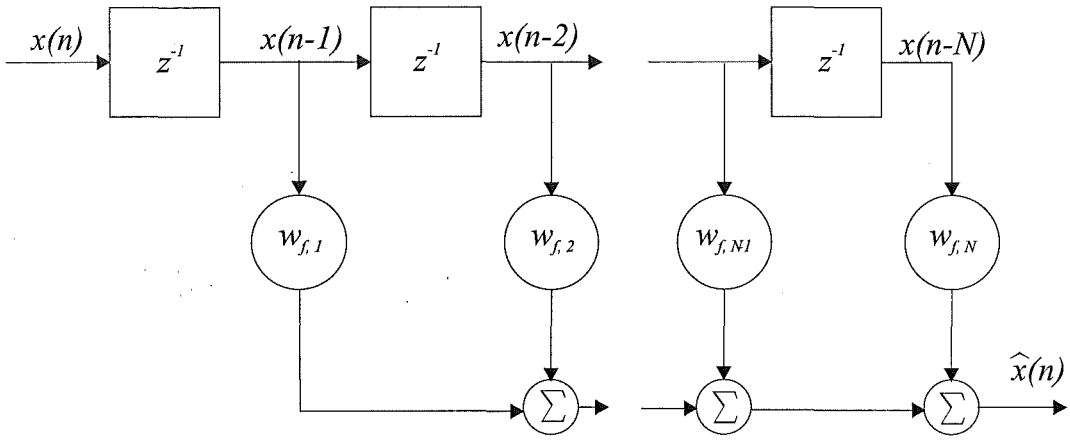

Figure A

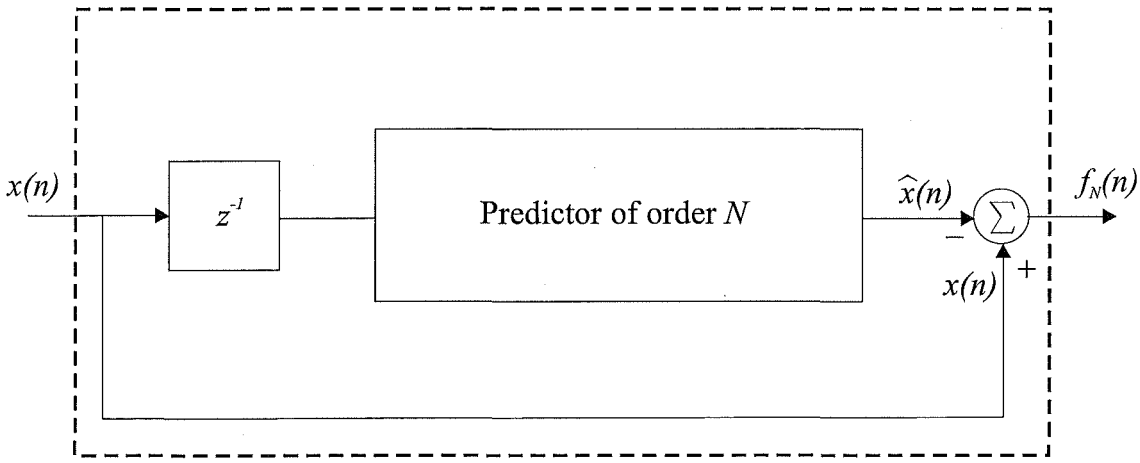

Figure B

Figure 5.1: (Figure A) Forward predictor; (Figure B) Block diagram of forward prediction error filter

A forward predictor consisting of a linear transversal filter is shown in Figure 5.1A. We assume that the tap weights are optimized in the mean-square sense in

accordance with the Wiener filter theory [43]. In this situation the desired response is $x(n)$ and the *forward prediction error* $f_N(n)$ as depicted in Figure 5.1B, is the difference between $x(n)$ and $\hat{x}(n)$. N signifies the order of the predictor defined as the number of unit-delay elements needed to store the given set of samples used to make the prediction. To solve the Wiener-Hoft equations for the $N \times 1$ tap weight vector defined as

$$\boldsymbol{w}_f = [w_{f,1}, w_{f,2}, \ldots, w_{f,N}]^T, \tag{5.12}$$

the $N \times N$ correlation matrix of the tap inputs $x(n-1), x(n-2), \ldots, x(n-N)$ and the $N \times 1$ cross-correlation vector between these tap inputs and the desired response $x(n)$ must first be evaluated. If $\boldsymbol{x}(n-1) = [x(n-1), x(n-2), \ldots, x(n-N)]^T$ then the correlation matrix is given by

$$\boldsymbol{R} = E[\boldsymbol{x}(n-1)\boldsymbol{x}^H(n-1)] \tag{5.13}$$

$$\boldsymbol{R} = \begin{bmatrix} r(0) & r(1) & \ldots & r(N) \\ r(1)^T & r(0) & \ldots & r(N-1) \\ \vdots & \vdots & \ddots & \vdots \\ r(N-1)^T & \ldots & r(0) & r(1) \\ r(N)^T & \ldots & r(1)^T & r(0) \end{bmatrix} \tag{5.14}$$

and the cross-correlation vector equals

$$\boldsymbol{r} = E[\boldsymbol{x}(n-1)\boldsymbol{x}^*(n)] \tag{5.15}$$

$$= \begin{bmatrix} r^*(1) \\ r^*(2) \\ \vdots \\ r^*(N-1) \\ r^*(N) \end{bmatrix} \tag{5.16}$$

In compact matrix form, we can write

$$\boldsymbol{R}\boldsymbol{w}_f = \boldsymbol{r} \tag{5.17}$$

To evaluate the minimum mean-squared prediction error or the forward prediction error power given by

$$P_M = E[|f_N(n)|^2], \tag{5.18}$$

the variance of $x(n)$ must be known. The variance of $x(n)$ equals $r(0)$, since $x(n)$ has zero mean.

It it shown in [43] that the Wiener-Hopf equation(5.17) for linear prediction and the Yule-Walker equations for an autoregressive (AR) model are of exactly the same mathematical form. The average power (i.e., variance) of the forward prediction error is also of the same mathematical form as the variance of the white-noise process used to excite an AR model. If the model order N of an AR process is known, we may say that when a forward predictor is optimized in the mean-square sense, in theory, its tap weights take on the same values as the corresponding parameters of the process.

To proceed, we will introduce the concept of *innovations* first introduced by Kaliath [153, 154]. We define the forward prediction error

$$f_{n-1}(n) = x(n) - \hat{x}(n|\mathbb{X}_{n-1}), \qquad n = 1, 2, \cdots \tag{5.19}$$

where $\mathbb{X}_{n-1}$ denotes the space spanned by $x(1), \cdots, x(n-1)$ and $\hat{x}(n|\mathbb{X}_{n-1})$ is the *one-step prediction* of the observed random variable $x(n)$ at time n, using *all* past observations available up to and including time $n-1$. The order of the forward prediction-error filter is $n-1$ and *increases linearly with* n. We refer to the forward prediction error as the *innovation*, and for simplicity of notation write

$$i(n) = f_{n-1}(n), \qquad n = 1, 2, \cdots \tag{5.20}$$

and define the *innovation process* as

$$i(n) = x(n) - \hat{x}(n|\mathbb{X}_{n-1}), \qquad n = 1, 2, \cdots \tag{5.21}$$

It is shown in Haykin [43] that the innovation $i(n)$, associated with the observed variable $x(n)$, is orthogonal to the past observations $x(1), x(2), \cdots, x(n-1)$. Also the innovations $i(1), i(2), \cdots, i(n)$ are orthogonal to each other and there is a one-to-one correspondence between the observed data $\{x(1), \cdots, x(n)\}$ and the innovations $\{i(1), i(2), \cdots, i(n)\}$. One sequence can be obtained from the other by means of a causal invertible filter without any loss of information.

The process x will be said to be autoregressive if there exists a finite N such that the innovation $i(n)$ coincides with the Nth-order innovation $i_N(n) =$

$x(n) - \hat{x}(n|\mathbb{X}_{n-1}), \qquad n = 1, 2, \cdots, N$. The *order* of an autoregressive process is defined as the minimal value of N for which $i(n) = i_N(n)$.

The basic idea behind the use of linear prediction for blind identification resides in the *generalised Bezout identity* [155]. Let us define the $M \times 1$ polynomial vector

$$\boldsymbol{H}(z) = [H_0(z), H_1(z), \cdots, H_{M-1}(z)]^T \tag{5.22}$$

where $H_i(z)$ is the transfer function of the ith subchannel. Under the condition that $\boldsymbol{H}(z)$ is irreducible, the generalized Bezout identity states there exists a $1 \times M$ polynomial vector

$$\boldsymbol{G}(z) = [G_0(z), G_1(z), \cdots, G_{M-1}(z)] \tag{5.23}$$

such that

$$\boldsymbol{G}(z)\boldsymbol{H}(z) = 1 \tag{5.24}$$

that is

$$\sum_{i=0}^{M-1} G_i(z)H_i(z) = 1 \tag{5.25}$$

The implication of this identity is that a set of moving average processes described in terms of a white noise process $s(k)$ by the operation $\boldsymbol{x}(k) = \boldsymbol{H}[s(k)]$ may also be represented by an autoregressive process of finite order. Using the generalised Bezout identity, we show that

$$\sum_{i=1}^{M} G_i(z)[x_i(k)] = s(k) \tag{5.26}$$

and $s(k)$ is thus reproduced exactly with $G_i(z)$ as an operator.

In order to compute a linear prediction error filter $G(z)$, it is first necessary to extract the innovation $i(n)$ of $x(n)$ by calculating a $M \times M$ linear prediction error filter $A(z) = I + \sum_{k=1}^{N} A_k z^{-k}$ where I is the identity matrix and the coefficients $[A(1), \cdots, A(N)]$ of the $M \times M$ prediction error filter $A(z)$ are defined by the orthogonality relationship

$$[A(z)]x(n)[x^T(n-1), \cdots, x^T(n-N)]) = 0 \tag{5.27}$$

that is

$$[A(1), \cdots, A(N)]R_{N-1} = -[r(1), \cdots, r(N)]. \tag{5.28}$$

and

$$[A(1), \cdots, A(N)] = -[r(1), \cdots, r(N)]R_{N-1}^{\#} \tag{5.29}$$

where the superscript # denotes the Moore-Penrose pseudoinverse.

Given the assumption that $H(z)$ is irreducible, it is shown with proof in [123] that if $x(n)$ is an autoregressive process with order less than N, its innovation process is given by $i(n) = H(0)s(n)$. The space generated by $i(n)$ is monodimensional and is generated by the (scalar) random variable $s(n)$, i.e., $s(n)$ is the normalized innovation of $x(n)$. As $x(n)$ is AR of order less than N, it is possible to compute the normalized innovation $s(n)$ as a linear combination of $x(n), \cdots, x(n-N)$, i.e., there exists a $1 \times M$ filter such that $s(n) = [G(z)]x(n)$.

Next, we compute a M-dimensional vector f for which $s(n) = f^T i(n)$ such that $G(z) = f^T A(z)$ satisfies $[G(z)]x(n) = s(n)$ where

$$f = \frac{1}{\sqrt{\lambda}} l_v \tag{5.30}$$

and λ and l_v are respectively, the eigenvalue and the unit norm eigenvector of the innovation covariance matrix D defined as

$$D = H(0)H^T(0) = r(0) + \sum_{k=1}^{N} A(k)r^T(k). \tag{5.31}$$

The prediction error filter $G(z) = f^T A(z)$ allows the identification of $H(z)$. In fact, $H(k)$ corresponds to the kth covariance coefficient of $x(n)$ and the shifted normalized innovation $s(n-k)$, as extracted by the prediction error filter. For $0 \leq k \leq N$

$$H(k) = E(x(n)s(n-k)) = E(x(n)[G(z)]x(n-k)). \tag{5.32}$$

5.4 Implementation

This section covers the steps to implement the linear prediction channel estimation method of Karem *et al.* [123] which we will refer to as the linear prediction engine

(LPE) in this thesis. This engine is used iteratively in our algorithm for channel order estimation. To implement the LP method in practice requires the knowledge of several unknowns which must be determined. They are summarized below

1. *Calculating the autocovariance coefficients for the covariance matrix* $\boldsymbol{R}$. From T successive samples of the observations and given $T > Q$ samples of the process $x, x_T = [x(1), \ldots, x(T)]$ and that Q is greater than the order of the filter, N, then the $Q+1$ autocovariance coefficients can be computed according to

$$\hat{r}(n) = \frac{1}{T-n} \sum_{t=1}^{T-n} x(t+n)x(t)^T \qquad 0 \leq n \leq Q \tag{5.33}$$

and the sample estimate $\hat{\boldsymbol{R}}_Q$ of the $M(Q+1) \times M(Q+1)$ covariance matrix of the vectorized observation X_Q is given by

$$\hat{\boldsymbol{R}}_Q = \begin{bmatrix} \hat{r}(0) & \hat{r}(1) & \ldots & \hat{r}(Q) \\ \hat{r}(1)^T & \hat{r}(0) & \ldots & \hat{r}(Q-1) \\ \vdots & \vdots & \ddots & \vdots \\ \hat{r}(Q-1)^T & \ldots & \hat{r}(0) & \hat{r}(1) \\ \hat{r}(Q)^T & \ldots & \hat{r}(1)^T & \hat{r}(0) \end{bmatrix} \tag{5.34}$$

2. *Estimation of the noise power* $\hat{\sigma}^2$. The noise is assumed to be additive white Gaussian noise. The noise covariance $\hat{\sigma}^2$ can be estimated by calculating the average of the $M(Q+1) - (N+Q+1)$ smallest eigenvalues of the convariance matrix $\hat{R}_Q$.

3. *Estimation of the order* $\hat{N}$ *of the prediction filter.* A standard model order estimation procedure based on the information theoretic criteria is normally used. In practice, when the antennas are close together, there is a high degree of correlation between the received signals and the information theoretic criteria models fail. The next section will describe in detail an algorithm that does not use information theoretic criteria based algorithms [102] but uses the intrinsic properties of the LP method to give robust estimates of the channel order.

4. *Estimation of the prediction coefficients* $\hat{A}$. This is obtained by solving the Yule-Walker equations

$$\hat{A} = [I, \hat{A}(1), \ldots, \hat{A}(\hat{N})]^T \tag{5.35}$$

$$\hat{A} = -[\hat{r}(1), \ldots, \hat{r}(\hat{N})](\hat{\boldsymbol{R}}_{\hat{N}-1} - \hat{\sigma}^2 \boldsymbol{I})^{\#} \tag{5.36}$$

where the superscript # stands for the pseudoinverse.

5. *Estimation of the innovation covariance matrix* $\hat{D}$. This is obtained as a direct byproduct of the solution of the Yule-Walker system

$$\hat{D} = \hat{r}(0) - \hat{\sigma}^2 I_M + \sum_{k=1}^{N} \hat{A}(k)\hat{r}(k)^T \tag{5.37}$$

$$\hat{D} = \hat{r}(0) - \hat{\sigma}^2 I_M + [\hat{A}(1), \ldots, \hat{A}(\hat{N})][\hat{r}(1), \ldots, \hat{r}(\hat{N})]^T \tag{5.38}$$

6. *Estimation of the prediction error filter* $\hat{G}$. The filter coefficient $\hat{f}$ can now be estimated from the eigen-decomposition of the estimated covariance matrix $\hat{D}$ where $\hat{\lambda}$ is the greatest eigenvalue of D and $\hat{l_v}$ is the associated eigenvector of $\hat{D}$ such that $\hat{f} = \frac{\hat{l_v}}{\sqrt{\hat{\lambda}}}$. The prediction error filter $\hat{G}$ is a $1 \times M(\hat{N}+1)$ matrix computed using the equation

$$\hat{G} = \hat{f}^T \hat{A}. \tag{5.39}$$

7. *Estimation of the channel coefficients* $\hat{H}$. $\hat{H}$ is the $M(\hat{N}+1) \times 1$ vector

$$\hat{H} = \hat{S}(\hat{N})\hat{G}^T \tag{5.40}$$

where

$$\hat{S}(\hat{N}) = \begin{bmatrix} \hat{r}(\hat{N}) & 0 & 0 & \ldots & 0 \\ \hat{r}(\hat{N}-1) & \hat{r}(\hat{N}) & 0 & \ldots & 0 \\ \vdots & \vdots & \vdots & \ddots & \vdots \\ \hat{r}(0) - \hat{\sigma}^2 I_q & \hat{r}(1) & \ldots & \ldots & \hat{r}(\hat{N}) \end{bmatrix} \tag{5.41}$$

5.5 The Dynamic Channel Order Estimator algorithm

In this section, we will describe an algorithm which will be referred to in this Thesis as the Dynamic Channel Order Estimator (DYCOE) algorithm. The flowchart for the algorithm is depicted in Figure 5.2.

At initialization, the order of the filter is set to 1. The sample covariance matrix $\hat{\boldsymbol{R}}_Q$ is computed from 1000 received samples. Next an eigen decomposition of $\hat{\boldsymbol{R}}_Q$ is performed to estimate the noise power and the channel coefficients are calculated using the linear prediction engine outlined in steps 4 to 7 in the previous section.

It has been shown in [123] that when the covariance sequence is exactly known, the prediction method remains valid when N is replaced by $Q \geq N$ and the coefficients defined by

$$[A_Q(1), \ldots, A_Q(Q)] = [r(1), \ldots, r(Q)](\boldsymbol{R}_{Q-1} - \sigma^2 \boldsymbol{I})^{\#} \tag{5.42}$$

correspond to a prediction error filter $A_Q(z) = I + \sum_{k=1}^{Q} A_Q(k) z^{-k}$ and the innovation covariance matrix is still equal to $D = r(0) - \sigma^2 I + \sum_{k=1}^{Q} A_Q(k) r^T(k)$. A degree Q, $1 \times M$ prediction error filter $g_Q(z)$ can thus be found as $g_Q(z) = f^T A_Q(z)$. The first $M(N+1)$ components of the vector $M(Q+1) \times 1$ vector $H_Q = S_Q G_Q^T$, correspond to the true filter coefficients and if we assume the noiseless case where $\sigma^2 = 0$, then the last $M(Q-N)$ coefficients are equal to zero. For example, when $Q = N+1$ which represents an over-estimation by 1, there will be M number of coefficients equal to zero. Thus, an algorithm that detects the number of coefficients equal to zero will be able to determine the channel order. However, when dealing with sample statistics, the last coefficients are not equal to zero but to some residual noise level and thus $\sigma^2 \neq 0$. The algorithm depicted in Figure 5.2 compares the coefficients of $\boldsymbol{H}$ with a threshold set above the residual noise level and computes the number of coefficients, J_c below this set threshold. If there are none, it indicates that the original channel order estimate is $\hat{N} \leq N$ which implies either an under estimation or a correct estimation. The algorithm increases the channel order estimate (step 3) by 1 and recalculates channel coefficients until $J_c \geq M$ which implies that $\hat{N} > N$.

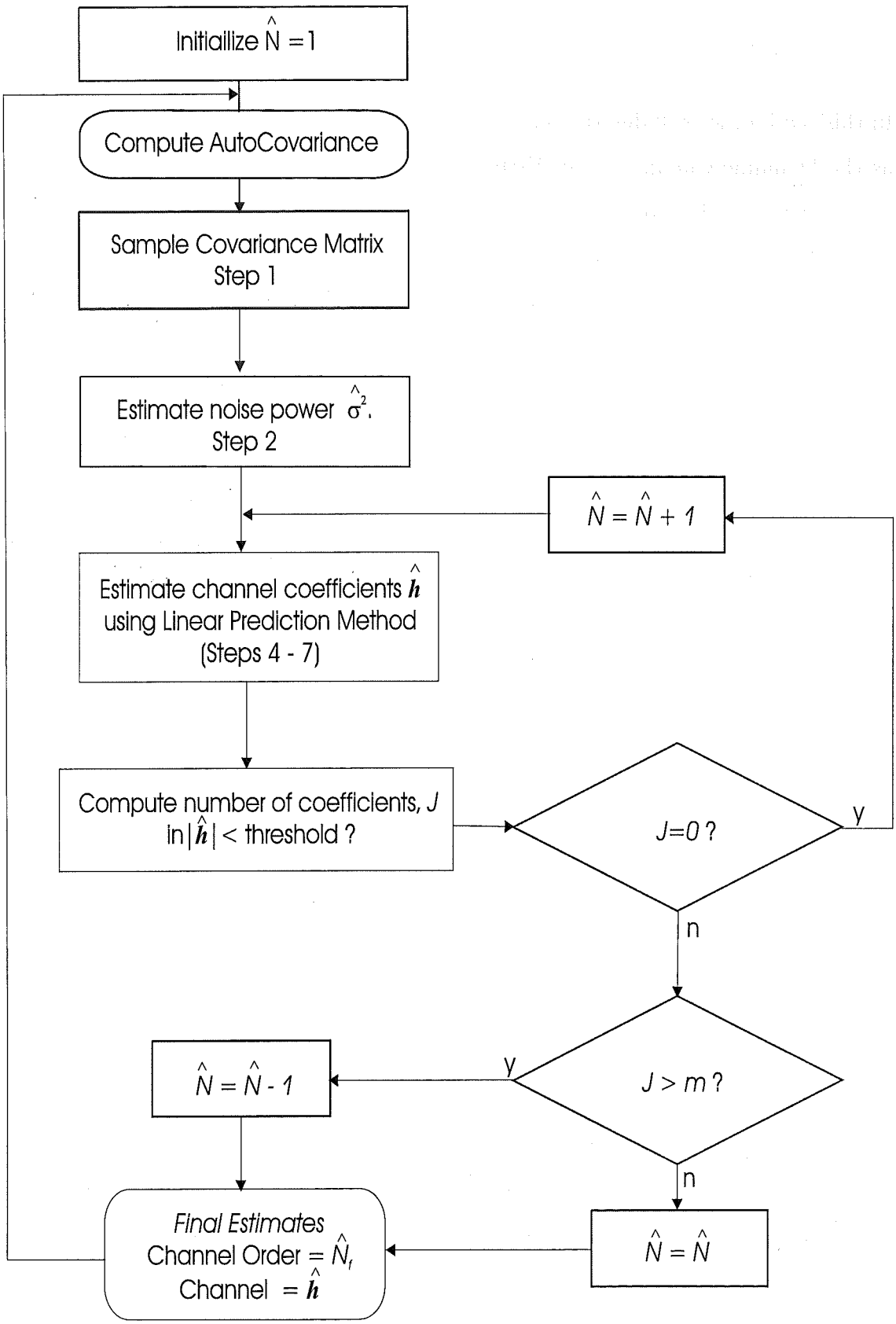

Figure 5.2: Adaptive Channel Order and Channel Estimation Algorithm

If $J_c = M$, then the channel order is overestimated by one and the final estimate $\hat{N}_f = \hat{N} - 1$ is computed. If $J_c < M$, the algorithm will not compute $\hat{N}_f$ but will increase $\hat{N}$ by 1 and recalculate channel coefficients until $J_c \geq M$. The algorithm must over estimate by at least one before a final estimate is computed.

There will be occasions when the channel characteristics change over time and the previous channel order estimate used in the current computation of $\boldsymbol{H}$ is too big. In this situation, $J_c = i \times M$ where $i = 2, 3, \ldots$ and the final estimate is $\hat{N}_f = \hat{N} - \frac{J_c}{M}$. The new channel order estimate for the next computation is reduced by 1 at each iteration until $J_c = M$. Conservely, when the previous channel order estimate used in the current computation of $\boldsymbol{H}$ is too small, the algorithm detects that $J_c < M$ and will iteratively increase the channel estimate by 1 until $J_c = M$. The algorithm will thus adapt to changing channel conditions.

5.6 Simulation Results

Example 1 : In this example, the performance of the adaptive channel order estimation algorithm is assessed by Monte-Carlo experiments. For each experiment there are 100 independent trials and each trial consist of 1000 identical and independently distributed (i.i.d.) sequence of binary variables taking its value in $-1, +1$ with equal probabilities. The output observation noise is an i.i.d. sequence of zero-mean Gaussian variables. For comparison, the performance is compared with the MDL algorithm which is the standard algorithm used for channel order estimation. We will first investigate the performance of algorithm for a 4 variate model to depict the situation of one transmiter and 4 receive antennas sampled at symbol rate with the channel coefficients given in Table 5.1. The channel coefficients are chosen to give mixed-phase channel responses. h_1, h_2 and h_3 have nonminimum-phase channel responses with some of the zeros outside the unit circle in the z-plane. h_4 has a minimum phase channel response with all zeros inside the the unit circle in the z-plane. h_3 and h_4 however, have all their zeros close to the unit circle. Note that it is quite common to find nonminimum-phase zeros close or even on the unit circle in a typical mobile radio communication environment [156]. These coefficients represent 4 distinct channels with $N = 5$ and refered to in this Thesis as Type 1 channel

coefficients. We will look at selecting a threshold value for the algorithm. This is determined by using Monte Carlo experiments using various values of thresholds at 5 dB SNR as shown in Table 5.2.

Table 5.1

Type 1 channel coefficients

Channel	Channel coefficients					
		z^{-1}	z^{-2}	z^{-3}	z^{-4}	z^{-5}
$h_1(z)$	-0.0419	-0.2993	-1.2808	-0.5301	0.1417	-0.2624
$h_2(z)$	0.9097	-0.2021	-0.4401	-1.0153	-0.5364	-0.0817
$h_3(z)$	-1.1836	0.4906	-0.3093	0.4011	0.1269	-1.8522
$h_4(z)$	1.2965	0.0525	0.3410	-0.0260	0.3991	0.8817

Table 5.2

Performance of DYCOE algorithm at various threshold values (5dB SNR)

threshold	Estimated Channel Order $\hat{N}$							
	1	2	3	4	5	6	7	8
0.125	0	0	0	0	63	15	12	10
0.15	0	0	0	0	93	7	0	0
0.2	0	1	0	1	98	0	0	0
0.25	1	0	0	0	99	0	0	0
0.3	5	2	0	2	91	0	0	0
0.35	3	2	0	9	86	0	0	0
0.4	24	4	1	4	67	0	0	0

Table 5.2 shows that the best threshold is between 0.2 and 0.25. The threshold value is fixed at 0.2 for the simulations. Later an automatic threshold equation based on the range of eigenvalues will be introduced. Higher thresholds will result in under estimation because it fails to detect the low value channels coefficients and treats them as noise and counts only the high coefficients. Thresholds below 0.2 on the

other hand results in a over estimation because more noise samples are mistaken for channel coefficients.

The performance of the DYCOE and MDL algorithms also depend on the number of samples used per trial as shown in Table 5.3. The results of the DYCOE algorithm at a threshold setting of 0.2 and 10 dB SNR are shown in Table 5.3A. The performance is excellent above 800 samples but degrades significantly below 600 samples for the DYCOE algorithm. The MDL algorithm (Table 5.3B) on the otherhand is excellent above 500 samples but degrades gradually with acceptable performance down to 300 samples. The simulations throughout this chapter use a sample size of 1000 as they provide perfect estimates and will not be a factor in limiting the performance of both algorithms.

The performance of the DYCOE algorithm as a function of SNR is compared with the standard MDL algorithm. This is shown in Tables 5.4. Table 5.4A shows excellent performance of the DYCOE algorithm from 50 dB down to 0 dB SNR. At -5 dB SNR, the algorithm still works and is able to estimate the correct channel order with a probability of 0.87. The number of under estimates increases as the SNR decreases.

It is shown in Table 5.4B that the MDL algorithm works within a narrow SNR range of between 5 and 15 dB SNR. This phenomenon is also reported by Liavas *et al.*[118]. At SNR of 0 dB and below, the MDL algorithm severely underestimates and above 20 dB grossly overestimates the channel order. The dynamic behaviour of the algorithms is depicted in Figure 5.3.

Figure 5.3A, Figure 5.3B and Figure 5.3C show the dynamic performance of the DYCOE and MDL algorithms at -5 dB, 10dB and 20dB SNR respectively. We can clearly see from Figure 5.3 and Table 5.4 that the DYCOE algorithm has superior performance over MDL and shows robust operation over a wide SNR range from -5 to 50 dB SNR. At -5dB SNR, the DYCOE algorithm initially ramps up and settles down within the first 18 trials with 4 occasions of under estimates after the first 18 trials. The MDL algorithm under estimates *all* 100 trials at -5dB SNR. The MDL algorithm gave the best performance at 5 dB SNR. At 20 dB SNR, the DYCOE algorithm gives perfect channel order estimates while the MDL algorithm severely overestimates the channel order.

Table 5.3

Performance of DYCOE and MDL algorithms at various number of samples at $10dB$ SNR

Sample Size	A: DYCOE ALGORITHM Estimated Channel Order $\hat{N}$								
	1	2	3	4	5	6	7	8	≥ 9
100	3	4	0	5	29	24	23	12	0
200	0	1	0	1	56	24	14	4	0
300	0	0	0	1	55	32	11	1	0
400	0	0	0	1	74	25	0	0	0
500	0	0	0	0	75	15	8	2	0
600	0	0	0	0	99	1	0	0	0
700	0	0	0	0	89	9	2	0	0
800	0	0	0	0	99	1	0	0	0
900	0	0	0	0	99	1	0	0	0
1000	0	0	0	0	100	0	0	0	0
Sample Size	B: MDL ALGORITHM Estimated Channel Order $\hat{N}$								
	1	2	3	4	5	6	7	8	≥ 9
100	0	0	0	0	79	6	12	0	3
200	0	0	0	0	91	2	3	0	4
300	0	0	0	0	96	3	1	0	0
400	0	0	0	0	98	2	0	0	0
500	0	0	0	0	100	0	0	0	0
600	0	0	0	0	100	0	0	0	0
700	0	0	0	0	100	0	0	0	0
800	0	0	0	0	100	0	0	0	0
900	0	0	0	0	100	0	0	0	0
1000	0	0	0	0	100	0	0	0	0

Table 5.4

Performance of DYCOE algorithm (threshold = 0.2) and the MDL algorithm as a function of SNR

	A: DYCOE ALGORITHM Estimated Channel Order $\hat{N}$									
SNR	0	1	2	3	4	5	6	7	8	≥ 9
-5	0	1	0	0	7	87	3	2	0	0
0	0	0	0	1	3	96	0	0	0	0
5	0	0	0	0	1	99	0	0	0	0
10	0	0	0	0	1	98	2	0	0	0
15	0	0	0	0	0	100	0	0	0	0
20	0	0	0	0	0	100	0	0	0	0
30	0	0	0	0	0	97	3	0	0	0
50	0	0	0	0	0	99	1	0	0	0
	B: MDL ALGORITHM Estimated Channel Order $\hat{N}$									
SNR	0	1	2	3	4	5	6	7	8	≥ 9
-5	7	23	70	0	0	0	0	0	0	0
0	0	0	0	0	28	72	0	0	0	0
5	0	0	0	0	0	100	0	0	0	0
10	0	0	0	0	0	100	0	0	0	0
15	0	0	0	0	0	94	0	5	1	0
20	0	0	0	0	0	0	1	7	9	83
30	0	0	0	0	0	0	0	0	0	100
50	0	0	0	0	0	0	0	0	0	100

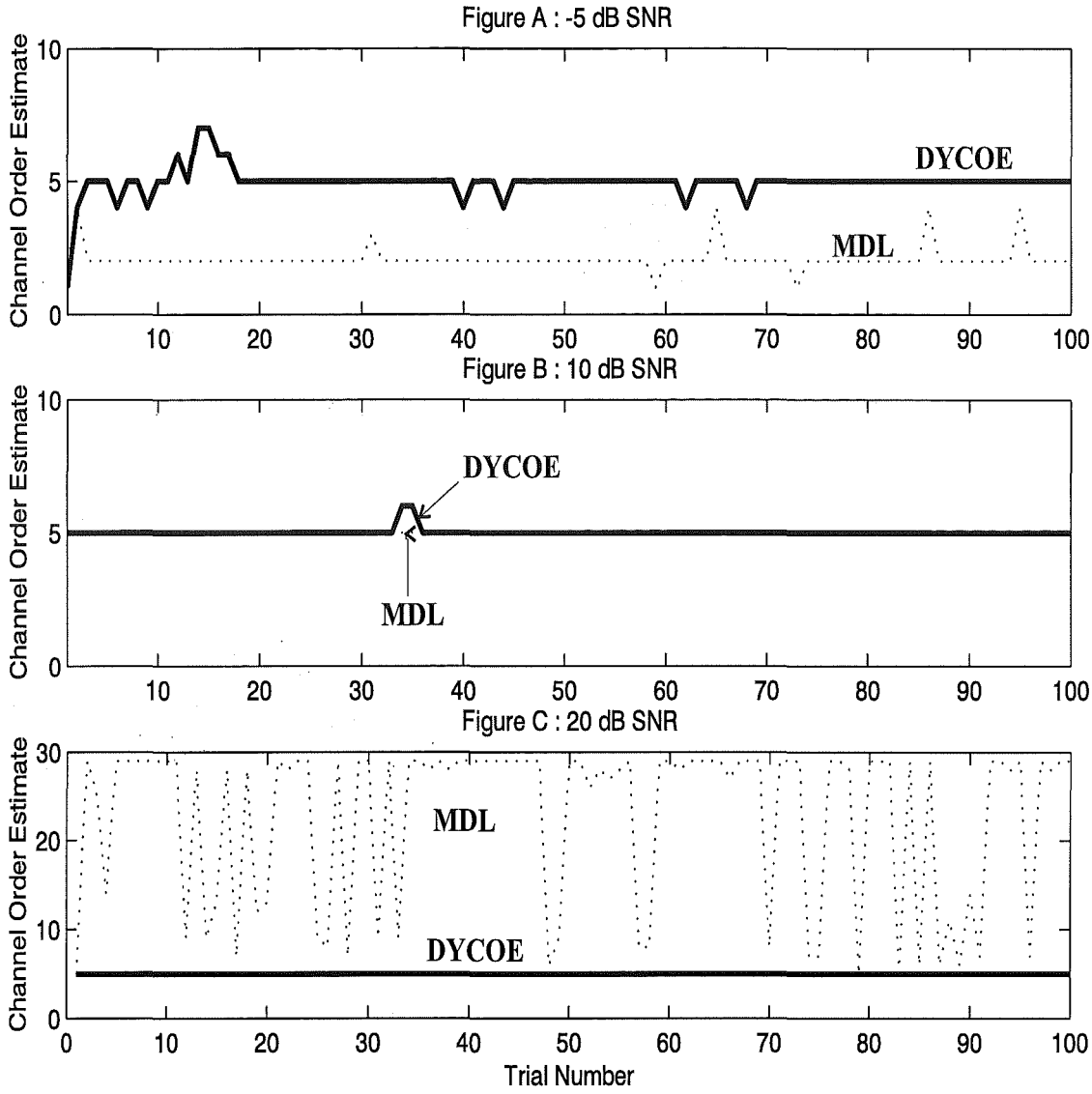

Figure 5.3: Dynamic performance of algorithm at -5, 10 and 20 dB SNR

Example 2 : The experiment is repeated and performance is then investigated under different channel conditions. The channel coefficients of Table 5.5 are used for this set of trials and are referred in this Thesis as Type 2 channel coefficients.

Table 5.5

Type 2 Channel coefficients

Channel	Channel coefficients					
		z^{-1}	z^{-2}	z^{-3}	z^{-4}	z^{-5}
$h_1(z)$	-0.0419	-0.2993	-1.2808	-0.5301	0.1417	-0.2624
$h_2(z)$	-1.1836	0.4906	-0.3093	0.4011	0.1269	-1.8522
$h_3(z)$	-1.1836	0.4906	-0.3093	0.4011	0.1269	-1.8522
$h_4(z)$	-1.1836	0.4906	-0.3093	0.4011	0.1269	-1.8522

The Type 2 channel coefficients represent an extreme case scenario where 3 out of 4 channels are exactly the same. They thus possess common zeros and usually lead to poor performance of second-order schemes. The DYCOE and MDL algorithms are subjected to this Type 2 channel and the performance is tabulated in Table 5.6.

It can be seen in Table 5.6A that the performance of the DYCOE algorithm is very good with an average probability of correct channel order estimation of 0.897 from 0 to 50 dB SNR. The errors are mainly an over estimation by a factor of 1. The frequency of under estimation is very small and occurs only at startup. The performance of the MDL algorithm shown in Table 5.6B by comparison is extremely poor. There is severe under and over estimation thoroughout the range of SNRs'. These experiments show the robustness of the DYCOE algorithm over SNR and highly correlated channels. The MDL algorithm performance is restricted to a much smaller SNR range and works best when the channels are uncorrelated.

Table 5.6

Performance of DYCOE algorithm (threshold = 0.2) and the MDL algorithm as a function of SNR using Type 2 channel coefficients

	A: DYCOE ALGORITHM Estimated Channel Order $\hat{N}$									
SNR	0	1	2	3	4	5	6	7	8	≥ 9
-5	0	0	0	0	5	65	30	0	0	0
0	0	0	1	0	2	88	9	0	0	0
5	0	0	0	0	1	89	8	2	0	0
10	0	0	0	0	2	92	6	0	0	0
15	0	0	0	0	0	90	10	0	0	0
20	0	0	0	0	1	83	16	0	0	0
30	0	0	0	0	1	93	6	0	0	0
50	0	0	0	0	0	93	7	0	0	0
	B: MDL ALGORITHM Estimated Channel Order $\hat{N}$									
SNR	0	1	2	3	4	5	6	7	8	≥ 9
-5	3	68	29	0	0	0	0	0	0	0
0	0		100	0	0	0	0	0	0	0
5	0	0	2	2	96	0	0	0	0	0
10	0	0	0	0	43	57	0	0	0	0
15	0	0	0	0	0	95	5	0	0	0
20	0	0	0	0	0	55	19	12	1	13
30	0	0	0	0	0	0	2	20	30	48
50	0	0	0	0	0	0	0	0	0	100

Table 5.7

Performance of DYCOE algorithm with *AUTOMATIC* threshold as a function of SNR using Type 1 and Type 2 channel coefficients

	A: TYPE 1 CHANNEL Estimated Channel Order $\hat{N}$								
SNR	1	2	3	4	5	6	7	8	≥ 9
-5	1	0	0	3	96	0	0	0	0
0	0	1	0	4	95	0	0	0	0
5	0	0	0	0	100	0	0	0	0
10	0	0	0	0	100	0	0	0	0
15	0	1	0	0	99	0	0	0	0
20	0	0	0	0	92	8	0	0	0
30	0	0	0	0	94	3	3	0	0
50	0	0	0	0	97	3	0	0	0
	B: TYPE 2 CHANNEL Estimated Channel Order $\hat{N}$								
SNR	1	2	3	4	5	6	7	8	≥ 9
-5	1	0	0	1	80	18	0	0	0
0	0	0	0	4	91	5	0	0	0
5	0	0	0	1	91	6	2	0	0
10	0	0	0	1	80	19	0	0	0
15	1	0	0	0	88	11	0	0	0
20	0	0	0	0	81	11	0	0	0
30	0	0	0	0	91	9	0	0	0
50	0	0	0	0	84	16	0	0	0

Example 3: The threshold of the DYCOE algorithm in the previous examples is optimized for the Type 1 channel coefficients and set to 0.2. In a real system however , the channel coefficients and signal SNR will change over time. It is therefore necessary to establish an automatic threshold based on the signal and noise powers. An

equation based on the eigenvalues of the sample covariance matrix $\hat{\boldsymbol{R}}_Q$ is empirically determined and given as

$$T_H = 0.1 + \frac{0.2}{log_{10}[\frac{\hat{\lambda}_1}{\hat{\lambda}_{mQ}}]} \tag{5.43}$$

where $\hat{\lambda}_1$ is the largest eigenvalue and $\hat{\lambda}_{mQ}$ the smallest eigenvalue of $\hat{\boldsymbol{R}}_Q$. The constants were empirically determined by simulation for a variety of channel coefficients over a wide range of SNRs. The logarithm function compresses the range between the largest and smallest eigenvalues. It gives the desired effect of increasing the threshold when the SNR is low and has the converse effect on the threshold at high SNR. Table 5.7A shows excellent performance from -5db to 50 dB SNR using Type 1 channel coefficients. In comparison with the results obtained using a fixed threshold of 0.2 in Table 5.4A, the performance is slightly inferior with degradation in performance at higher SNR. The overall performance is still excellent.

The algorithm's performance using Type 2 channel coefficients is shown in Table 5.7B. Here the average probability of correct channel order estimation over -5 to 50 dB SNR is 0.86 and the main errors are over estimations. They occur with an average probability of 0.13. This is still an acceptable level of performance compared to the MDL algorithm. Furthermore, Viterbi algorithm equalizers that rely on correct channel order estimates will still work with an over estimation despite increased computational complexity. The DYCOE algorithm with adaptive threshold has slighly inferior performance at high SNR when compared to the fixed threshold version in Table 5.6. The adaptive threshold has better performance at low SNR range of between -5 and 5 dB SNR. The adaptive threshold version also has less under estimates compared to the fixed threshold version.

5.7 Summary

The chapter has presented a robust channel order estimation algorithm which will work over a wide range of SNRs' and correlated channels. The performance is clearly superior to the MDL algorithm which operates within a small range of SNRs and fails completely when the channels are correlated. An adaptive threshold for the algorithm copes with the dynamic nature of real channels and signals compared

with a fixed threshold version of the algorithm. The algorithm however, is limited to SIMO channels of the same order.

Chapter 6

Conclusions and Suggestions for Future Work

In this chapter, the main conclusions of the work presented will be discussed. We will also consider some suggestions to future research.

6.1 Thesis Conclusions

We have developed a flexible and versatile smart antenna architecture that has been fully developed into a real test platform called SASRATS that can be used to evaluate smart antenna architectures and algorithms. The modular approach makes it easy to reconfigure the hardware for different hardware architectures if required. A flexible data bus allows for options for batch, pseudo-real time and real time mode of operation. The flexible 'digital software radio' approach makes the system easy to calibrate, compensate for antenna mutual coupling effects and most importantly make changes to algorithms and retesting them almost immediately. The developed test platform has been successfully used to verify both the cyclostationary beamforming algorithm of [132] and the signal enumeration algorithm developed by the author. We have also proposed a 'one-cable' architecture that will eliminate the need for multiple cables that is between the antennas and the receivers using conventional architecture.

We have also developed a robust signal emuneration (DSE) algorithm that will correctly enumerate the number of signals impinging on an antenna array. Most

high resolution parameter estimation algorithms critically depend on the knowledge of the number of incident signals and our algorithm will ensure that correct enumeration always occur. The algorithm is robust to the degree of correlation between signals and also works in a flat fading channel environment. It has been shown that the adaptive nature of the algorithm responds to the dynamic nature of incoming and outgoing signals and minimizes the number of antennas needed to correctly enumerate the signals so as reduce the computational load. During off-peak periods when the usage is low, there is no need to operate all the antenna arrays. All current systems use *fixed* sized arrays and that do not have the dynamic variable size property that we use to reduce computation complexity. We have successfully verified the operation of the algorithm in limited field trials.

The performance of the DSE is limited to the resolution capacity of the antenna array. If the signals are closely spaced, the algorithm under-estimates the number of signals present and a different approach will be needed.

The second algorithm developed is a channel order estimation algorithm based on linear prediction error filter theory for SIMO systems. Current channel order estimators operates over limited signal to noise ratios and underestimates the order when some of the channels are correlated. The result is poor channel estimates and will result in total failure of trellis-based equalization algorithms like the maximum likelihood sequence estimator which is realized in a recursive manner using the Viterbi algorithm. We have presented a robust algorithm that overcomes these limitations and should give more reliable operation in the field. Our channel order estimation algorithm will operate over a wide range of SNRs' and is relatively insensitive to correlated channels. Our simulation results show its superior performance over the information theoretic based algorithm like the AIC and MDL algorithms. Our DYCOE algorithm and also the MDL algorithm is limited to SIMO systems with channnels of the same order.

In conclusion we have presented in this thesis SASRATS, a flexible and versatile smart antenna test platform architecture and two useful signal processing algorithms for signal enumeration and channel order estimation.

6.2 Suggestions for Future Research

The smart antenna architecure proposed and adopted in the design and development of SASRATS is primarily focussed on the receiver side to cope with beamforming and receive diversity algorithms. To extend the capabilities of SASRATS, research can be done to develop architectures suitable for transmit diversity and space time coding. Suggestions for engineering improvements to SASRATS can be found in [125] which includes descriptions of RF, digital hardware, software and system architecture. Research into synchronization problems of smart antenna systems is another area open to research. For diversity experiments and multi-user applications, each receiver must be able to synchronize to the desired signal independently. Methods to combine and synchronize these independent signals is a field open to research.

In the field of signal enumeration, there are many interesting avenues to persue. One obvious research area is to find ways to resolve closely spaced signals which are beyond the resolution capability of the antenna array. Here the different channel characterictics of closely spaced sources may be used to separate the signals using diversity arrays and to improve the enumeration performance. A combination of beamforming array and diversity techniques may improve the performance of the enumeration algorithm when the system is overloaded. The current enumeration algorithm will work only when the number of signals is less than the number of antennas.

Finally, in the field of blind channel order estimation, research can be extended to estimate SIMO channels of different orders. Current work assumes that all channels have the same order. In practice, the order of the channels from diversity antennas may not be the same. Research can also be extended to estimate the channel orders of multiple-input-multiple-output (MIMO) systems. The system is more complex as there is more than one transmitter. The use of unique signatures at each transmitter is *one* possible way of extending the work to include MIMO systems. Each transmitter can be given a unique cyclostationary property as a proper 'signature' and at the receiver, spatial diversity antennas and the linear prediction engine can then be used to estimate the channel order and the channel transfer function.

Appendix A

Glossary of Abbreviations

ACT	Advanced Communication Technology and Services
AIC	Akaike information-theoretic criterion
ACI	adjacent channel interference
AOA	angle of arrival
ADC	analogue and digital converter
AR	auto-regressive model
ASIC	application specific integrated circuit
bps	bits per second
BLAST	Bell Labs Layered Space Time
BPSK	binary phase shift keying
CCI	co-channel interference
CDMA	code division multiple access
CM	constant modulus
CMA	constant modulus algorithm
DARPA	United States Defence Advanced Research Project Agency
DC	direct current
DDC	digital down converter
DDS	direct digital synthesizer
DOA	direction-of-arrival
DQPSK	differential phase shift keying

DS-CDMA	direct sequence code division multiple access
DSP	digital signal processor
DYCOE	Dynamic Channel Order Estimator algorithm
EMI	electromagnetic interference
ESPRIT	estimation of signal parameters via rotational invariance technique
ESSI	enhanced synchronous serial interface ports
FA	finite alphabet
FFT	Fast Fourier Transform
FPGA	field programmable gate arrays
GAIC	Gerschgorin AIC
GLE	Gerschgorin likelihood estimator
GMDL	Gerschgorin MDL
GMSK	gaussian minimum shift keying
GHz	giga Hertz
GSM	Global System for Mobile Communications
HOS	higher order statistics
I	in-phase
IC	integrated circuit
IF	intermediate frequency
IF-Baseband	intermediate frequency-to-baseband
IF-RF	intermediate frequency-to-radio frequency
IMT-2000	third generation mobile systems approved by ITU
IS-136	North America TDMA Standard
IS-95	North America CDMA Standard
ISI	inter-symbol interference
ISM	Industrial, Scientific and Medical frequency bands
ITU	International Telecommunication Union
Kbps	kilo bits per second
KSPS	kilo samples per second
KHz	kilohertz

LNA	low noise amplifier
LMS	least mean squares
LO	local oscillator
LP	linear prediction
Mbps	mega bits per second
MDL	minimum description length
MHz	megahertz
MIMO	multiple-input-multiple-output
ML	maximum likelihood
MLSE	maximum likelihood sequence estimation
MMITS	Modular Multifunction Information Transfer System
MMSE	minimum mean squared error
MRC	maximal ratio combining
MSE	mean square error
MVDR	minimum variance distortionless response
MUD	multi-user detection
MUI	multi-user interference
NIDAQ	National Instruments Data Acquisition Card
PC	personal computer
PN	pseudo noise
PSD	power spectral density
Q	quadrature phase
QAM	quadrature amplitude modulation
QPSK	quadrature phase shift keying
RACE	Research and Development in Advanced Communication in Europe
RF	Radio Frequency
RF-IF	radio frequency-to-intermediate frequency
RLS	recursive least squares
RX	receiver
SAW	surface acoustic wave

SASRATS	Smart Antenna Software Radio Test System
SCB	Special Communication Bus
SCORE	Spectral self COherence REstoral technique
SDR	software defined radio
SH	sequential hypothesis
SIMO	single-input-multiple-output
SINR	signal-to-interference-plus-noise ratio
SMI	sample matrix inversion
SNR	signal-to-noise ratio
SNOI	signal-not-of-interest
SOCS	second order cyclic statistics
SOI	signal-of-interest
ST	space-time
ST-MMSE	space-time minimum mean square error
SUNBEAM	Smart Universal Beamform (an ACT project)
TDMA	time division multiple access
TX	transmitter
VLSI	very large scale integrated circuit
WSF	weighted subspace fitting
2G	second generation cellular system - digital
3G	third generation cellular system - digital

Appendix B

Glossary of Symbols

$a(\phi)$	steering vector of the array in direction ϕ
$a_k(\phi)$	gain of the k-th element in the direction ϕ
A	prediction coefficients
$\hat{A}$	estimate of prediction coefficients
$\boldsymbol{A}$	steering matrix of the array of size $M \times K$
$\boldsymbol{a}$	steering vector of the array of size $M \times 1$
BW	bandwidth of a signal
$\boldsymbol{B}$	noise free array covariance matrix
B_C	coherence bandwidth
$\boldsymbol{C}$	vector of mutual coupling coefficients
c_{kk}	self coupling coefficient
c_{kl}	mutual coupling coefficient between antenna elements
$C_\bullet$	information-theoretic criteria of type $\bullet$
d	spacing between the elements of a linear array
D	innovation covariance matrix
$\hat{D}$	estimate of innovation covariance matrix
D_{SNR}	degradation of SNR
$\boldsymbol{d}^*$	reference signal
$\boldsymbol{E}$	diagonal matrix of steering vectors
$E\{\bullet\}$	expectation operator

E_k	incident field on element k
E_l	incident field on element l
E_θ	amplitude of the plane wave from direction θ
$f(\varphi)$	isolated antenna element pattern
f_c	carrier frequency
f_m	maximum Doppler shift
f_{IF}	intermediate frequency
f_N	forward prediction error
f_S	sampling frequency
Δ_f	small frequency offsets
$F(\theta)$	normalized array factor
$\hat{g}$	prediction error filter
$g_m(\varphi)$	complex voltage pattern of elements in an array
$g(\bullet)$	pulse shaping function
G	prediction error filter
$\hat{G}$	estimate of prediction error filter
$\boldsymbol{G}$	vector of prediction error filter
h_i	ith channel impulse response
$\boldsymbol{h}$	channel impulse response vector
H	channel impulse response matrix
$\boldsymbol{H}$	channel impulse response vector
i	innovation
$i(n)$	innovation process
I	current induced in an antenna element
$\boldsymbol{I}$	identity matrix
$I_g[x]$	floor function of the largest integer of x
j	a positive integer number
J	cost function
J_c	number of channel coefficients
$\boldsymbol{J}$	exchange matrix

k	an integer number
K	number of narrowband sources
$\hat{K}$	estimate of K
l	a positive integer number
l_v	unit norm eigenvector
L	number of estimates
L_I	likelihood function
m	a positive integer number
m_p^α	p^{th} order cyclic moment at frequency α
M	number of elements in a linear antenna array
n	a positive integer number
N	channel order
$\hat{N}$	estimate of channel order
$\hat{N}_f$	final estimate of channel order
N_{in}	in-band noise power density
$\boldsymbol{n}$	noise vector
n_k	additive white Gaussian noise at the k source
N_{out}	out-of-band noise power density
p	a positive integer number
P	a positive integer number
P_M	prediction error power
Q	a positive integer number
r'	a unique rank
$\boldsymbol{r}$	cross correlation vector
$\boldsymbol{R}$	covariance matrix
$\hat{\boldsymbol{R}}$	estimate of covariance matrix
S	signal power
SNR_S	signal to noise ratio in bandpass sampling
$\boldsymbol{s}$	signal vector
s	transmitted symbols

s_k	signal at the k-th source
t	an integer number
T	symbol period (baud rate)
T_C	coherence time
T_H	auto threshold constant for LPE
$\hat{u}$	estimate of uncorrelated sources
$\boldsymbol{u}$	eigenvectors
V	voltage output from antenna
$\boldsymbol{V}$	vector of uncompensated output voltage from antenna
$\boldsymbol{V^d}$	vector of compensated output voltage from antenna
v	mobile velocity
v^d	desired nutual coupling free received signal
v_k	total voltage of the received signal
W_k	complex weight at antenna element k
$\boldsymbol{w}$	weight vector of an array
x_i	noiseless baseband signal at i^{th} antenna
$x(n)$	sample at time n
$\boldsymbol{x}(t)$	receive vector of an antenna array
$\boldsymbol{X}$	observation vector
$\mathbb{X}_{n-1}$	Space spanned by $x(1), \cdots, x(n-1)$
$y(t)$	output of an array
$\boldsymbol{y}(t)$	output vector of an array
$\boldsymbol{Y}$	generalized matrix decomposition
z	z-transform
Z	estimation performance constant
Z_{kk}	self impedance
Z_{kl}	mutual impedance between antenna elements k and l

∇	complex gradient operator
α	frequency of spectral line
α_R	amplitude of Rayleigh distribution
β	eigenvalues of covariance matrix
γ	variable for maximum array factor response in direction θ_O
ϵ	error
ε	matrix decomposition function
π	3.14159
λ	wavelength of propagating wave
λ_i	ith ordered eigenvector
κ	wavenumber of the antenna in the antenna array
μ	step size
ω_0	frequency of impinging signals on the array
τ_k	propagation delay bewteen reference and k-th sensor
Θ	parameter vector of a model
$\hat{\Theta}$	maximum likelihood estimate of Θ
θ	direction of arrival of plane wave
θ_O	desired look direction of antenna array
$\hat{\theta}$	estimate of θ
ϕ	direction of arrival of plane wave
χ	phase of incoming signal
ψ	sine of the direction of arrival of plane wave multiplied by π
σ	variance
υ	eigenvalues
φ	sine of the angle of arrival θ
$\#$	pseudoinverse
$(.)^p$	raised to the power of p
$\langle . \rangle$	time average operation

Bibliography

[1] M. Haardt and W. Mohr, "The complete solution for third-generation wireless communications: Two modes on air, one winning strategy," *IEEE Personal Communnications*, vol. 7, no. 6, pp. 18–24, Dec. 2000.

[2] R.D. Carsello et al., "IMT-2000 standards: Radio aspects," *IEEE Personal Communication*, pp. 30–40, Aug. 1997.

[3] Theodore S. Rappaport, *Wireless Communications Principles and Practice*, Prentice Hall, 1996.

[4] R.M. Buehrer et al., "Intelligent antennas for wireless communications-uplink," *Bell Labs Technical Journal*, pp. 73–103, July 1999.

[5] A.J. Paulraj and C.B. Papadias, "Space-time processing for wireless communications," *IEEE Signal Processing Magazine*, pp. 49–83, Nov. 1997.

[6] G.E. Zysman et al., "Technnology evolution for mobile and personal communication," *Bell Labs Technical Journal*, pp. 107–129, Jan. 2000.

[7] G.V. Tsoulos, "Smart antennas for mobile communication systems: benefits and challenges," *Electronics and Communication Engineering Journal*, pp. 84–94, Apr. 1999.

[8] J. Mitola, "The software radio architecture," *IEEE Communications Magazine*, pp. 26–38, May 1995.

[9] Lal C. Godara, "Application of antenna arrays to mobile communications, part 2: Beam-forming and direction-of-arrival consideration," *Proceedings of the IEEE*, vol. 85, no. 8, pp. 1195–1245, Aug. 1997.

[10] S. J. Grant and J. K. Cavers, "Performance enhancement through joint detection of cochannel signals using diversity arrays," *IEEE Transactions on Communications*, vol. 46, no. 8, pp. 1038–1049, Aug. 1998.

[11] Simon Haykin, "Signal processing: Where physics and mathematics meet," *IEEE Signal Processing Magazine*, vol. 18, no. 4, pp. 6–7, 2001.

[12] J. H. Cozzens and M. J. Sousa, "Source enumeration in a correlated signal environment," *IEEE Transactions on Signal Processing*, vol. 42, no. 2, pp. 304–317, Feb. 1994.

[13] J.H. Winters, "Smart antennas for wireless systems," *IEEE Personal Communications*, vol. 5, no. 1, pp. 23–27, Feb. 1998.

[14] Jr. Joseph Liberti and T.S. Rappaport, *Smart Antennas for Wireless Communications*, Prentice Hall, 1999.

[15] J.G. Proakis, *Digital Communications-2nd Edition*, McGraw-Hill, 1989.

[16] H. Arslan, S.C. Gupta, G.E. Bottomley, and S. Chennakeshu, "New approaches to adjacent channel interference suppression in FDMA/TDMA mobile radio systems," *Vehicular Technology, IEEE Transactions on*, vol. 49, no. 4, pp. 1126–1139, July 2000.

[17] D. Murotake, J. Oates, and A. Fuchs, "Real-time implementation of a reconfigurable IMT-2000 base station channel modem," *IEEE Communications Magazine*, vol. 38, no. 2, pp. 148–152, Feb. 2000.

[18] H.V. Poor and G.W. Wornell, Eds., *Wireless Communications : Signal Processing Perspectives*, Prentice-Hall International, Inc., 1998.

[19] J.D. Laster and J.H. Reed, "Interference rejection in digital wireless communications," *IEEE Signal Processing Magazine*, vol. 14, no. 3, pp. 37–62, May 1997.

[20] Alle-Jan van der Veen and A. Paulraj, "An analytical constant modulus algorithm," *IEEE Transaction on Signal Processing*, vol. 44, no. 5, pp. 1136–1155, May 1996.

[21] R.C. North, R.A. Axford, and J.R. Zeidler, "The performance of adaptive equalization for digital communication systems corrupted by interference," *Asilomar 1993*, vol. 2, pp. 1548–1554.

[22] I. Howitt et al., "Recent developments in applying neural nets to equalization and interference rejection," in *Virginia Tech's Third Symposium on Wireless Personal Communications. Proceedings*, 1993.

[23] B.G. Agee, S.V. Schell, and W.A. Gardner, "Spectral self-coherence restoral: A new approach to blind adapative signal extraction using antenna arrays," *Proceedings of the IEEE*, vol. 78, pp. 753–767, Apr. 1990.

[24] T. Nagayasu and S. Sampei, "Elimination of adjacent channel interference via nonlinear filters," *Electronics and Communications in Japan, Part 1 : Communications*, vol. 77, no. 5, pp. 23–32.

[25] D.C. Shin and C.L. Nikias, "Adaptive interference canceler for narrowband/wideband interferences using higher-order statistics," *IEEE Transactions on Signal Processing*, vol. 42, no. 10, pp. 2715–2728, Oct. 1994.

[26] F. Takawira and L.B. Milstein, "Narrowband interference rejection in PN spread spectrum communications systems using decision feedback filters," *MILCOM'86*, vol. 2, pp. 20.4/1–5, Oct. 1986.

[27] F. Amoroso, "Adaptive A/D converter to suppress CW interference in DSPN spread spectrum communications," *IEEE Transactions on Communications*, vol. 31, pp. 1117–1123, Oct. 1983.

[28] R. Vijayan and H.V. Poor, "Nonlinear techniques for interference suppression in spread-spectrum systems," *IEEE Transaction on Communications*, vol. 38, no. 7, pp. 1060–1065, July 1990.

[29] S. Verdu, Ed., *Multiuser Detection*, Cambridge University Press, 1998.

[30] S. Verdu, "Adaptive multiuser detection," *Proceedings of the 1994 International Symposium on Spread Spectrum Technology and Applications*, pp. 43–50, 1994.

[31] J. Litva and K.Y.L. Titus, *Digital Beamforming in Wireless Communications*, Artech House Publishers, 1996.

[32] B. Widrow, P.E. Mantey, L.J. Griffiths, and B.B. Goode, "Adaptive antenna systems," *IEEE Proceedings*, vol. 55, no. 12, pp. 2143–2159, Dec. 1967.

[33] G.V. Tsoulos, Ed., *Adaptive Antennas for Wireless Communications*, IEEE Press, 2000.

[34] P. Howells, "Intermediate frequency side-lobe canceller," *U.S. Patent 3,202,990*, 1965.

[35] S.P. Applebaum, "Adaptive arrays," *Syracuse University Research Corporation Report SPL, TR66-1*, 1996.

[36] B. Widrow, "Adaptive filters," in *Aspects of Network and System Theory*, R.E. Kalman and N. DeClaris, Eds. New York, Holt, Rinehart and Wilson, 1970.

[37] J. Capon et al., "Multidimensional maximum likelihood processing of a large aperture seismic array," *Proceedings of IEEE*, vol. 55, pp. 192–211, Feb. 1967.

[38] O.L. Frost, "An algorithm for linearly constrained adaptive array processing," *Proceedings of the IEEE*, vol. 60, pp. 926–935, 1972.

[39] L.J. Griffiths and C.W. Jim, "An alternative approach to linearly constrained adaptive beamforming," *IEEE Transactions on Antennas and Propagation*, vol. 30, pp. 27–34, May 1982.

[40] A.N. Kolgomorov, "Sur l'interpolation et extrapolation des suites stationaries," *C. R. Acad. Sci. Paris*, vol. 208, pp. 2043–2045, 1939.

[41] N. Wiener, *Extrapolation, Interpolation and smoothing of stationary time series with engineering applications*, MIT Press, Cambridge, Massachusetts, 1949.

[42] D.H. Brandwood, "A complex gradient operator and its application in adaptive array theory," *Proc. Inst. Elect. Eng.*, vol. 130, pp. 11–16, Feb. 1947.

[43] Simon Haykin, *Adaptive filter theory-3rd Edition*, Prentice Hall, 1996.

[44] Lal C. Godara, "Application of antenna arrays to mobile communications, part 1: Performance improvement, feasibility, and system consideration," *Proceedings of the IEEE*, vol. 85, no. 7, pp. 1031–1060, 1997.

[45] D. J. Goodman, *Wireless personal communication systems*, Addison-Wesley-Longman Inc., 1997.

[46] J. Salz J.H. Winters and R.D. Gitlin, "The impact of antenna diversity on the capacity of wireless communication systems," *IEEE Trans. Comm*, vol. 42, pp. 1740–1750, Feb. 1994.

[47] P. Petrus and J.H. Reed, "Least squares CM adaptive arrays for cochannel interference rejection for amps and is-54 signals," in *Wireless'95*, July 1995.

[48] T. Ohgane et al., "An implementation of a CMA adaptive array for high speed GMSK transmission in mobile communication," *IEEE trans. veh. technol.*, vol. 42, pp. 282–288, Aug. 1993.

[49] N. Kikuma et al., "Consideration on performance of the CMA adaptive adaptive array for 16-QAM signals," in *Sixth IEEE Int. Symposium on Personal, Indoor, and Mobile Radio Communications*, 1995, pp. 677–681.

[50] M.V. Clark et al., "MMSE diversity combining for wide-band digital cellular radio," *IEEE transactions on communications*, vol. 40, no. 6, pp. 1128–1135, June 1992.

[51] M.V. Clark et al., "Optimum linear diversity receivers for mobile communications," *IEEE Transactions on Vehicular Technologgy*, vol. 43, no. 1, pp. 47–56, Feb. 1994.

[52] M.V. Clark, *Diversity and equalization in digital cellular radio*, Ph.D. thesis, University of Canterbury, Christchurch, New Zealand, 1992.

[53] A.J. Paulraj and B.C. Ng, "Space-time modems for wireless personal communications," *IEEE Personal Communications*, vol. 5, no. 1, pp. 36–48, Feb. 1998.

[54] R.B. Ertel et al., "Overview of spatial channel models for antenna array communication systems," *IEEE Personal Communications*, vol. 5, no. 1, pp. 10–22, Feb. 1998.

[55] M. Simon and M. Alouini, *Digital Communication over Fading Channels*, John Wiley and Sons, 2000.

[56] J.H. Winters, "Optimum combining in digital mobile radio with co-channel interference," *IEEE Trans. Veh. Technology*, vol. 33, pp. 144–155, Aug. 1984.

[57] W.R. Bennet M. Schwartz and S. Stein, *Communicationn Systems and techniques*, IEEE Press, 1996.

[58] S. Ratnavel et al., "MMSE space-time equalization for GSM cellular systems," in *IEEE 46th Vehicular Technology Conference 1996. Mobile Technology for the Human Race.*, 1996, vol. 1, pp. 331–335.

[59] M. Wax and Y. Anu, "Performance analysis of the minimum variance beamformer," *IEEE Transactions on Signal Processing*, vol. 44, no. 4, pp. 928–937, 1996.

[60] M. Torlak and Guanghan Xu, "Maximum likelihood detection of co-channel communication signals exploiting the spatio-temporal diversity," *Signals, Systems and Computers, 1996. Conference Record of the Thirtieth Asilomar Conference on*, vol. 1, pp. 728–732, 1997.

[61] R.O. Schmidt, "Multiple emitter location and signal parameter estimation," *IEEE transactions on antennas and propagation*, vol. 34, pp. 276–280, 1986.

[62] R. Roy and T. Kailath, "ESPRIT - estimation of signal parameters via rotational invariance techniques," *IEEE Transactions on Acoustic, Speech and Signal processing*, vol. 37, no. 7, pp. 984–995, July 1989.

[63] Theodore S. Rappaport, Ed., *Smart Antennas*, IEEE Press, 1998.

[64] A. Perez-Neira, X. Mestre, and J.R. Fonollosa, "Smart antennas in software radio base stations," *IEEE Communication Magazine*, pp. 166–173, Feb. 2001.

[65] R. Baines, "The DSP bottleneck," *IEEE Communication Magazine*, vol. 33.

[66] A.K. Salkintzis et al., "ADC and DSP challenges in the development of software radio base stations," *IEEE Personal Communications*, vol. 6, no. 4, pp. 47–55, Aug. 1999.

[67] L. Huang et al., "Space-time multirate blind multiuser detection for synchronous DS-CDMA systems," *Global Telecommunications Conference, 2001. GLOBECOM 2001.IEEE*, vol. 1, pp. 146–150, Nov. 2001.

[68] J.K. Han et al., "Performance comparison of the systems employing multiple antennas over spatially correlated rayleigh fading channel," *Global Telecommunications Conference, 2001. GLOBECOM 2001.IEEE*, vol. 5, pp. 3217–3221, Nov. 2001.

[69] A. Czylwik and A. Dekorsy, "System level simulations for downlink beamforming with different array topologies," *Global Telecommunications Conference, 2001. GLOBECOM 2001.IEEE*, vol. 5, pp. 3222–3226, Nov. 2001.

[70] K. Kopsa et al., "Space-time combining in the uplink of UTRA/FDD," *Global Telecommunications Conference, 2000. GLOBECOM 2000.IEEE*, vol. 3, pp. 1844–1848, Nov. 2000.

[71] Ryuji Kohno, "Spatial and temporal communication theory using adaptive antenna array," *IEEE Personal Communications*, vol. 5, no. 1, pp. 28–35, Feb. 1998.

[72] R. Yonezawa et al., "A combination of two adaptive algorithms:SMI and CMA," *Global Telecommunications Conference, 1998. GLOBECOM 1998. The Bridge to Global Integration. IEEE*, vol. 6, pp. 3181–3186, Nov. 98.

[73] R. Miura et al., "Maximal-ratio-combining array beamforming assisted by training sequences for SDMA mobile radios," *Global Telecommunications Conference, 1998. GLOBECOM 1998. The Bridge to Global Integration. IEEE*, vol. 6, pp. 3204–3208, Nov. 98.

[74] P. Vandenameele et al., "An SDMA algorithm for high speed wlan. performance and complexity," *Global Telecommunications Conference, 1998.*

GLOBECOM 1998. The Bridge to Global Integration. IEEE, vol. 1, pp. 189–194, Nov. 98.

[75] Mei Feng and K.D. Kammeyer, "Blind direction of arrival estimation using antenna arrays in multipath communication environment," *Global Telecommunications Conference, 1998. GLOBECOM 1998. The Bridge to Global Integration. IEEE*, vol. 1, pp. 165–170, Nov. 98.

[76] Yuying Dai et al., "Combined adaptive interference cancellation with antenna array for CDMA systems," *Global Telecommunications Conference, 2000. GLOBECOM 2000.IEEE*, vol. 1, pp. 143–146, Nov. 2000.

[77] M. Barrett and R. Arnott, "Adaptive antennas for mobile communications," *Electronics and Communication Engineering Journal*, pp. 203–214, Aug. 1994.

[78] P.J. Green, "Universal digital test platform and bandpass sampling receiver," M.S. thesis, University of Canterbury, 1996.

[79] J. Mitola, "Software radios-survey, critical evaluation and future directions," in *Telesystems Conference, 1992. NTC-92., National , 1992*, 1992, pp. 13/15–13/23.

[80] J. Mitola, "Software radio architecture: A mathematic perspective," *IEEE Journal on Selected areas in Communications*, vol. 17, no. 4, pp. 514–538, 1999.

[81] R.I. Lackey and D.W. Upmal, "The SPEAKeasy: The military software radio," *IEEE Communications Magazine*, vol. 33, no. 5, pp. 56–61, May 1995.

[82] R. Vidano, "SPEAKeasy II - an IPT approach to software programmable radio development," in *Proceedings of MILCOM 97*, 1997, vol. 3, pp. 1212–1215.

[83] J. Mitola, "Technical challenges in the globalization of software radio," *IEEE Communications Magazine*, vol. 37, no. 2, pp. 84–89, 1999.

[84] ITU Rec. M.1036, Geneva, Switzeland, *Spectrum Considerations for Implementation of IMT-2000 in the bands 1885 - 2025 MHz and 2100 - 2200 MHz.*

[85] V. Bose et al., "Virtual radios," *IEEE Journal on Selected areas in Communications*, vol. 17, no. 4, pp. 591–602, 1999.

[86] T. Turletti, H.J. Bentzen, and D. Tennenhouse, "Toward the software realization of a GSM base station," *IEEE Journal on Selected areas in Communications*, vol. 17, no. 4, pp. 603–612, 1999.

[87] J. Razavilar, F. Rashid-Farrokhi, and K.J. Ray Liu, "Software radio architecture with smart antennas: A tutorial on algorithms and complexity," *IEEE Journal on Selected areas in Communications*, vol. 17, no. 4, pp. 662–676, 1999.

[88] J.E. Gunn, K.S. Barron, and W. Ruczczyk, "A low-power DSP core-based software radio architecture," *IEEE Journal on Selected areas in Communications*, vol. 17, no. 4, pp. 574–590, 1999.

[89] N.S. Correal, R.M. Buehrer, and B.D. Woerner, "A DSP-based DS-CDMA multiuser receiver employing partial interference cancellation," *IEEE Journal on Selected areas in Communications*, vol. 17, no. 4, pp. 613–630, 1999.

[90] I. Seskar and N.B. Mandayam, "Software-defined radio architectures for interference cancellation in DS-CDMA," *IEEE Personal Communications*, vol. 6, no. 4, pp. 26–34, Aug. 1999.

[91] Jean-Francois Frigon annd Babak Daneshrad, "Field measurements of an indoor high-speed QAM wireless system using decision feedback equalization and smart antenna array," *IEEE Transactions on Wireless Communications*, vol. 1, no. 1, pp. 134–144, Jan. 2002.

[92] B. Hagerman et al., "Field test performance for D-AMPS in PCS bands with array processing," *IEEE VTC*, vol. 3, pp. 1582–1586, May 1997.

[93] J.H. Winters and G.D. Golden, "Adaptive antenna applique field test," in *4th Wksp. Smart Antennas in Wireless Mobile Communication*, Stanford, CA, July 1997.

[94] D. H. Johnson and D.E. Dudgeon, *Array Signal Processing: Concepts and Techniques*, Prentice Hall, 1993.

[95] Lal C. Godara, "Limitations and capabilities of direction-of-arrival estimation techniques using an array of antennas: a mobile communications perspective," in *IEEE International Symposium on Phased Array Systems and Technology, 1996.*, Oct., pp. 327–333.

[96] M. Wax and I. Ziskind, "Maximum likelihood localization of multiple sources by alternating projection," *IEEE Trans. Acoust. Speech Signal Processing*, vol. 36, no. 10, pp. 1553–1560, Oct. 1988.

[97] M. Wax et al., "Spatio-temporal spectral analysis by eigen structure methods," *IEEE Transactions on Acoustics, Speech and Signal Processing*, vol. 32, pp. 817–827, 1984.

[98] M. Viberg et al., "Detection and estimation in the sensor arrays using weighted subspace fitting," *IEEE Transaction on Signal Processing*, vol. 39, no. 11, pp. 2436–2449, Nov. 1991.

[99] M. S. Bartlett, "Further aspects of the theory of multiple regressions," *Proc. Cambridge Philos. Soc.*, vol. 34, pp. 33–40, 1938.

[100] D. N. Lawley, "Tests of significance in canonical analysis," *Biometrika*, vol. 46, pp. 59–66, 1959.

[101] T.W. Anderson, "Asymptotic theory for principle component analysis," *Ann. Math. Stat.*, vol. 34, pp. 122–148, 1963.

[102] M. Wax and T. Kailath, "Detection of signals by information theoretic criteria," *IEEE Trans. Acoust., Speech, Signal Processing*, vol. 33, no. 2, pp. 387–392, Apr. 1985.

[103] H. Akaike, "A new look at statistical model identification," *IEEE Trans. Automat. Contr.*, vol. 19, pp. 716–723, Dec. 1974.

[104] J. Rissanen, "A universal prior for integers and estimation by minimum description length," *Ann. Stat.*, vol. 11, no. 2, pp. 416–431, 1983.

[105] Q.T. Zhang et al., "Statistical analysis of the performance of information theoretical criteria in the detection of the number of signals in an array,"

IEEE Transactions on Acoustic, Speech and Signal Processing, vol. 37, no. 10, pp. 1557–1567, Oct. 1989.

[106] H. Wang and M. Kaveh, "On the performance of signal-subspace processing-part 1: Narrowband systems," *IEEE Transactions on Acoustics, Speech and Signal Processing*, vol. 34, pp. 1201–1209, 1986.

[107] Y. Yin and P. Krishnaiah, "On some nonparametric methods for detection of the number of signals," *IEEE Trans. Acoust. Speech Signal Processing*, vol. 35, pp. 1533–1538, 1987.

[108] K. M. Wong et al., "On information theoretic criteria for determining the number of signals in high resolution array processing," *IEEE Trans. Acoust. Speech Signal Processing*, vol. 38, no. 11, pp. 1959–1971, Nov. 1990.

[109] H.T. Wu et al., "Source number estimators using transformed Gerschgorinn radii," *IEEE Trans. on Signal Processing*, vol. 43, no. 6, pp. 1325–1333, June 1995.

[110] M. Wax and I. Ziskind, "Detection of the number of coherent signals by the MDL principle," *IEEE Trans. Acoust. Speech Signal Processing*, vol. 37, no. 8, pp. 1190–1196, Aug. 1989.

[111] M. Wax, "Detection and localization of multiple sources in noise with unknown covariance," *IEEE Trans. on Signal Processing*, vol. 40, no. 1, pp. 245–249, Jan. 1992.

[112] M. Wax, "Detection and localization of multiple sources via stochastic signal model," *IEEE Trans. on Signal Processing*, vol. 39, no. 11, pp. 2450–2456, Nov. 1991.

[113] T. J. Shan et al., "On spatial smoothing for directional of arrival estimation of coherent signals," *IEEE Trans. Acoust. Speech Signal Processing*, vol. 33, pp. 806–811, 1985.

[114] J.F. Yang and C.J. Tsai, "A further analysis of decorrelation performance of spatial smoothing techniques for real multipath sources," *IEEE Transactions on Signal Processing*, vol. 40, no. 8, pp. 2109–2112, Aug. 1992.

[115] H. Lee and F.Li, "An eigenvector technique for detecting the number of emitters in a cluster," *IEEE Transactions on Signal Processing*, vol. 42, no. 9, pp. 2380–2388, 1994.

[116] A. Di and L. Tain, "Matrix decomposition and multiple sources location," in *Proceedings of IEEE ICASSP'84*, 1985, pp. 33.4.1–33.4.4.

[117] A. Di, "Multiple source location-a matrix decomposition approach," *IEEE Trans. Acoust. Speech Signal Processing*, vol. 33, no. 4, pp. 1086–1091, Oct. 1985.

[118] A.P. Liavas, P.A. Regalia, and J. Delmas, "Blind channel approximation: Effective channel order determination," *IEEE Transactions on Signal Processing*, vol. 47, no. 12, pp. 3336–3344, 1999.

[119] W. Xu and M. Kaveh, "Analysis of the performance and sensitivity of eigendecomposition-based detectors," *IEEE Transactions on Signal Processing*, vol. 43, no. 6, pp. 1413–1426, 1995.

[120] A.P. Liavas and P.A. Regalia, "On the behavior of information theoretic criteria for model order selection," *IEEE Transactions on Signal Processing*, vol. 49, no. 8, pp. 1689–1695, Aug. 2001.

[121] W.H. Gerstacker and D.P. Taylor, "Blind channel estimation based on prediction and interpolation," Tech. Rep., University of Canterbury, School of Engineering, Department of Electrical and Electronic Enginnering, 2000.

[122] A.P. Liavas, P.A. Regalia, and J. Delmas, "Robustness of least-squares and subspace methods for blind channel identification/equalization with respect to effective channel undermodeling/overmodeling," *IEEE Transactions on Signal Processing*, vol. 47, no. 6, pp. 1636–1645, 1999.

[123] K. Abed-Meraim et al., "Prediction error method for second-order blind identification," *IEEE Transactions on Signal Processing*, vol. 45, no. 3, pp. 694–704, Mar. 1997.

[124] D. Slock, "Blind fractionally-spaced equalization, perfect reconstructionn filter-banks and multichannel linear prediction," *Proceedings of ICASSP*, vol. 4, pp. 585–588, 1994.

[125] P.J. Green, "Smart antenna software radio test system user manual version 1.0," Tech. Rep., University of Canterbury, School of Engineering, Department of Electrical and Electronic Enginnering, 2001.

[126] R.G. Vaughan, N.L. Scott, and D.R. White, "The theory of bandpass sampling," *IEEE Transaction on Signal Processing*, vol. 39, no. 9, pp. 1973–1984, 1991.

[127] A.J. Coulson, R.G. Vaughan, and N.L. Scott, "Signal combination using bandpass sampling," *IEEE Transaction on Signal Processing*, vol. 43, no. 8, pp. 1809–1818, Aug. 1995.

[128] S.P. Stapleton and J.K. Cavers, "A DSP-based alternative to direct conversion receiver for digital mobile communications," *IEEE Globecom'90*, vol. 3, pp. 2024–2027, 1990.

[129] Harris Semiconductor, *1996 Wireless Communications Design Seminar Handbook*, 1996.

[130] Harris Semiconductor, *Digital Signal Processing Databook 1994*, 1994.

[131] J. A. Cadzow, "A high resolution direction-of-arrival algorithm for narrow-band coherent and incoherent sources," *IEEE Trans. Acoust. Speech Signal Processing*, vol. 36, no. 7, pp. 965–979, July 1988.

[132] L. Castedo and A.R. Figueiras-Vidal, "An adaptive beamforming technique based on cyclostationary signal properties," *IEEE Transactions on Signal Processing*, vol. 43, no. 7, pp. 1637–1650, July 1995.

[133] Hans Steyskal and J. S. Herd, "Mutual coupling compensation in small array antennas," *IEEE Transactions on Antennas and Propagation*, vol. 38, no. 12, pp. 1971–1975, Dec. 1995.

[134] B. Strait and K. Hirasawa, "Array design for a specified pattern by matrix methods," *IEEE Transactions on Antenna and Propagation*, pp. 237–239, Mar. 1969.

[135] W.L. Stutzman and G.A. Thiele, *Antenna Theory and Design*, John Wiley and Sons, 1981.

[136] I. J. Gupta and A. A. Ksienski, "Mutual coupling compensation in small array antennas," *IEEE Transactions on Antennas and Propagation*, vol. 31, no. 5, pp. 785–791, Sept. 1983.

[137] P. Papazian, P. Wilson, and Y. Lo, "Phase calibration of a PCS wideband antenna array system," *Vehicular Technology Conference, 2000. IEEE VTS Fall VTC 2000. 52nd*, vol. 1, pp. 135–141.

[138] W. A. Gardner, *Statistical Spectral Analysis: A Nonprobabilistic Theory*, Prentice Hall, 1987.

[139] D.E. Reed and M.A. Wickert, "Nonstationary moments of a random binary pulse train," *IEEE Transactions on Information Theory*, vol. 35, pp. 700–703, May 1989.

[140] S. Mayrarque, "Spatial equalization of a radio-mobile channel without beamforming using the constant modulus algorithm (CMA)," in *Proceedings of ICASSP'93*, Apr. 1993, pp. 344–347.

[141] M. S. Bartlett, "Multivariate analysis," *J. Roy. Stat. Soc.*, vol. 9, pp. 176–197, 1947.

[142] J. A. Cadzow, Y. S. Kim, and D. C. Shiue, "Signal eigenvector method for general array signal processing," *Proc. SPIE Advanced Algorithms Architectures Signal Processing II*, pp. 56–72, 1987.

[143] T. J. Shan, A. Paulraj, and T. Kailath, "On smoothed rank profile tests in eigenstructure methods for direction-of-arrival estimation," *IEEE Trans. Acoust. Speech Signal Processing*, vol. 35, no. 10, pp. 1377–1385, 1987.

[144] T. E. Shrimpton and S. V. Schell, "Source enumeration using a signal-selective information theoretic criterion," *MILCOM 97 Proceedings*, vol. 3, pp. 1092–1097, 1997.

[145] T.M. Cover and J.A. Thomas, *Elements of Informationn theory*, Wiley-Interscience, 1991.

[146] G.H. Golub and C.F. VanLoan, *Matrix Computations*, Baltimore: Johns Hopkins University Press, 1983.

[147] Y. Bresler and A. Macovski, "On the number of signals resolvable by a uniform linear array," *IEEE Transactions on Acoustic, Speech and Signal Processing*, vol. 34, no. 6, pp. 1361–1375, Dec. 1986.

[148] Z. Ding, "Blind channel identification and equalization using spectral correlation measurements,part1:frequency-domain analysis," in *Cyclostationarity in communication and signal processing*, W.A. Gardner, Ed.

[149] L. Tong, G. Xu, and T. Kailath, "Blind identification and equalization of multipath channels: a time domain approach," *IEEE Transactions on Information Theory*, vol. 40, no. 2, pp. 340–349, Mar. 1994.

[150] W. A. Gardner, Ed., *Cyclostationarity in communications and signal processing*, IEEE Press, 1994.

[151] L. Tong, G. Xu, and T. Kailath, "Blind identification and equalization of multipath channels," in *IEEE International Conference on Communications, 1992*, 1992, pp. 1513–1517.

[152] L. Tong, G. Xu, B. Hassibi, and T. Kailath, "Blind identification and equalization of multipath channels: a frequency-domain approach," *IEEE Transactions on Information Theory*, vol. 41, no. 1, pp. 329–334, Jan. 1995.

[153] T. Kailath, "An innovations approach to least-squares estimation: Part 1. linear filtering in additive white noise," *IEEE Transactions on Automatic Control*, vol. 13, pp. 646–655, 1968.

[154] T. Kailath, "The innovations approach to detection and estimation theory," *Proceedings of the IEEE*, vol. 58, pp. 680–695, 1970.

[155] T. Kailath, *Linear Systems*, Englewood Cliffs, NJ:Prentice-Hall, 1980.

[156] J. Alyuna and B. Mulgrew, "A comparison of cyclostationary blind equalisation techniques," *IEE Colloquium on Multipath Countermeasures*, pp. 8/1–8/6, 1996.